UNIVERSIDADE FEDERAL DE SANTA CATARINA
CAMPUS FLORIANÓPOLIS
PROGRAMA DE PÓS-GRADUAÇÃO EM ENGENHARIA MECÂNICA

Carlos Humberto Pinzón Cuta

ON THE MOBILITY ANALYSIS OF RECTANGULAR ORIGAMI WITH MULTIPLE VERTICES

Florianópolis
2024

Carlos Humberto Pinzón Cuta

ON THE MOBILITY ANALYSIS OF RECTANGULAR ORIGAMI WITH MULTIPLE VERTICES

Dissertação submetida ao Programa de Pós-Graduação em Engenharia Mecânica da Universidade Federal de Santa Catarina para a obtenção do título de mestre em Engenharia Mecânica.
Orientador: Prof. Daniel Martins, Dr. Eng.
Co-orientador: Marina Baldissera de Souza, Dra. Eng.

Florianópolis
2024

Ficha catalográfica gerada por meio de sistema automatizado gerenciado pela BU/UFSC.
Dados inseridos pelo próprio autor.

Pinzón Cuta, Carlos Humberto
ON THE MOBILITY ANALYSIS OF RECTANGULAR ORIGAMI WITH MULTIPLE VERTICES / Carlos Humberto Pinzón Cuta ; orientador, Daniel Martins, coorientadora, Marina Baldissera de Souza, 2024.
106 p.

Dissertação (mestrado) - Universidade Federal de Santa Catarina, Centro Tecnológico, Programa de Pós-Graduação em Engenharia Mecânica, Florianópolis, 2024.

Inclui referências.

1. Engenharia Mecânica. 2. Origami. 3. Multicêntricos. 4. Método de Davies. 5. Mobilidade. I. Martins, Daniel . II. Baldissera de Souza, Marina . III. Universidade Federal de Santa Catarina. Programa de Pós-Graduação em Engenharia Mecânica. IV. Título.

Carlos Humberto Pinzón Cuta

ON THE MOBILITY ANALYSIS OF RECTANGULAR ORIGAMI WITH MULTIPLE VERTICES

O presente trabalho em nível de mestrado foi avaliado e aprovado por banca examinadora composta pelos seguintes membros:

Prof. Andrea Piga Carboni, Dr. Eng.
Universidade de Federal de Santa Catarina

Prof. Antônio Carlos Valdiero , Dr. Eng.
Universidade Federal de Santa Catarina

Rodrigo Luis Pereira Barreto, Dr. Eng.
Universidade Federal de Santa Catarina

Certificamos que esta é a **versão original e final** do trabalho de conclusão que foi julgado adequado para obtenção do título de mestre em Engenharia Mecânica.

Documento assinado digitalmente
Henrique Simas
Data: 13/09/2024 14:06:28-0300
CPF: ***.194.639-**
Verifique as assinaturas em https://v.ufsc.br

Prof. Henrique Simas, Dr. Eng.
Coordenador do Programa

Documento assinado digitalmente
Daniel Martins
Data: 13/09/2024 17:00:33-0300
CPF: ***.746.219-**
Verifique as assinaturas em https://v.ufsc.br

Prof. Daniel Martins, Dr. Eng.
Orientador

Florianópolis, 28 de agosto de 2024.

This work is dedicated to my family.

ACKNOWLEDGEMENTS

Upon analyzing the process experienced during my master's degree, I realize that the work developed was quite satisfactory, and the obstacles overcome were significant. But it wouldn't have been possible without the faith and support of the people I shared this project with.

I would like to begin by acknowledging God, because with Him, everything was possible, for guiding my path and giving me strength in difficult times.

To my parents, Esperanza Cuta and Julio Pinzón, I am grateful for their unconditional support, patience, and understanding. To my siblings, Jhon, Julio, Diego, and Sara, because they have always believed in me and have been there when I needed them.

I am immensely grateful to Professor Daniel for his patience, for finding solutions when I did not have them, for his guidance both academically and emotionally throughout this challenging process. To my co-advisor, Marina, for all the time made available to assist me when required, thank you. I also want to thank Professor Henrique Simas and Rodrigo Vieira for their teachings.

To Professor Gonzalo and my friends Marlon and Mishel, for being the first to encourage me to undertake this master's study. To my Colombian friends, Ruben, Alex, Jhon, Antonio, Duvan, Richard, Viviana, Jorge, for welcoming me, embracing me, and making me part of that beautiful Colombian community in Florianópolis, you were my family in Brazil.

I would like to especially thank Álvaro, Neider, and Fernando, for those evenings of coffee, stories, music, literature, and geography; I learned a lot from you. Also, I appreciate my colleagues from meu LAR, Gustavo, Valdatti, Luan, Esdras, Leonardo, Guilherme, for being part of this process.

I thank to the Programa de Pós-Graduação em Engenharia Mecânica of the Universidade Federal de Santa Catarina and the Conselho Nacional de Desenvolvimento Centifico e Tecnologico (CNPq) for their financial support.

“Whether you think you can or you think you can’t, you’re right”

Henry Ford

RESUMO

A análise cinemática dos origamis oferece uma compreensão profunda de suas características de movimento e restrições redundantes. Neste estudo, o método de Davies foi aplicado para determinar a mobilidade e as restrições redundantes de vários padrões de origami, incluindo um origami de vértice de grau 4 (D4V). Foram examinadas configurações completamente desdobradas, parcialmente dobradas e completamente dobradas do origami D4V, bem como outros padrões de origami de múltiplos vértices. Cada configuração foi analisada meticulosamente, desde a representação esquemática e estrutural até a construção dos helicoides e a matriz de movimentos. Os graus de liberdade líquidos foram identificados e as restrições redundantes foram calculadas pelo método de Davies e pelo princípio do trabalho virtual. Além disso, uma equação que define a mobilidade dos origami rectangulares com multiplos vértices foi proposta com base em critérios cinemáticos clássicos e nas características geométricas e estruturais dos origamis. Os resultados revelaram a importância da seleção adequada das árvores geradoras e da simetria topológica para obter resultados precisos. Este estudo fornece uma base sólida para entender a cinemática de origamis e oferece uma ferramenta útil para o projeto e análise de mecanismos dobraveis em diversas aplicações.

Palavras-chave: Origami. Extruturas dobraveis. Método de Davies. Mobilidade. Restrições redundantes.

RESUMO EXPANDIDO

Introdução

Tradicionalmente, a palavra *origami* está associada à arte da dobradura de papel, derivada da palavra japonesa "Ori", que significa dobrar, e "Kammi", que se traduz como papel. Por décadas, diferentes técnicas têm sido usadas com o objetivo de obter esculturas tridimensionais a partir da dobradura de uma folha quadrada de papel, sem a necessidade de cortá-la, colá-la ou rasgá-la . A prática do origami gera marcas no papel, as quais têm atraído a atenção de pesquisadores, que encontraram relações geométricas e matemáticas que contribuíram para avanços significativos em áreas como robótica, medicina e aeroespacial, aproveitando recursos como reconfigurabilidade, flexibilidade, compatibilidade e multifuncionalidade proporcionadas pelo origami.

Projetos para essas aplicações envolvem mecanismos compostos por múltiplos painéis conectados por juntas rotativas que permitem dobrar e desdobrar os paneis como um origami, o que é alcançado pelo arranjo sistemático e organizado dos painéis conectados como padrões de origami. Padrões tradicionalmente conhecidos como Miura-ori, Tachi-Miura e suas variações têm sido usados, caracterizados por terem padrões de dobra geometricamente simétricos e/ou a capacidade de repetir os padrões linearmente ou radialmente, facilitando a tarefa de armazenamento compacto e desdobramento em áreas.

Alguns estudos foram realizados para definir a cinemática de mecanismos inspirados em origami. Pesquisadores como Tachi e Dai propuseram algumas equações para estabelecer sua mobilidade; Bowen et al analisam a posição dos vértices de sistemas acoplados de mecanismos esféricos repetidos; Peng desenvolve um método para analisar a capacidade de dobragem rígida de padrões de origami, modelando-os como montagens ligadas esfericamente; Wilcox estuda movimentos fundamentais e atuação em mecanismos inspirados em origami; Barreto et al apresentaram uma nova classe de mecanismos chamados Multiloop Origami-inspired Spherical Mechanisms (MOISM); e Brown et al propuseram uma metodologia que permite eliminar restrições redundantes em padrões de origami.

O objetivo desta dissertação de mestrado é obter uma equação de mobilidade geral para mecanismos inspirados em origami com múltiplos vértices, que será aplicada a alguns padrões de origami e cujos resultados serão comparados com os resultados de mobilidade e restrições redundantes obtidos usando o Método de Davies.

Objetivos

O principal objetivo deste trabalho é propor uma equação geral para determinar a mobilidade de origamis retangurales com múltiplos vértices. Para atingir o objetivo principal, são delineados os objetivos específicos:

- Identificar as posições singulares de mecanismos inspirados em origami aplicando o Método de Davies.

- Quantificar as restrições redundantes presentes em alguns padrões de origami aplicando o método de Davies.
- Analisar o comportamento cinemático de mecanismos inspirados em origami usando o Método de Davies para validar sua mobilidade e restrições redundantes.
- Propor uma equação de mobilidade para os origami retangualasres com múltiplos vértices.

Metodologia

Há pesquisas que demonstram a relação entre os mecanismos esféricos e o origami. Os mecanismos esféricos têm a característica de ter todos ou alguns eixos dos pares cinemáticos encontrando-se num ponto específico no espaço, conhecido como centro esférico. Equivalentemente, as dobras do origami tendem a se encontrar num ponto específico no padrão, denominado vértice do origami. Assim, os vértices do origami são semelhantes aos centros esféricos do mecanismo, as dobras do origami podem ser interpretadas como os pares cinemáticos, e as facetas do origami representam os elos de um mecanismo esférico. Porém, os teoremas do origami podem ser utilizados para analisar os mecanismos esféricos, e as técnicas, métodos e teorias para analisar mecanismos podem ser aplicados ao origami.

A análise cinemática de origamis é essencial para compreender seu comportamento e aplicações. Utilizando o Método de Davies, foram investigadas a mobilidade e as restrições redundantes de alguns padrões de origami retangulares. Sua estrutura foi decomposta em topologia, geometria e características cinemáticas para entender seu comportamento mecânico. O estudo começou com a representação esquemática e estrutural dos origamis, identificando pares cinemáticos e gerando grafos que mostravam as conexões entre os elementos.

As características cinemáticas de cada junta e a propagação de movimentos através do mecanismo foram analisadas detalhadamente. Seus circuitos independentes foram identificados, com os quais foram calculados seus graus de liberdade bruto e liquido, além de serem calculadas as restrições redundantes. Observou-se como as características cinemáticas e as restrições redundantes mudam à medida que o origami se transforma entre configurações (totalmente dobrado, parcialmente dobrado e totalmente desdobrado). A simetria da árvore geradora mostrou-se crucial na análise dos origamis, visto que origamis com árvores geradoras simétricas possuem resultado que são ais fáceis de serem interpretados em comparação com aqueles origamis com árvores geradoras assimétricas.

Os resultados foram comparados com pesquisas anteriores, encontrando um acordo geral que valida o Método de Davies utilizado. Este estudo proporciona uma compreensão detalhada da cinemática de origamis e destaca a importância da simetria da árvore geradora.

Resultados e Discussão

O método de Davies foi aplicado a um origami de vértice de grau 4 (D4V) e usando o sistema de helicoides de ordem $\lambda = 6$ para determinar sua mobilidade e restrições redundantes. Representações esquemáticas e estruturais foram definidas e o método de Davies foi aplicado. No caso do origami D4V simples na configuração totalmente aberto teve $F_N = 2$ graus de liberdade líquida e $C_N = 4$ restrições redundantes. Para origamis parcialmente e totalmente dobrados, o mesmo método foi usado. Os resultados variaram dependendo da configuração. No

estado parcialmente dobrado, a mobilidade foi $F_N = 1$ com $C_N = 3$ restrições redundantes. No totalmente dobrado, foi $F_N = 2$ com $C_N = 4$ restrições redundantes. Esses resultados indican que o origami entre em singularidade nas configurações totalmente aberto e totalmente fechado, porem, ele ganhou um grau de liberdade.

Alguns padrões com múltiplos circuitos foram estudados: Para um padrão de dobra de dois vértices, no estado semi-dobrado, onde o origami não está em singularidade, a mobilidade foi $F_N = 1$ com $C_N = 6$ restrições redundantes. No padrão com três facetas por cada lado (padrão em forma de 3x3), duas árvores geradoras diferentes foram analisadas, resultando em diferentes restrições redundantes. A simetria na árvore geradora facilitou a interpretação dos resultados da cinemática do origami.

Em resumo, o método de Davies foi aplicado com sucesso para analisar a mobilidade e as restrições redundantes de diferentes padrões de origami, oferecendo informação sobre seu comportamento cinemático.

Considerações Finais

O método de Davies provou ser eficaz para analisar a mobilidade e as restrições nos padrões de origami, especialmente ao aplicá-lo aos origamis D4V. Isso ajudou a determinar as posições de singularidade do origami D4V. Ao examinar origamis abertos, parcialmente e completamente dobrados, foram observadas variações nos resultados, destacando a importância de uma análise detalhada para entender seu comportamento cinemático. Ao estudar padrões de múltiplos centros esféricos, como os de dois vértices e o padrão com treis facetas por lado, foram encontradas diferentes configurações de mobilidade e restrições redundantes. A análise cuidadosa da simetria nas árvores geradoras facilitou a interpretação dos resultados da cinemática desses padrões. Em resumo, o método de Davies forneceu valiosas percepções sobre a cinemática dos origamis, destacando sua versatilidade e aplicabilidade no design de estruturas dobraveis complexas.

Palavras-chave: Origami, Multicêntricos, Estructuras dobraveis, Método de Davies, Mobilidade, Restições redundantes.

ABSTRACT

The kinematic analysis of origamis offers a deep understanding of their motion characteristics and redundant constraints. In this study, the Davies method was applied to determine the mobility and redundant constraints of various origami patterns, including a degree-4-vertex (D4V) origami. Fully unfolded, partially folded, and fully folded configurations of the D4V origami were examined, as well as other multi-loops origami patterns. Each configuration was meticulously analyzed, from schematic and structural representation to the construction of screws and the motion matrix. Net degrees of freedom were identified, and redundant constraints were calculated using the Davies method and the principle of virtual work. Additionally, an equation defining the mobility of rectangular origami with multiple vertices was proposed based on classical kinematic criteria and the geometric and structural characteristics of origamis. The results revealed the importance of correct selection of spanning trees and topological symmetry to achieve accurate results. This study provides a solid foundation for understanding the kinematics of origamis and offers a useful tool for the design and analysis of foldable mechanisms in various applications.

Keywords: Origami. Deployable structures . Davies method. Mobility. Redundant constraints.

LIST OF FIGURES

LIST OF TABLES

LIST OF ABBREVIATIONS AND ACRONYMS

D4V	Degree-4-Vertex
MOISM	Multiloop Origami-inspired Spherical Mechanisms
rref	Reduced row echelon form

LIST OF SYMBOLS

$\$$	Screw
l	Line
h	Screw pith
O_{xyz}	Inertial system
$\$^M$	Twist
$\$_i^M$	Direction vector
$\vec{S}_{Oi}$	Position vector
ω	Angular velocity
V_p	Linear velocity
τ	Velocity Parallel to the Screw axis
$\$^a$	Wrench
$[\hat{\mathbf{M}}_{\mathbf{D}}]_{\lambda\nu\times F}$	Unit motion matrix for direct couplings
$\left[\hat{\mathbf{M}}_{\mathbf{N}}\right]_{\lambda\times F}$	Network unit motion matrix
$\{\vec{\psi}\}$	Twists' magnitudes vector
$[\mathbf{B}_{\mathbf{M}}]_{\nu\times F}$	Circuit matrix
G_M	Motion Graph
F	Gross degree of freedom
F_N	Net degree of freedom
m	Rank of matrix
R	Moment around x axis
S	Moment around y axis
T	Moment around z axis
U	Force around x axis
V	Force around y axis
W	Force around Z axis
λ	Screw system
j	Kinematic pairs or creases
ν	Independent Loops
C_N	Net degree of constraint
m_f	Number of mountain folds
V_f	Number of valley folds
f_i	Number of degree of freedom of kinematic pair i
B	Number of edges on the boundary at origami
H	Number of holes in the pattern
P_k	Number of k-gon facets
F_{N_c}	Mobility in the closed loop
F_{N_o}	Mobility in the open loop
G_C	Coupling graph

l_e	Number of lateral edges
m_e	Number of vertical edges

CONTENTS

1 INTRODUCTION

Origami has significantly influenced modern engineering, inspiring fields such as medicine, robotics and aerospace engineering. Research is currently underway to harness its potential to develop innovative solutions in engineering and science. In this introduction, we will explore how origami principles have penetrated various fields and their role in creating new technologies and devices.

1.1 MOTIVATION AND APPLICATIONS

During the Edo period (1603-1868), a type of art emerged in Japan that transcended paper to become the inspiration for modern engineering: origami. During that time, precise and delicate folds brought elegant and symbolic forms to life, which used to accompany religious ceremonies and festivities (HATORI, 2011). As origami evolved, it has become integrated into other artistic expressions such as painting and sculpture, later expanding to impact seemingly unrelated fields, like science and engineering.

The practice of origami leaves distinctive marks on paper that have captured the attention of designers and scientists. They have discovered geometric and mathematical relationships that laid the foundation for origami principles, later adopted in engineering applications to create remarkable devices (BROWN et al., 2022).

The precise folds of origami have inspired the development of foldable mechanisms in fields such as robotics, acoustics, active structures, airbags, batteries, deployable shelters, energy absorption, foldable bridges, medical devices, and aerospace applications (BROWN et al., 2022; MELONI et al., 2021). A striking example is the creation of deployable solar panels for aerospace applications, which can fold compactly during launch and unfold in space to maximize the solar panel area and increase the collected energy (YUE, 2023).

Another significant contribution is found in the field of medicine, where origami principles have been employed in the creation of foldable stents. These medical devices are used to keep narrow blood vessels open, incorporating origami patterns that allow them to be easily introduced into the bloodstream and then deployed in a controlled manner (LIMA et al., 2021).

In the realm of robotics, origami concepts have been applied to create foldable and autonomous robots. These robots can fold into compact shapes to navigate through narrow spaces and later unfold to perform various tasks (LIU; YOU; MAIOLINO, 2022).

The designs for these applications involve mechanisms composed of multiple panels connected by rotating joints that allow them to fold and unfold like origami. This is achieved through the systematic and organized arrangement of connected panels in origami patterns (BROWN et al., 2022; KIM; EOM; CHO, 2022). Traditionally, origami patterns such as Miura-Ori, Tachi-Miura, and their variations have been used. These are characterized by geometrically symmetric folding patterns, which can transform rotational movements into linear movements and vice versa, and can reconfigure into multiple forms (BOWEN et al., 2013; SAREH; GUEST,

2015). This repeatability and periodicity make some origami patterns, especially those with rectangular facets like the Miura-Ori, to be considered unique origami with redundant behaviors. This results in errors in the calculation of degree of freedom and difficulty in determining redundant constraints.

Some studies have been conducted to define the kinematics of origami-inspired mechanisms. Tachi (2010) and Dai and Jones (1999) have proposed some equations to establish their mobility. Bowen et al. (2013) analyzed the position vectors of repeated spherical mechanism linkages. Peng, Ma, and Chen (2018) developed a method to analyze the rigid folding capability of origami patterns by modeling their linkages as spherical joints. Wilcox (2014) studied the fundamental actuation movements in origami-inspired mechanisms. Barreto et al. (2021) introduced a new class of mechanisms called Origami Inspired Spherical Multiloop Mechanisms (MOISM). Finally, Brown et al. (2022) has proposed a methodology to eliminate redundant constraints in origami patterns.

Despite significant advances in the development of origami-inspired mechanisms, it is crucial to conduct an exhaustive investigation of their kinematic behavior to overcome the limitations present in the current methods and equations that define their mobility. This would not only facilitate the discovery of new mechanisms but also allow for the design of lighter, more compact, and efficient structures.

1.2 OBJECTIVES

The main objective of this work is to propose a general equation to determine the mobility of rectangular origami with multiple vertices. To achieve the main objective, some specific objectives are outlined:

- To identify the singular positions of origami by applying the Davies Method.
- To analyze the kinematic behavior of rectangular origami using the Davies Method to validate their mobility and redundant constraints.
- To quantify the redundant constraints present in some origami patterns by applying Davies' method.
- To establish for a mobility equation for rectangular origami with multiple vertices.

1.3 MASTER´S THESIS CONTRIBUTIONS

This dissertation mainly contributes with the kinematic analysis of origami patterns and provides an equation to calculate their mobility and redundant constraints. The kinematic analysis was based on screw and graph theories, which allowed the study of the kinematic behavior of some origami patterns in defined positions.

The specific contributions of this work are as follows:

- A singularity analysis of rectangular origami patterns, using screw and graph theories.

- A comprehensive analysis of mobility and redundant constraints in rectangular origami patterns, employing graph and screw theories through the application of Davies' method.
- A conjecture for calculating the mobility of rectangular origami patterns is proposed.
- A methodology for quantifying redundant constraints in rectangular origami patterns is established.

To the best of the author's knowledge, this is the first time where graph theory and screw theory have been combined to analyze the kinematics of origami patterns.

1.4 OVERVIEW OF THIS WORK

In this chapter, an introduction to origami-inspired mechanisms is presented, along with the objectives and contributions of this dissertation. An overview of the dissertation is also provided.

In chapter 2, screw theory and origami mechanisms are analyzed, with a presentation of Davies' notation and a review of relevant literature. The relationship between spherical mechanisms and origami patterns is established. Spherical mechanisms, are connected with origami structures, and Multiloop Origami-inspired Spherical Mechanisms (MOISM) are highlighted.

The Davies method was used, for the first time, to study the Degree-4-Vertex (D4V) origami in three states: fully unfolded, partially folded, and fully folded. The singular positions of D4V mechanism were found by analyzing mobility and redundant constraints through schematic, structural, and graphical representations. This information is found in Chapter 3.

In Chapter 4, the analysis is extended to origami with multiloops and multiple vertices. A particular behavior was found in the redundant constraints of these origami. Furthermore, it was observed that symmetry in the spanning tree facilitates the calculation of origami kinematics, while asymmetry can produce unexpected results in displacement and rotation constraints.

In Chapter 5 an equation is proposed to define origami mobility based on kinematic pairs, links, screw system, and redundant constraints. The equation proposed is applicable to origamis with at least one vertex, offering results consistent with the Davies Method.

The conclusions of this dissertation and future works are presented in Chapter 6.

2 BIBLIOGRAPHIC REVIEW

This chapter presents key theoretical foundations related to screw theory. It introduces Davies' notation and elucidates the freedoms of motion and constraints in kinematic pairs. Furthermore, it conducts a comprehensive literature review to explore the principles of origami-inspired mechanisms. The chapter establishes the connection between spherical mechanisms and origami patterns, and defines crucial concepts of mobility and constraint.

2.1 SCREW THEORY REVIEW

The screw theory is a tool capable of representing the instantaneous state of motions (kinematics) and actions (statics) of rigid bodies in space. It is based on the concept that any rigid body motion can be represented as the inseparable union of a rotation around an axis and a translation along the same axis. Geometrically, a screw \$ is defined by a directed straight line l and an associated pitch h, i.e. $\$ = l, h$ (BALL, 1998; SOUZA et al., 2023).

This dissertation adopts the notation introduced by Davies (2006). The instantaneous state of motions of a rigid body relative to an inertia system O_{xyz} can be described by a screw called *twist* $\$^M$, this screw is composed of an angular velocity vector and a linear velocity vector, and can be conveniently expressed through six homogeneous coordinates as shown in Equation (1).

$$\$_i^M = \begin{pmatrix} \vec{S}_i^M \\ \cdots\cdots\cdots\cdots \\ \vec{S}_{0_i} \times \vec{S}_i^M + h\vec{S}_i^M \end{pmatrix} \omega_i = \begin{pmatrix} \omega_x \\ \omega_y \\ \omega_z \\ \cdots \\ V_{px} \\ V_{py} \\ V_{pz} \end{pmatrix} = \begin{pmatrix} r \\ s \\ t \\ \cdots \\ u \\ v \\ w \end{pmatrix} \quad \text{Davies notation} \tag{1}$$

where the $\$_i^M$ represents the direction vector along the screw axis, ω_i denotes the twist magnitude, and $\vec{S}_{Oi}$ is the position vector of any point on the screw axis relative to the origin of the coordinate system. The vector ω ($\vec{\omega} = (r \quad s \quad t)^T = (\omega_x \quad \omega_y \quad \omega_z)^T$) represent the angular velocity of the body with respect to the inertial system. while the vector $V_p = \tau$ ($\vec{V_p} = (u \quad v \quad w)^T = (V_{px} \quad V_{py} \quad V_{pz})^T$) refers to the linear velocity of a body point at the origin O_{xyz}. The ratio of the linear velocity to the angular velocity is called the pitch of the screw, consequently $h = \|\tau\|/\|\omega\|$.

The velocity vector $\vec{V}_p$ comprises two components: a component parallel to the instantaneous screw axis, represented by $\tau = h\omega$, and the velocity normal to the instantaneous screw axis, represented by $\vec{S}_0 \times \vec{\omega}$.

Similarly, force vector $\vec{Q} = [U \quad V \quad W]^T$ and a moment vector $\vec{P} = [R \quad S \quad T]^T$ around the origin represent an action screw in the form $\$^{\mathbf{a}} = [R \quad S \quad T \quad U \quad V \quad W]^T$. Generally, a

action screw $\$^a$ can be called a $wrench$. The motion screw is said to be written in ray-coordinates and the action screw in axis-coordinates.

By arranging the normalized twist side by side, the unit motion matrix $[\hat{\mathbf{M}}_{\mathbf{D}}]_{\lambda\nu\times F}$ is generated. The subscript λ represents the workspace of the screw system, F denotes the gross degree of freedom of a coupling network, and ν indicates the independent loops of the kinematic chain. This matrix contains one motion screw for each column, as illustrated in Equation (2).

$$\left[\hat{M}_D\right]_{\lambda\nu\times F} = \begin{bmatrix} \$_a^M & \$_b^M & \cdots & \$_F^M \end{bmatrix} \tag{2}$$

where the subscripts a and b represent the degrees of freedom of each kinematic pair of the mechanism.

Relations among the motions allowed by the couplings belonging to the same circuit are established using an analogy with the Kirchhoff´s Voltage Law: the algebraic sum of the twists around any circuit is zero. This statement can be mathematically translated by the homogeneous linear system presented in Equation (3).

$$\left[\hat{M}_N\right]_{\lambda\times F}\left[\vec{\psi}\right]_F = \{\overrightarrow{0}\}_\lambda \tag{3}$$

where $\left[\hat{\mathbf{M}}_{\mathbf{N}}\right]_{\lambda\times F}$ is the network unit motion matrix of the coupling network and $\{\vec{\psi}\}$ is the vector containing the F generalized motion magnitudes (angular or translation velocity). given by Equation (4).

$$\{\vec{\psi}\}_{F\times 1} = \begin{Bmatrix} \psi_a \\ \psi_b \\ \cdots \\ \psi_c \end{Bmatrix}_{F\times 1} \tag{4}$$

The matrix $\left[\hat{M}_N\right]_{\lambda\times F}$ is obtained via multiplying $[\hat{M}_D]_{\lambda\nu\times F}$ times by a diagonal matrix composed of a row of the circuit matrix, thus can be written as:

$$\left[\hat{M}_N\right]_{\lambda\nu\times F} = \begin{bmatrix} \left[\hat{M}_D\right]_{\lambda\times F}[B_1]_{F\times F} \\ \left[\hat{M}_D\right]_{\lambda\times F}[B_2]_{F\times F} \\ \cdots \\ \left[\hat{M}_D\right]_{\lambda\times F}[B_F]_{F\times F} \end{bmatrix}_{\lambda\nu\times F} \tag{5}$$

where $[B_i]_{F\times F}$, with $i = 1, 2, 3, \cdots, F$ are diagonal matrices with diagonal elements corresponding to row i of the circuit matrix $[\mathbf{B}_{\mathbf{M}}]_{\nu\times F}$, generated from the motion graph G_M.

The F unknowns related by $\lambda\nu$ equations can be written as a function of a subset of F_N primary variables, where F_N is the net degree of freedom of the kinematic chain. The net degree of freedom is computed via Equation (6).

$$F_N = F - m \tag{6}$$

where m is the rank of the matrix $\left[\hat{M}_N\right]_{\lambda\nu\times F}$.

In mechanical networks, circuit actions provide the same information as coupling actions. A circuit action cannot expend power on any of the motions that the couplings in the circuit allow when they are unconstrained by circuit closure (DAI; JONES, 1999). When examining a single loop mechanism, the actions within such circuits are reciprocally related to the F coupling motions spanning the connectivity of the kinematic pairs. Thus, F reciprocity equations can be written expressing conditions that the λ unknown circuit action components must satisfy (CARBONI et al., 2015). In the general case, considering that all screws belong to a screw system of order $\lambda = 6$, a circuit action can be generally represented by a wrench in axis-coordinates:

$$\hat{\$}^A = \begin{bmatrix} R \\ S \\ T \\ U \\ V \\ W \end{bmatrix}_{6,1} \tag{7}$$

where R, S, and T are moments around x, y, and z axes, and U, V, and W are forces along to x, y, and z axes, respectively.

Thus, the F reciprocity equations can be written by expressing conditions under which λ unknown circuit action components can be satisfied. Furthermore, the circuit actions must be incapable of working on the displacement of any joint, which means that it can be a screw reciprocal to the screw motion of all kinematic pair in the circuit (CARBONI et al., 2015). This condition is expressed as Equation (8):

$$\left[\hat{M}_D^T\right]_{F\times 6} \begin{bmatrix} R \\ S \\ T \\ U \\ V \\ W \end{bmatrix}_{6\times 1} = \begin{bmatrix} 0 \\ 0 \\ \vdots \\ 0 \end{bmatrix}_{F\times 1} \tag{8}$$

where matrix $\left[\hat{M}_D^T\right]_{F\times 6}$ has been introduced in Equation (2) and represents the motion screws of the joints of the circuit.

For multi-loop kinematic chain with j joints, ν independent loops and a screw system of order λ, the generic circuit actions $\$_1^A, \$_1^A, \cdots, \$_\nu^A$ have a total of $\lambda\nu$ unknown components. For this kinematic chain, we can write Equation (8) as:

$$\left[\hat{M}_N^T\right]_{F,\lambda\nu} \left[\vec{A}_l\right]_{\lambda\nu,1} = [0]_{F,1} \tag{9}$$

where the column vector $\left[\vec{A}_l\right]_{\lambda\nu,1}$ contains the $\lambda\nu$ components of the circuit actions:

$$\left[\vec{A}_1\right]_{\lambda\nu,1} = \begin{bmatrix} A_{11} \\ \vdots \\ A_{1\lambda} \\ A_{21} \\ \vdots \\ A_{\nu\lambda} \end{bmatrix}_{\lambda\nu,1} \tag{10}$$

Matrix $\left[\hat{M}_N^T\right]_{F\times\lambda\nu}$, also called freedom matrix, imposes F conditions on the $\lambda\nu$ components of the circuit actions. By evaluating the rank of the matrix $\left[\hat{M}_N^T\right]_{F\times\lambda\nu}$, we can determine the net degree of constraint C_N of the kinematic chain as:

$$C_N = \lambda\nu - m \tag{11}$$

where m is the rank of matrix $\left[\hat{M}_N^T\right]_{F\times\lambda\nu}$.

2.2 SCREW SYSTEM

The screw system defines the space in which the mechanism operates. Mathematically, the screw system is the vector space generated by the linear combination of the vectors representing the movements allowed by each kinematic pair. These linearly combined vectors form the vectorial basis of the screw system. Thus, the dimension of the screw system is the number of vectors in the basis of this vector space. The dimension of the working space is given by the number of independent motions possible within that space. This space may be contained in the planar space, three-dimensional space, or in some other subspaces (MARTINS; MURAI, 2020).

In the planar workspace, three motions are possible: two translational motions contained in the plane and a rotation whose axis is normal to the plane. Thus the dimension of this screw system is $\lambda = 3$. While in the three-dimensional space, six motions are possible: Three translations and three rotations. Therefore, the dimension of the screw system is $\lambda = 6$. These six degrees of freedom can be constrained or unconstrained (HOPKINS, 2007). When a connection is added between a body and a reference body in such a way that the number of degrees of freedom is reduced, the body is said to be constrained. There is a correspondence between the degrees of freedom removed and the constraints applied to an object (MARTINS; MURAI, 2020; BLANDING, 2000). So for each kinematic pair we can write:

$$\lambda = f_i + c_i \tag{12}$$

where f_i is the degree of freedom and c_i is the constraint of freedom of each kinematic pair.

Other examples of workspaces include the gear space and the spherical space. The latter will be examined more thoroughly in the following subsection.

2.2.1 The Screw System for Spherical Motions

During the analysis of motion and actions in origami, we make certain assumptions to reduce the complexity of screw systems. This, in turn, facilitates the resolution of homogeneous linear systems presented in Equation (3) and Equation (9).

It has been suggested that the motion of kinematic pairs in an origami-inspired mechanism belongs to the second special Three-system of screws, as classified by Hunt (1978). This three-system establishes that all axes of the screws of the kinematic pairs pass through the origin O_{xyz}; and each axis contains a screw with the same pitch. When the pitch of the screw is zero, this three-system defines the degrees of freedom in spherical motions (HUNT, 1978). In other words, it is possible to perform all rotations in space; thus, the dimension of the screw system is three ($\lambda = 3$).

2.3 ORIGAMI

Euclidean geometry has been the inspiration for the creation of most origami models (DUREISSEIX, 2012). Generally, the starting point is a flat sheet of paper that is folded in such a way that creases are generated. The creases are represented by straight lines. As the number of creases within the sheet of paper increases, they intersect. The points where the straight lines converge are known as vertices. Then, taking as a reference the distance between one vertex and another, the magnitude of a crease can be defined. On the other hand, the vertex degree can be defined as the number of folds that converge at the same point. Also, the areas bounded by the creases are known as faces (PERAZA-HERNANDEZ et al., 2014). Some of these concepts can be seen in Figure 1. For example, in Figure 1 the vertex of origami shown has degree 4, as 4 creases converge to it; also, it has 4 faces.

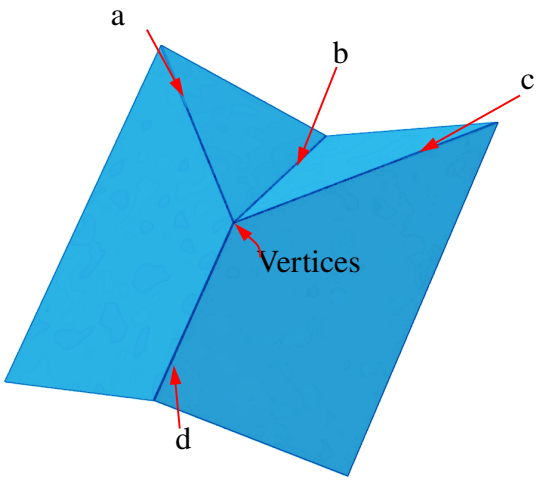

Figure 1 – Origami of degree four vertex. (BARRETO et al., 2021)

To determine the direction of a crease or the crease type, a mountain-valley assignment is generally used, considering that there are two types of creases: convex creases are considered mountain creases, while concave creases are considered valley creases. The origami shown in

Figure 1 has 3 mountain crease and 1 valley crease. A crease pattern is a schematic showing all the creases necessary to fold a structure in a sheet (DUREISSEIX, 2012). It should be noted that each crease pattern is composed of sequences of building blocks. In Figure 2, a Miura-Ori pattern is shown, this is composed of the building block presented in Figure 2a. When connected sequentially with other building blocks the fold pattern of Figure 2b is created, which can be observed folded in Figure 2c.

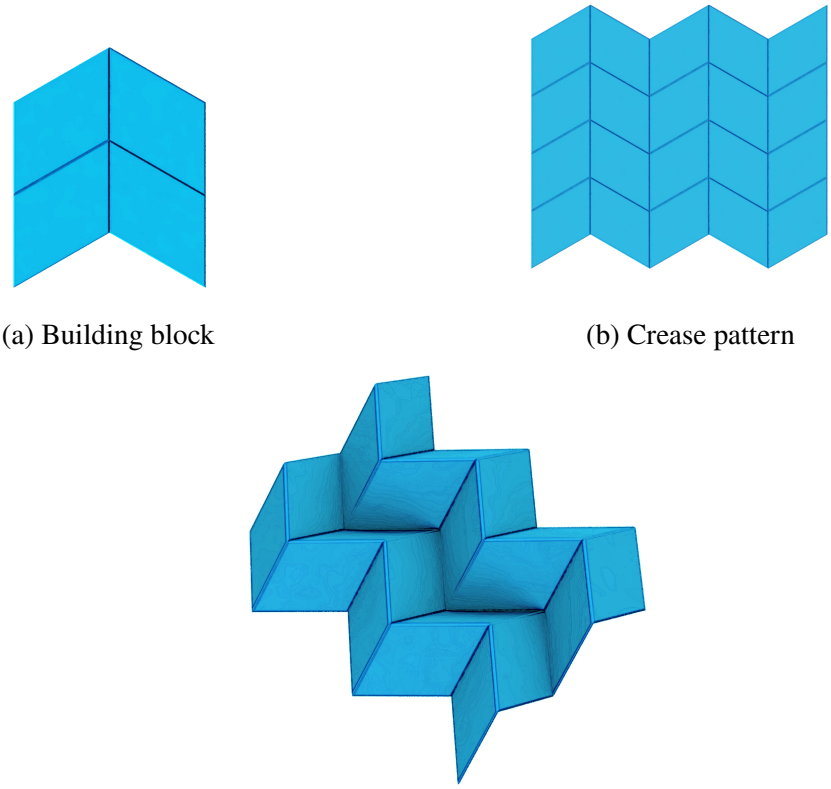

(a) Building block

(b) Crease pattern

(c) Folding of the Miura-ori pattern

Figure 2 – Miura-ori Pattern. (BARRETO et al., 2021)

Based on the concepts presented in this section, researchers have used some basic theorems have been used to establish the necessary conditions for origami folding, which are presented in the following subsection.

2.3.1 Origami Theorems

Origami, beyond being an ancient art form, possesses a rigorous mathematical foundation that governs its possibilities and limitations. This section explores two fundamental theorems that form the theoretical cornerstone of flat origami: the Kawasaki-Justin Theorem and the Maekawa-Justin Theorem.

Kawasaki-Justin Theorem: This theorem provides a necessary condition for having a flat folded state and states a condition in the vicinity of each vertex from which some straight crease radiate (DUREISSEIX, 2012), as shown in Figure 3. Let us consider a vertex with N folds, separated by angles α_i $(i = 1, ..., N)$, each at $[0, 2\pi]$. If the unfolded state is flat, they sum:

$$\sum_{i=1}^{N} \alpha_i = 2\pi \tag{13}$$

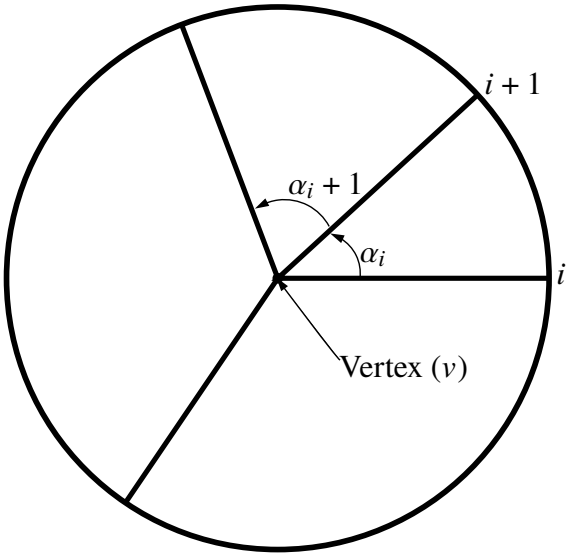

Figure 3 – Illustration of Kawsaki, Justin Theorem

Then the theorem states:

Theorem 1 *Let v be a vertex of degree 2N in a single vertex crease and let α_1 , α_2 , ..., α_{2N} be the consecutive angles between the creases. Then v is a plane vertex crease if and only if:*

$$\alpha_1 - \alpha_2 + \alpha_3 - \alpha_4 + \cdots - \alpha_{2N} = 0 \tag{14}$$

In other words, for an origami to fold flat, it is necessary to verify that N is even and that the sum of the even angles is equal to the sum of the odd angles, as given by Equation (15)

$$\sum_{1 \leq 2j+1 \leq N-1} \theta_{2j+1} = \sum_{2 \leq 2j \leq N} \theta_{2j} \tag{15}$$

Maekawa, Justin Theorem: This theorem allows calculating the number of mountain and valley creases converging to a vertex (HULL, 2002). It states that:

Theorem 2 *Let m_f be the number of mountain creases and V_f the number of valley creases adjacent to a vertex in a single-vertex fold. Then:*

$$m_f - V_f = \pm 2 \tag{16}$$

Proof. If N is the number of creases, then $N = m_f + V_f$. Fold the paper flat and consider the cross-section obtained by clipping the area near the vertex from the paper; the cross-section forms a flat polygon. If we view each interior 0° angle as a valley crease and each interior 360°

angle as a mountain crease, then $OV + 360\mathrm{m_f} = (\mathrm{N} - 2)180 = (\mathrm{m_f} + V - 2)180$, which gives $m_f - V = -2$. On the other hand, if we view each 0° angle as a mountain crease and each 360° angle as a valley crease (this corresponds to flipping the paper over), then we get $m_f - V = 2$ (HULL, 2002).

From this theorem, two corollaries were derived that are part of the important conceptual basis of the work.

Corollary 1: The number of creases at a vertex is even.

Corollary 2: If we consider an origami crease-pattern as a graph, then every flat origami crease-pattern is 2 face-colorable.

2.3.2 Origami and Spherical Mechanisms

A spherical mechanism is a mechanism in which all the axes of the rotation joints point towards a specific point in space and intersect with it. This point is known as the *spherical center* (BROWN et al., 2022). In that sense, an equivalence can be made between planar origami and spherical mechanisms, where the vertex of the origami behaves similarly to the spherical center of the mechanism, the origami faces represent the links of a spherical mechanism and the origami folds can be seen as kinematic pairs of revolution (BROWN et al., 2022). The Figure 4 shows this relationship. In Figure 4a, we can observe an origami with four folds and four faces, in Figure 4b we have a four-bar spherical mechanism, and in Figure 4c the Figure 4a and Figure 4b overlap.

Just as in origami, patterns of spherical mechanisms can be constructed, based on folding patterns, from spherical mechanisms with one independent circuit, which can be viewed as a building block. An example is illustrated in Figure 5, which contains two views of an origami overlapping with a series of kinematically equivalent spherical mechanisms. This folding pattern is referred to as a frog's tongue (BOWEN et al., 2013). Also, if a series origami patterns or building blocks are joined together to create patterns such as Miura-ori (Figure 2c), multicentric origami patterns are achieved.

Just as origami theorems can be employed in spherical mechanisms, some techniques can be applied to origami.

2.3.3 Multiloop Monocentric Origami-Inspired Spherical Mechanisms

Raul Guenter's Applied Robotics Lab (LAR) (BARRETO et al., 2021), introduces an innovative category of mechanisms called "Multi-Loop Origami Inspired Spherical Mechanisms" (MOISM). These new mechanisms, inspired by the art of origami, meet the structural criteria of conventional mechanisms and the flat folding principles of origami. In this study, it is assumed that the analyzed mechanisms are free of redundant constraints and belong to the so-called "second special three system" screw system, as shown in the subsection 2.2.1, implying that $\lambda = 3$.

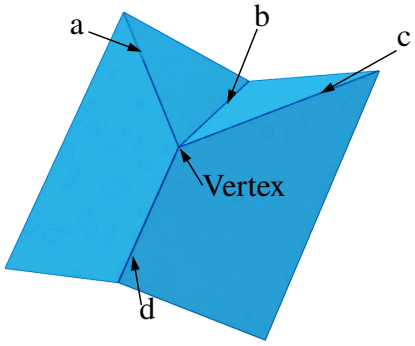

(a) Single vertex origami

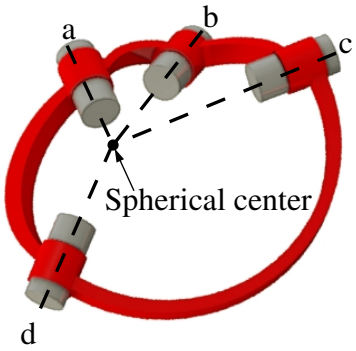

(b) Spherical four-bar mechanism

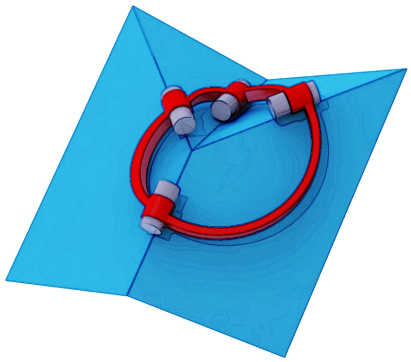

(c) Overlapping of origami and mechanism

Figure 4 – Comparison between origami and a mechanism. (BARRETO et al., 2021)

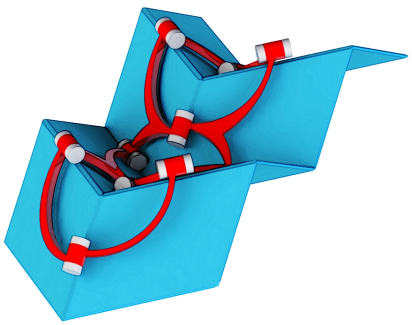

(a) Isometric view.

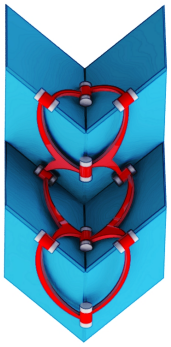

(b) Top view.

Figure 5 – Shaeffer's "Frog's Tongue" with a series of coupled spherical four-bar mechanisms kinematically equivalent to the origami. (BARRETO et al., 2021)

Two fundamental theorems of origami have been considered: the Maekawa Theorem and the Kawasaki-Justin Theorem. As described in section subsection 2.3.1, the Maekawa Theorem establishes a relationship between the number of valley-type folds and mountain-type folds. A similarity has been observed between this theorem and graph theory, especially with bipartite graphs. On the other hand, the Kawasaki-Justin Theorem was used to ensure that all kinematic pairs point toward a common spherical center. An example of a monocentric spherical mechanism with two independent circuits is shown in Figure 6. This spherical mechanism has $F_N = 1$, $\lambda = 3$

and $\nu = 2$.

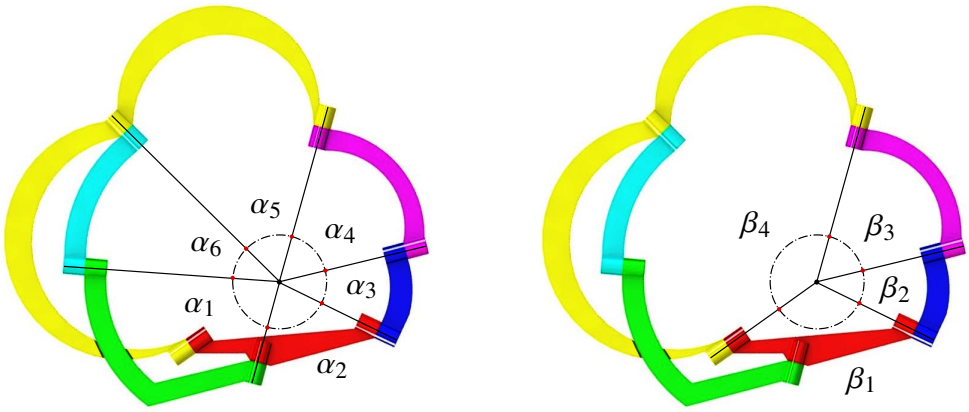

(a) (b)

Figure 6 – MOISM with $F_N = 1$, $\nu = 2$ and $\lambda = 3$: (a) Angles of the first loop (b) Angles of the second loop. (BARRETO et al., 2021)

The article written by Barreto et al. (2021) also modeled several other types of MOISM. For example, a mechanism with $F_N = 2$ and $\nu = 2$ was presented, as illustrated in Figure 7, and Figure 8 shows a MOISM with three independent loops.

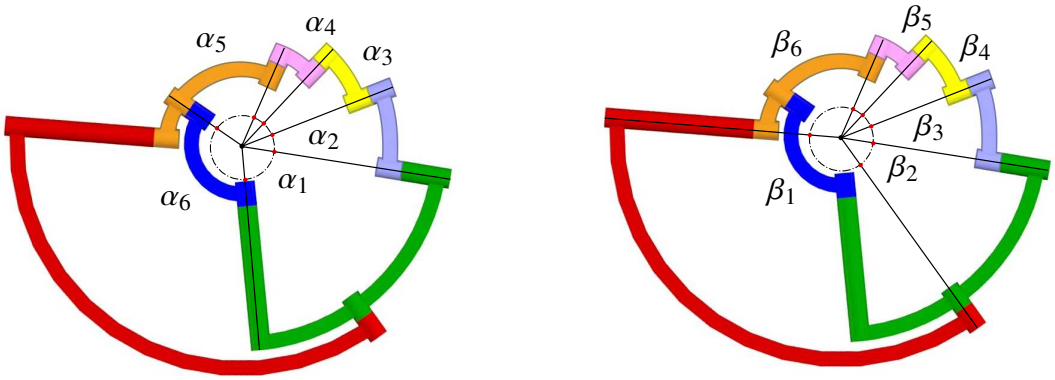

(a) (b)

Figure 7 – MOISM with $F_N = 2$, $\nu = 2$ and $\lambda = 3$: (a) Angles of the first loop (b) Angles of the second loop. (BARRETO et al., 2021)

In all cases, Kawasaki-Justin Theorem is satisfied in each of the independent circuits, which guarantees the flat-foldability condition. Therefore, origami-inspired mechanisms generated from the conditions established in the MOISM can be used in the spherical screw system ($\lambda = 3$), ensuring that all joints of the mechanism point towards a single spherical center.

This method allows the creation of a wide range of new spherical mechanisms. It is important to note that both Kawasaki-Justin Theorem and Maekawa, Justin Theorem are of great importance. For example, in mechanisms with even mobility and a single independent circuit, it is impossible to find a kinematic chain that satisfies the origami properties.

In all the cases presented in this subsection, it is crucial to perform dimensional optimization to avoid collisions between links and singularities.

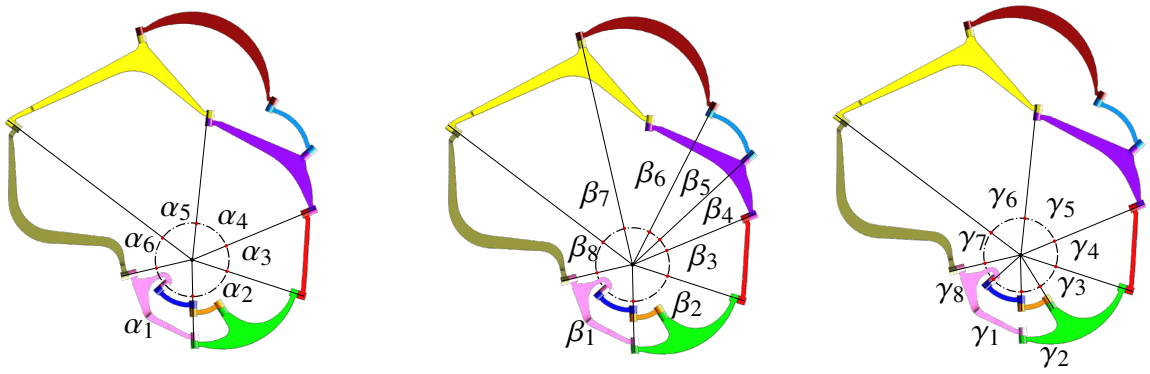

(a) (b) (c)

Figure 8 – MOISM with $F_N = 3$, $\nu = 3$ and $\lambda = 3$: (a) Angles of first loop (b) Angles of second loop and (c) Angles of third loop. (BARRETO et al., 2021)

2.3.4 Mobility of Origami

The mobility (F_N) of a kinematic chain or mechanism refers to the number of independent parameters required to define its configuration. In other words, mobility is the degree of freedom of relative movements within the kinematic chain or mechanism (MARTINS; MURAI, 2020). Mobility also determines the number of actuators needed to drive a mechanism and is used to verify the existence of mechanisms with specific structural characteristics (SIMONI; CARBONI; MARTINS, 2009).

The modified Kutzbach-Chebyshev-Gruebler equation is generally used to define the mobility of a kinematic chain (HUANG; LIU; ZENG, 2009), formulated as:

$$F_N - C_N = \lambda(n - j - 1) + \sum_{i=1}^{j} f_i \tag{17}$$

where λ is the order of the screw system to which all the kinematic pairs of the chain belong; n is the number of links; j is the number of kinematic pairs, f_i is the number of degrees of freedom of kinematic pair i , with respect to the relative motion allowed by that pair, and C_N is the number of redundant constraints present in the mechanism.

Based on some considerations such as symmetry, periodicity, redundant constraints, among others, some alternative equations have been proposed to calculate the mobility of origami-inspired mechanisms (BROWN et al., 2022). Tachi (2010) proposes that, for a general pattern such as Miura-ori, mobility can be calculated as:

$$M = B - 3H + S - 3 - \sum_{k=4} P_k(k - 3) \tag{18}$$

where B is the number of edges on the boundary of the pattern, H is the number of holes in the pattern, S is the number of redundant constraints, and P_k is the number of k-gon facets. Some of these meanings can be seen in Figure 9.

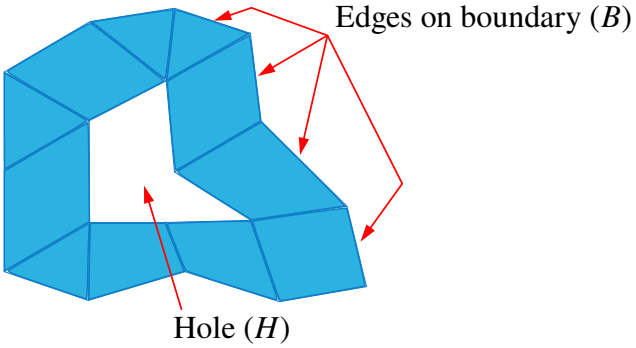

Figure 9 – Constraint origami

Although traditional mobility criteria in general underestimate the mobility of origami mechanisms, this equation accounts for redundant constraints in the system. Despite Equation (18) including a term for redundant constraints, denoted as S, identifying the exact number of these constraints within a pattern can be challenging. Moreover, Equation (18) is constrained to fold patterns that adhere to the "bird's-foot condition." Lang defined this condition as a vertex having (a) a set of three folds with the same fold assignment, sequentially separated by angles strictly between 0 and π, and (b) an additional fold with the opposite assignment (LANG, 2017). Some terms such as B, k, and P_k can be difficult to comprehend, requiring careful analysis of the equation for full comprehension.

On the other hand, Dai and Jones (1999) propose to study the mobility of origami using the Kutzbach-Chebyshev-Gruebler criterion for hybrid kinematic chains, formulating:

$$F_N = F_{N_c} + F_{N_o} = \lambda(n - j - 1) + j + j_o \tag{19}$$

where F_{N_c} is the mobility in the closed loop, F_{N_o} is the mobility in the open loop and j_o is the number of kinematic pairs within the open loop.

Some other methods have been proposed to predict the mobility of origami-inspired kinematic chain based on screws (WEI; CHEN; DAI, 2014) (WEI; DING; DAI, 2010), applying group theory (CHEN; FENG; LIU, 2016), and employing the Euler-Rodrigues formula (DAI, 2015).

Yu, Guo, and Wang (2018) demonstrated that an adjacency matrix could be used to define the number of degrees of freedom in any rigidly foldable origami pattern with multiple vertices. This method works well for conventional origami patterns that include uncut fold patterns. However, once cuts are introduced into the pattern, the adjacency matrix method is limited to single cuts between two vertices and cannot predict the degrees of freedom of patterns with holes involving external vertices or more than two internal vertices. It is worth noting that the method employed by Yu et al. is extensive, requiring several calculations to determine mobility, and solid mathematical foundations are necessary to avoid errors in the process.

For this reason, we believed it was necessary to study the kinematic behavior, identify the mobility, and the redundant constraints present in origami structures, Our aim was to then propose an equation capable of determining the degrees of freedom in rectangular origami with

multiple vertices. This equation is designed to provide clarity and accuracy, thus mitigating the risk of calculation errors stemming from unknown values like redundant constraints.

In Appendix B, some of these equations in origami patterns were explained in greater detail, alongside a comparison between the Tachi equation and the mobility criterion.

3 SINGULARITY AND SCREW SYSTEM IN ORIGAMI

This chapter analyzes the mobility and redundant constraints of degree-4-vertex origami (D4V) with a "bird's foot condition". The study examines the mobility and redundant constraints of the D4V origami in various configurations, including fully open, partially open, and fully closed states. The analysis uses Davies' method to determine the mobility and redundant constraints of a spatial D4V origami ($\lambda = 6$), as shown in Figure 10. The singularity analysis employs a spatial screw system ($\lambda = 6$) to encompass all possible movements and redundant constraints. For origami patterns where all folds converge to a single common center, a screw system of ($\lambda = 3$) could suffice. However, as demonstrated in this chapter, such an approach would disregard three redundant constraints.

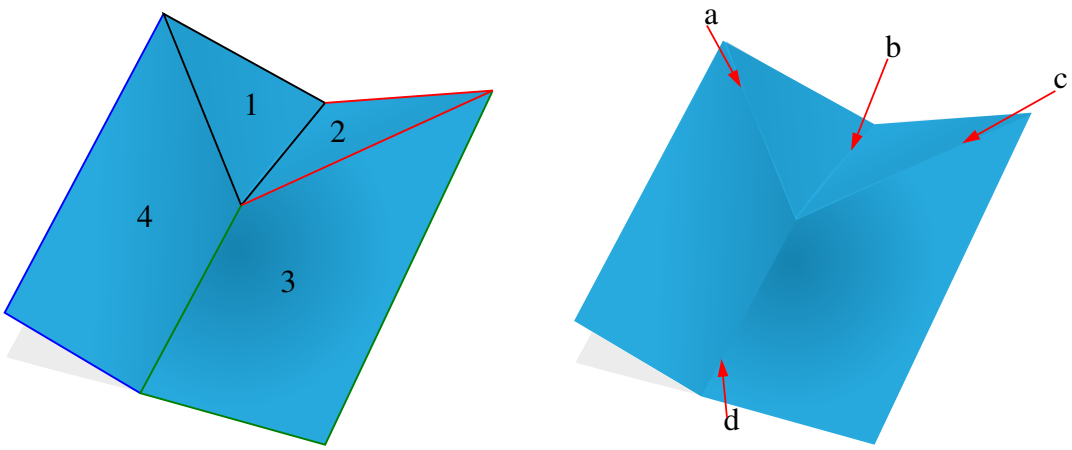

Figure 10 – Degree-4 vertices (D4V) with (a) faces and (b) creases labelled.

The origami of Figure 10 is composed of 4 facets ($n = 4$), named as shown in Figure 10a, while the number of folds within pattern is 4 ($j = 4$). In theory, a fold in origami has the same behavior as a revolution joint (BROWN et al., 2022), consequently, the couplings are all direct, of the rotational type and named as shown in Figure 10b. The origami D4V was analyzed in different configurations, which will be discuted in the next sections.

3.1 UNFOLDED ORIGAMI

The initial analysis focuses on the D4V origami in its fully unfolded configuration. This section establishes the schematic, structural, and graph representations of the origami and systematically applies Davies' method.

3.1.1 Origami representations

The initial analysis focuses on the D4V origami in its fully unfolded configuration. This section establishes the schematic, structural, and graph representations of the origami and systematically applies Davies' method.

3.1.1.1 Schematic Representation of D4V Origami

The schematic representation of the origami is depicted in Figure 11. This figure delineates the topology and geometry of the folding pattern alongside the O_{xyz} coordinate system. The origin of O_{xyz} is positioned at the origami vertex depicted in Figure 11a and at the spherical center of the mechanism shown in Figure 11b. It can be observed that the origami depicted in Figure 11a is equivalent to the spherical mechanism shown in Figure 11b. To facilitate comprehension, both the origami faces and the spherical mechanism links are color-coded consistently. Additionally, folds and joints have been identified with the same purpose of visual clarity. The O_z coordinate axis is oriented perpendicular to the origami's ground plane, defined as the plane containing the origami's fold pattern when completely unfolded. (WILCOX, 2014).

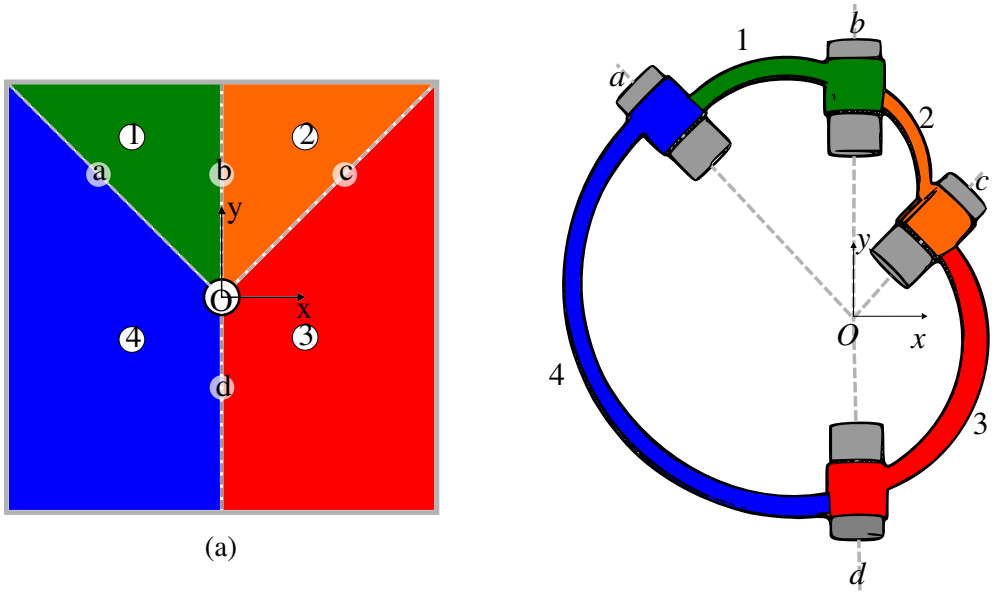

Figure 11 – Inertial system O_{xyz} and schematic representation of: (a) Origami of vertex of degree 4 and (b) Spherical four-bar mechanism.

3.1.1.2 Structural representation

The structural representation identifies the types of links within the coupling network. Binary links are represented by lines, while links connected to more than two links are depicted as polygons. The number of vertices in each polygon corresponds to the number of kinematic pair elements in the link (MARTINS; MURAI, 2020). The Figure 12 presents the structural representation of the D4V origami.

3.1.1.3 Coupling graph

The *coupling graph* G_C is derived from the coupling network. Links are represented as vertices, and direct kinematic pairs as edges. (MARTINS; MURAI, 2020). The coupling graph

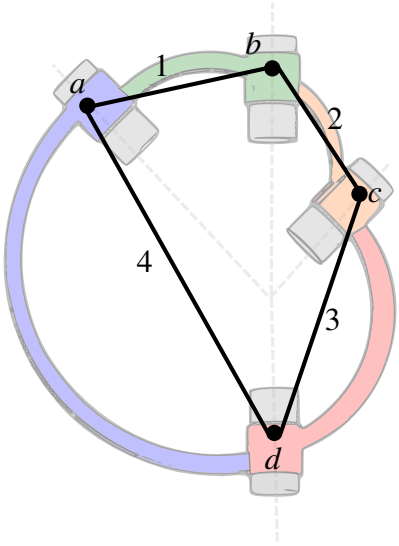

Figure 12 – Structural representation of spherical mechanism equivalent to D4V origami.

G_C is a digraph with edges oriented from minor vertices to major vertices (CAZANGI et al., 2008). Figure 13 illustrates the coupling graph G_C of the D4V origami.

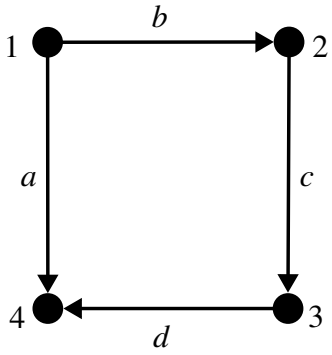

Figure 13 – Origami D4V coupling graph.

3.1.2 Kinematics: Degree 4 vertex origami

This section examines the kinematics of the fully deployed D4V origami, including coupling characteristics, motion graph construction, circuit matrix analysis, twist, motion matrix, and redundant constraints.

3.1.2.1 Coupling characteristics

The analysis requires the following data for twist elaboration and motion graph G_M construction: the *direction unit vector* $\vec{S}^M$, *vector position* $\vec{S}_0$ relative to the origin O_{xyz}, and pitch h^M. The motion graph necessitates the unitary motions f_i of each joint. All kinematic pairs in the origami are of the rotational type.

The kinematic pairs b and d, have twist axes parallel to the O_y axis, while the joints a and c have components on both O_x and O_y axes. The Figure 14 illustrates the $\vec{S}_0$ position vectors of the screw and the joint motions.

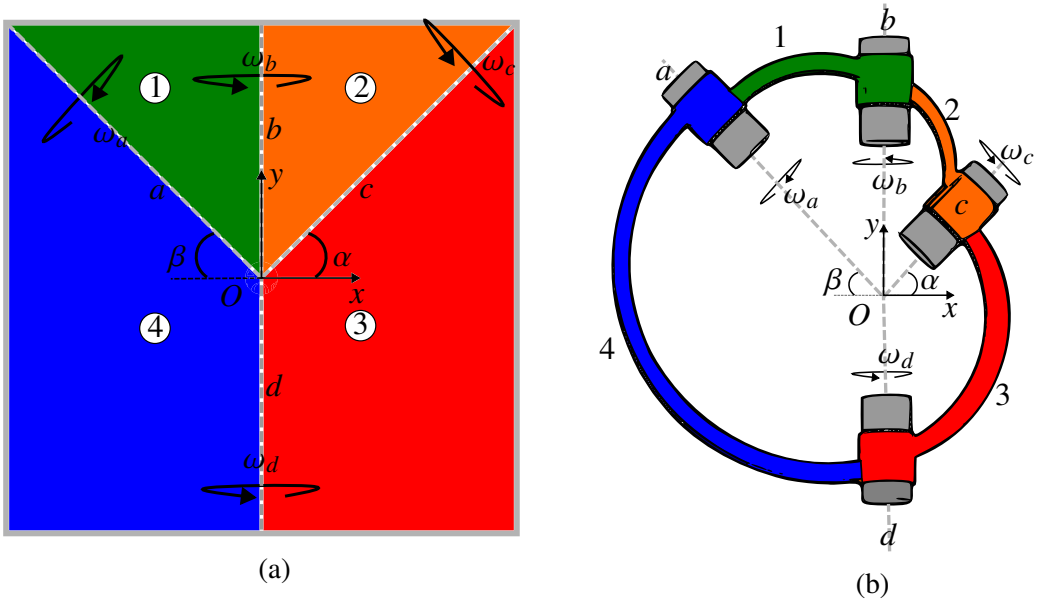

Figure 14 – Position vectors ($\vec{S}_0$) and respective motions in: (a) Origami D4V and (b) spherical four-bar mechanism.

All the joints of this kinematic chain are revolute. These joints have the characteristic that their mobility in space is $f = 1$, allowing only a rotation. Therefore, the unit direction vectors for the twists of each coupling are:

$$\vec{S}_a^M = \begin{Bmatrix} \cos\beta \\ -\sin\beta \\ 0 \end{Bmatrix} \quad ; \quad \vec{S}_y^M = \begin{Bmatrix} 0 \\ 1 \\ 0 \end{Bmatrix} \quad ; \quad \vec{S}_c^M = \begin{Bmatrix} -\cos\alpha \\ -\sin\alpha \\ 0 \end{Bmatrix} \tag{20}$$

where the subscripts a and c denote the direction of couplings a and c, respectively, while the subscript y indicates the direction of couplings along this axis.

The position vectors of the twists of the kinematic pairs are taken from the origin O_{xyz} to a point passing through the axis of the twists, therefore the position vector for all couplings is:

$$\vec{S}_{0_i} = \begin{Bmatrix} 0 \\ 0 \\ 0 \end{Bmatrix} \quad \text{for i = a, b, c and d} \tag{21}$$

For the D4V origami and the spherical 4-bar mechanism, the position vectors are as shown in Equation (21), since all twists pass through the origin O_{xyz}. Moreover, the *pitch* of the screws is $h^M = 0$ since there is pure rotation.

3.1.2.2 Motion Graph

Once the geometry and topology of the mechanism are known, the motion graph G_M shown in Figure 15 can be constructed. This is achieved by replacing the edges of the coupling graph G_C shown in Figure 13 by f_i edges in series, where $i = a, b, c, d$.

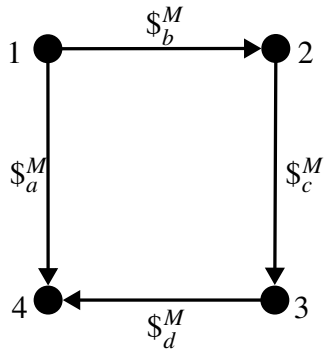

Figure 15 – Motion graph G_M of the origami D4V.

In this case, the graphs G_C and G_M are identical, because all kinematic pairs possess a single unitary motion ($f = 1$). Therefore, the gross degree of freedom (F) is:

$$F = \sum_{i=1}^{4} f_i = 1 + 1 + 1 + 1 = 4 \tag{22}$$

3.1.2.3 Circuit matrix

The next step is to determine the circuit matrix ($B_{M(\nu \times F)}$). For this, it is necessary to identify the number of independent loops (ν) contained in the origami. This can be done visually on the basis of Figure 15 or by using Euler's equation (Equation (23)).

$$\nu - 1 = j - n \tag{23}$$

Clearing ν:

$$\nu = j - n + 1 = 4 - 4 + 1 = 1 \tag{24}$$

There is only one independent loop in G_M graph of the origami D4V. However, for topologically more complex origami, it is important to perform this calculation.

Knowing the number of independent circuits, the spanning tree is determined. In this case, the edges *b, c and d* were selected as branches, identified in blue color in Figure 16, while edge a is the chord, represented by a dashed line in green color. The fundamental circuit is identified in red color, it carries the name and the direction of rotation of the chord.

From the Figure 16, we obtain the circuit matrix $B_{M(\nu \times F)} = [B_{i,j}]$, attending to the considerations below:

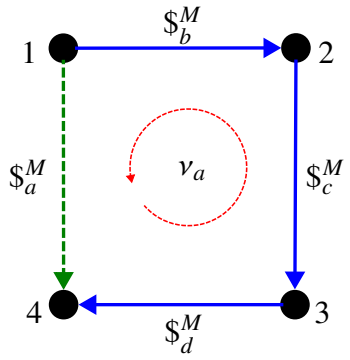

Figure 16 – D4V origami spanning tree and F-circuit.

$$B_{i,j} = \begin{cases} 1 \text{ if it belongs to the circuit-f } \nu_i \text{ and has the same direction as the chord,} \\ -1 \text{ if it belongs to circuit-f } \nu_i \text{ and has opposite direction to the chord,} \\ 0 \text{ if it does not belong to the circuit.} \end{cases}$$

Therefore, the circuit matrix is as shown in Equation (25).

$$[B_M]_{\nu \times F} = [B_M]_{1\times 4} = \begin{matrix} a & b & c & d \\ \left[1 \quad -1 \quad -1 \quad -1\right] & \nu_a \\ 1\times 4 \end{matrix} \tag{25}$$

The line of the matrix represents the fundamental circuit established by chord a, while the columns represent the edges (*a, b, c and d*).

3.1.2.4 Twist construction

Knowing the geometrical characteristics of the kinematic pairs, the twists are constructed using Equation (1). Subsequently, we replace the direction vectors from Equation (20) and the position vectors from Equation (21) into Equation (1) to obtain the twists of the kinematic pairs.

$$\$_a^M = \begin{pmatrix} \omega_a \cos\beta \\ -\omega_a \sin\beta \\ 0 \\ \cdots \\ 0 \\ 0 \\ 0 \end{pmatrix}; \quad \$_b^M = \begin{pmatrix} 0 \\ -\omega_b \\ 0 \\ \cdots \\ 0 \\ 0 \\ 0 \end{pmatrix}; \quad \$_c^M = \begin{pmatrix} -\omega_c \cos\alpha \\ -\omega_c \sin\alpha \\ 0 \\ \cdots \\ 0 \\ 0 \\ 0 \end{pmatrix}; \quad \$_d^M = \begin{pmatrix} 0 \\ \omega_d \\ 0 \\ \cdots \\ 0 \\ 0 \\ 0 \end{pmatrix} \tag{26}$$

In order to determine the screw system, a screw system with order $\lambda = 6$ will be considered. Therefore, the action circuit can be represented by a circuit of actions on a coordinate axis:

$$\$^a = \begin{pmatrix} R \\ S \\ T \\ \cdots \\ U \\ V \\ W \end{pmatrix}_{(6\times1)} \tag{27}$$

where all 6 actions are unknown.

3.1.2.5 Motion Matrix

The motion matrix $[M_D]_{\lambda\times F}$ of the D4V origami in fully opened state is shown in Equation (28).

$$[M_D]_{6\times4} = \begin{bmatrix} \omega_a\cos\beta & 0 & -\omega_c\cos\alpha & 0 \\ -\omega_a\sin\beta & -\omega_b & -\omega_c\sin\alpha & \omega_d \\ 0 & 0 & 0 & 0 \\ 0 & 0 & 0 & 0 \\ 0 & 0 & 0 & 0 \\ 0 & 0 & 0 & 0 \end{bmatrix}_{6\times4} \tag{28}$$

where the columns correspond to the twists $\$_a^M, \$_b^M, \$_c^M, \$_d^M$, respectively.

By separating the magnitudes of the twists, it is possible to obtain the unit motions matrix $[\hat{M}_D]_{\lambda\times F}$:

$$\left[\hat{M}_D\right]_{6\times4} = \begin{bmatrix} \cos\beta & 0 & -\cos\alpha & 0 \\ -\sin\beta & -1 & -\sin\alpha & 1 \\ 0 & 0 & 0 & 0 \\ 0 & 0 & 0 & 0 \\ 0 & 0 & 0 & 0 \\ 0 & 0 & 0 & 0 \end{bmatrix}_{6\times4} \tag{29}$$

where the columns are the normalized screw $\hat{\$}_a^M, \hat{\$}_b^M, \hat{\$}_c^M, \hat{\$}_d^M$.

On the other hand, the magnitude vector of the motions $\{\vec{\psi}\}_{F\times1}$ Equation (30) is formed by:

$$\{\vec{\psi}\}_{4\times1} = \begin{Bmatrix} \omega_a \\ \omega_b \\ \omega_c \\ \omega_d \end{Bmatrix}_{4\times1} \tag{30}$$

Thus, we have the kinematic variables of the problem.

3.1.3 Network unit motion matrix

The next step is to regroup the topological and geometrical information into a single mathematical element, the network unit motion matrix $[\hat{M}_N]_{\lambda.l\times F}$. This is obtained by inserting the information from the motion matrix $[\hat{M}_D]_{\lambda\times F}$ into the circuit matrix $B_M(\nu\times F)$. As shown in Equation (31).

$$\left[\hat{M}_N\right]_{6\times4} = \begin{bmatrix} \cos\beta & 0 & \cos\alpha & 0 \\ -\sin\beta & 1 & \sin\alpha & -1 \\ 0 & 0 & 0 & 0 \\ 0 & 0 & 0 & 0 \\ 0 & 0 & 0 & 0 \\ 0 & 0 & 0 & 0 \end{bmatrix}_{6\times4} \tag{31}$$

3.1.4 System of kinematic equations

Kirchhoff's circuit laws are applied, as shown in Equation (3), resulting in a system of equations for the kinematics of the origami D4V, presented in Equation (32).

$$\left[\hat{M}_N\right]_{6\times4}\{\vec{\psi}\}_{4\times1} = \{\overrightarrow{0}\}_{6\times1} \quad \therefore$$

$$\begin{bmatrix} \cos\beta & 0 & \cos\alpha & 0 \\ -\sin\beta & 1 & \sin\alpha & -1 \\ 0 & 0 & 0 & 0 \\ 0 & 0 & 0 & 0 \\ 0 & 0 & 0 & 0 \\ 0 & 0 & 0 & 0 \end{bmatrix}_{6\times4} \begin{Bmatrix} \omega_a \\ \omega_b \\ \omega_c \\ \omega_d \end{Bmatrix}_{4\times1} = \begin{Bmatrix} 0 \\ 0 \\ 0 \\ 0 \\ 0 \\ 0 \end{Bmatrix}_{6\times1} \tag{32}$$

The rank of matrix $\left[\hat{M}_{\mathbf{N}}\right]_{6,4}$ is $m = 2$ and thus Equation (6) state that the origami of Figure 1 has $F_N = 2$.

Therefore, replacing the matrix of Equation (29) in Equation (8) yields a homogeneous linear system with $F = 4$ equations and $\lambda = 6$ unknowns. Thus, the Equation (8) for the origami D4V can be written as:

$$\begin{bmatrix} \cos\beta & -\sin\beta & 0 & 0 & 0 & 0 \\ 0 & 1 & 0 & 0 & 0 & 0 \\ \cos\alpha & \sin\alpha & 0 & 0 & 0 & 0 \\ 0 & -1 & 0 & 0 & 0 & 0 \end{bmatrix}_{4\times6} \begin{bmatrix} R \\ S \\ T \\ \cdots \\ U \\ V \\ W \end{bmatrix}_{6\times1} = \begin{bmatrix} 0 \\ 0 \\ 0 \\ 0 \end{bmatrix}_{4\times1} \tag{33}$$

By determining the rank m of the matrix $[\hat{M}_N^T]$ and applying the Equation (11), the number of redundant constraints of the origami can be calculated.

The rank of $[\hat{M}_N^T]$ was 2 ($m = 2$), then applying the Equation (11), it can be said that the origami D4V has $C_N = 6 \cdot 1 - 2 = 4$ redundant constraints.

The Reduced row echelon form (rref) of Equation (33) is shown in Equation (34):

$$\begin{bmatrix} 1 & 0 & 0 & 0 & 0 & 0 \\ 0 & 1 & 0 & 0 & 0 & 0 \\ 0 & 0 & 0 & 0 & 0 & 0 \\ 0 & 0 & 0 & 0 & 0 & 0 \end{bmatrix}_{4\times6} \begin{bmatrix} R \\ S \\ T \\ \cdots \\ U \\ V \\ W \end{bmatrix}_{6\times1} = \begin{bmatrix} 0 \\ 0 \\ 0 \\ 0 \end{bmatrix}_{4\times1} \tag{34}$$

According to Equation (34) columns 1 and 2 are pivot columns and columns 3, 4, 5 and 6 are free columns. Thus, T, U, V and W are the free variables of the action circuit generated by the $C_N = 4$ redundant constraints:

$$\hat{\$}^a = \begin{bmatrix} 0 & 0 & T & U & V & W \end{bmatrix}^T \tag{35}$$

The analysis of Equation (34) shows that the order of the screw system is $\lambda = 2$ for the kinematics (since the reduced row echelon form of $\left[\hat{M}_N\right]_{6\times4}$ has only two pivot columns) and $\lambda = 4$ for the statics, as there are four free variables. These results do not agree with the order of the screw system of the spherical mechanism in space, which is $\lambda = 3$ for both kinematics and statics (HUNT, 1978). Therefore, it is presumed that the origami is in a singular position, corresponding to its unfolded state. For this reason, the origami D4V was analyzed in different configurations, which will be discussed in detail in the next sections.

3.2 PARTIALLY FOLDED ORIGAMI

The same procedure applied in the previous section to compute the mobility and the redundant constraints of the D4V origami in its unfolded state is applied in other two different configurations: in partially folded state and fully folded state.

Davies' method will be applied to the D4V origami in the position shown in Figure 17. A reference coordinate system O_{xyz} is attached again to the origami vertex.

The creases d and b are parallel to the O_y axis, while the crease a is parallel to the O_z axis, and the crease c has components on axes O_x and O_z. Thus, the unit direction vector of the joints is:

$$\vec{S}_c^M = \begin{Bmatrix} \sin\theta \\ 0 \\ \cos\theta \end{Bmatrix} \quad ; \quad \vec{S}_y^M = \begin{Bmatrix} 0 \\ 1 \\ 0 \end{Bmatrix} \quad ; \quad \vec{S}_z^M = \begin{Bmatrix} 0 \\ 0 \\ 1 \end{Bmatrix} \tag{36}$$

The position vectors of the kinematic pairs are maintained as in Equation (21), and the screw pitch is $h^M = 0$ because they are pure rotational motions.

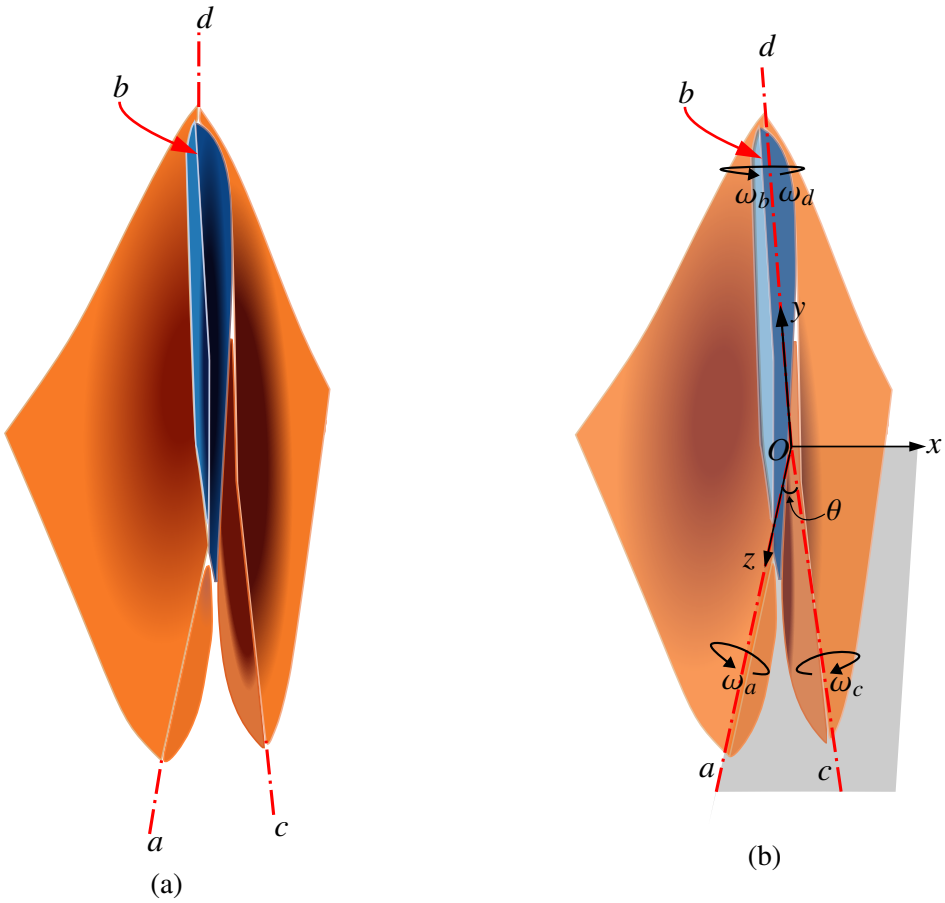

Figure 17 – Partially folded Origami D4V

In addition, the motion graph, the number of independent circuits, and the circuit matrix do not change with respect to the unfolded D4V origami.

Consequently, the creases screws of the folded origami are shown in Equation (37):

$$\$_a^M = \begin{pmatrix} 0 \\ 0 \\ \omega_a \\ \cdots \\ 0 \\ 0 \\ 0 \end{pmatrix}; \quad \$_b^M = \begin{pmatrix} 0 \\ \omega_b \\ 0 \\ \cdots \\ 0 \\ 0 \\ 0 \end{pmatrix}; \quad \$_c^M = \begin{pmatrix} \omega_c \sin\theta \\ 0 \\ \omega_c \cos\theta \\ \cdots \\ 0 \\ 0 \\ 0 \end{pmatrix}; \quad \$_d^M = \begin{pmatrix} 0 \\ \omega_d \\ 0 \\ \cdots \\ 0 \\ 0 \\ 0 \end{pmatrix} \tag{37}$$

For this case, the coordinates u, v, and w (the last three lines of the twists) are null, showing that the motions associated with the origami are restricted to the coordinates r, s, and t, representing rotations around the x, y and z axes, corresponding to to the spherical screw system, whose order is 3 ($\lambda = 3$) (HUNT, 1978).

The motion matrix $[M_D]_{\lambda \times F}$ of the D4V origami in partially folded state is shown in Equation (38).

$$[M_D]_{6\times4} = \begin{bmatrix} 0 & 0 & \omega_c \sin\theta & 0 \\ 0 & \omega_b & 0 & \omega_d \\ \omega_a & 0 & \omega_c \cos\theta & 0 \\ 0 & 0 & 0 & 0 \\ 0 & 0 & 0 & 0 \\ 0 & 0 & 0 & 0 \end{bmatrix}_{6\times4} \tag{38}$$

where the columns correspond to the twists $\$_a^M, \$_b^M, \$_c^M, \$_d^M$, respectively.

By separating the magnitudes of the twists, it is possible to obtain the unit motion matrix $[\hat{M}_D]_{\lambda\times F}$:

$$\left[\hat{M}_D\right]_{6\times4} = \begin{bmatrix} 0 & 0 & \sin\theta & 0 \\ 0 & 1 & 0 & 1 \\ 1 & 0 & \cos\theta & 0 \\ 0 & 0 & 0 & 0 \\ 0 & 0 & 0 & 0 \\ 0 & 0 & 0 & 0 \end{bmatrix}_{6\times4} \tag{39}$$

where the columns are the normalized screw $\hat{\$}_a^M, \hat{\$}_b^M, \hat{\$}_c^M, \hat{\$}_d^M$.

Thus, the network unit motion matrix can be writte as:

$$\left[\hat{M}_N\right]_{6\times4} = \begin{bmatrix} 0 & 0 & -\sin\theta & 0 \\ 0 & -1 & 0 & -1 \\ 1 & 0 & -\cos\theta & 0 \\ 0 & 0 & 0 & 0 \\ 0 & 0 & 0 & 0 \\ 0 & 0 & 0 & 0 \end{bmatrix}_{6\times4} \tag{40}$$

$$\left[\hat{M}_N\right]_{6\times4} \{\vec{\psi}\}_{4\times1} = \{\overrightarrow{0}\}_{6\times1} \quad \therefore$$

$$\begin{bmatrix} 0 & 0 & -\sin\theta & 0 \\ 0 & -1 & 0 & -1 \\ 1 & 0 & -\cos\theta & 0 \\ 0 & 0 & 0 & 0 \\ 0 & 0 & 0 & 0 \\ 0 & 0 & 0 & 0 \end{bmatrix}_{6\times4} \begin{Bmatrix} \omega_a \\ \omega_b \\ \omega_c \\ \omega_d \end{Bmatrix}_{4\times1} = \begin{Bmatrix} 0 \\ 0 \\ 0 \\ 0 \\ 0 \\ 0 \end{Bmatrix}_{6\times1} \tag{41}$$

The rank of the matrix $[\hat{M}_N]_{6\times4}$ shown in Equation (32) is $m = 3$. Consequently, the mobility for this configuration using Equation (6) is $F_N = 1$. Therefore, only one unitary motion (primary variable) is necessary to describe the behavior of the other m unitary motions (secondary variables) of the system.

Also, the number of redundant origami constraints can be determined by applying the Equation (8). In this case, we work with spatial screw system $\lambda = 6$ and consequently the Equation (8) can be written as:

$$\begin{bmatrix} 0 & 0 & 1 & 0 & 0 & 0 \\ 0 & -1 & 0 & 0 & 0 & 0 \\ -\sin\theta & 0 & -\cos\theta & 0 & 0 & 0 \\ 0 & -1 & 0 & 0 & 0 & 0 \end{bmatrix}_{4\times6} \begin{bmatrix} R \\ S \\ T \\ \cdots \\ U \\ V \\ W \end{bmatrix}_{6\times1} = \begin{bmatrix} 0 \\ 0 \\ 0 \\ 0 \end{bmatrix}_{4\times1} \tag{42}$$

By finding the rank $m = 3$ of the $[\hat{M}_N^T]$ matrix of the Equation (42), the number of redundant constraints of the origami were computed by applying the Equation (11). For this origami, in the partially folded configuration, the number of redundant constraints were $C_N = 3$. On the other hand, the Equation (42) can be rearranged in this reduced echelon form:

$$\begin{bmatrix} 1 & 0 & 0 & 0 & 0 & 0 \\ 0 & 1 & 0 & 0 & 0 & 0 \\ 0 & 0 & 1 & 0 & 0 & 0 \\ 0 & 0 & 0 & 0 & 0 & 0 \end{bmatrix}_{4\times6} \begin{bmatrix} R \\ S \\ T \\ \cdots \\ U \\ V \\ W \end{bmatrix}_{6\times1} = \begin{bmatrix} 0 \\ 0 \\ 0 \\ 0 \end{bmatrix}_{4\times1} \tag{43}$$

Then columns 1, 2 and 3 are pivot columns and columns 4, 5 and 6 are free columns. According to Equation (43), *U, V and W* are the free variables of the action circuit generated by the $C_N = 3$ redundant constraints:

$$\hat{\$}^a = \begin{bmatrix} 0 & 0 & 0 & U & V & W \end{bmatrix}^T \tag{44}$$

It is important to note that U, V, and W represent the forces along the x, y, and z axes, respectively. The analysis of Equation (43) shows that the order of the screw system is $\lambda = 3$ for the kinematics (since the reduced row echelon form of $\left[\hat{M}_N\right]_{6\times4}$ has three pivot columns) and $\lambda = 3$ for the statics, as there are three free variables. These results are in accordance with the order of the screw system of the spherical mechanism in space (HUNT, 1978).

3.3 FOLDED ORIGAMI

Additionally, the Origami D4V is analyzed in the configuration depicted in Figure 18b(b). i.e. in fully folded state. This is achieved by reducning the angle θ of Figure 17b until it reaches zero ($\theta = 0$). In this representation, folds b and d are parallel to the y axis, while folds a and c are parallel to the z axis.

$$\vec{S}_y^M = \left\{ \begin{array}{c} 0 \\ 1 \\ 0 \end{array} \right\} \quad ; \quad \vec{S}_z^M = \left\{ \begin{array}{c} 0 \\ 0 \\ 1 \end{array} \right\} \tag{45}$$

The position vector, the screw pitch, the motion graph, the number of independent circuits, and the circuit matrix do not change in relation to the Equation (21) and the unfolded D4V origami.

On the other hand, the fully folded origami twist are:

$$\$_a^M = \begin{pmatrix} 0 \\ 0 \\ \omega_a \\ \cdots \\ 0 \\ 0 \\ 0 \end{pmatrix}; \quad \$_b^M = \begin{pmatrix} 0 \\ \omega_b \\ 0 \\ \cdots \\ 0 \\ 0 \\ 0 \end{pmatrix}; \quad \$_c^M = \begin{pmatrix} 0 \\ 0 \\ \omega_c \\ \cdots \\ 0 \\ 0 \\ 0 \end{pmatrix}; \quad \$_d^M = \begin{pmatrix} 0 \\ \omega_d \\ 0 \\ \cdots \\ 0 \\ 0 \\ 0 \end{pmatrix} \tag{46}$$

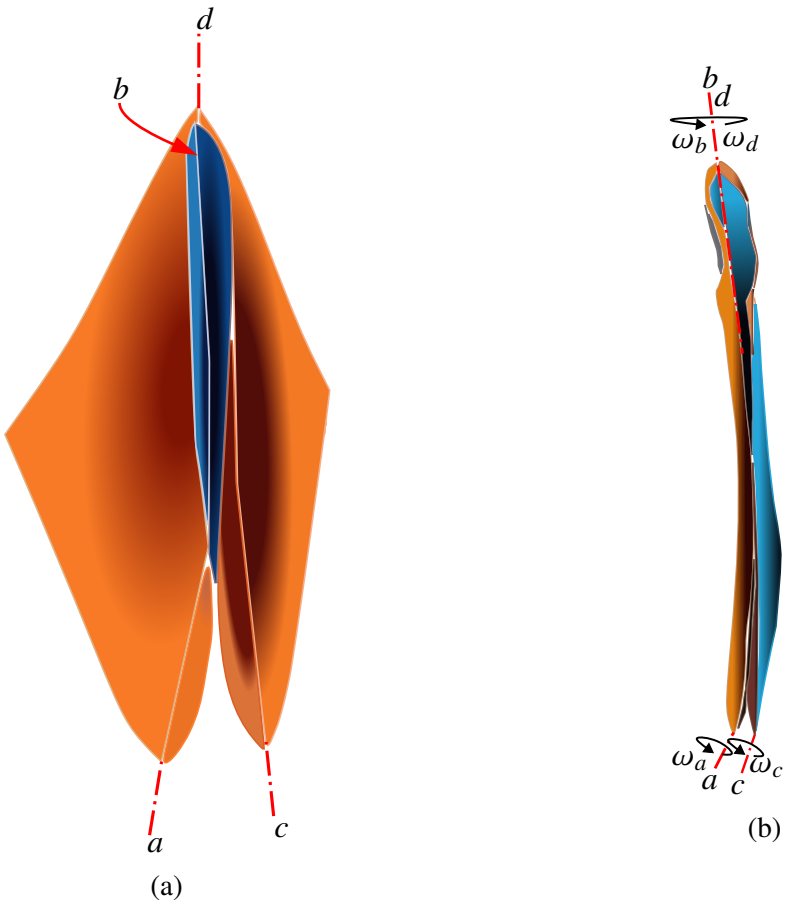

Figure 18 – Origami D4V: (a) Partially folded e (b) fully folded

The motion matrix $[M_D]_{\lambda \times F}$ of the fully folded D4V origami is shown in Equation (47):

$$[M_D]_{6\times4} = \begin{bmatrix} 0 & 0 & 0 & 0 \\ 0 & \omega_b & 0 & \omega_d \\ \omega_a & 0 & \omega_c & 0 \\ 0 & 0 & 0 & 0 \\ 0 & 0 & 0 & 0 \\ 0 & 0 & 0 & 0 \end{bmatrix}_{6\times4} \tag{47}$$

where the columns correspond to the twists $\$_a^M, \$_b^M, \$_c^M, \$_d^M$, respectively.

By separating the magnitudes of the twists, it is possible to obtain the unit motion matrix $[\hat{M}_D]_{\lambda\times F}$:

$$\left[\hat{M}_D\right]_{3\times4} = \begin{bmatrix} 0 & 0 & 0 & 0 \\ 0 & 1 & 0 & 1 \\ 1 & 0 & 1 & 0 \\ 0 & 0 & 0 & 0 \\ 0 & 0 & 0 & 0 \\ 0 & 0 & 0 & 0 \end{bmatrix}_{3\times4} \tag{48}$$

The network unit motion matrix $\left[\hat{M}_N\right]_{6\times4}$ is:

$$\left[\hat{M}_N\right]_{6\times4} = \begin{bmatrix} 0 & 0 & 0 & 0 \\ 0 & -1 & 0 & -1 \\ 1 & 0 & -1 & 0 \\ 0 & 0 & 0 & 0 \\ 0 & 0 & 0 & 0 \\ 0 & 0 & 0 & 0 \end{bmatrix}_{6\times4} \tag{49}$$

From the Equation (49), we determine the *rank m* of the matrix $[\hat{M}_N]_{\lambda\times F}$ and subsequently calculate the mobility of the origami, resulting in $F_N = F - m = 4 - 2 = 2$.

Subsequently, the number of redundant constraints of the origami is calculated by applying the Equation (8), giving that the rank of $[\hat{M}_N^T]$ was $m = 2$ and therefore, this configuration has $C_N = 4$. The matrix $\left[\hat{M}_N^T\right]_{6\times4}$ is rearranged in reduced row echelon form, shown in Equation (50):

$$\begin{bmatrix} 0 & 1 & 0 & 0 & 0 & 0 \\ 0 & 0 & 1 & 0 & 0 & 0 \\ 0 & 0 & 0 & 0 & 0 & 0 \\ 0 & 0 & 0 & 0 & 0 & 0 \end{bmatrix}_{4\times6} \begin{bmatrix} R \\ S \\ T \\ \cdots \\ U \\ V \\ W \end{bmatrix}_{6\times1} = \begin{bmatrix} 0 \\ 0 \\ 0 \\ 0 \end{bmatrix}_{4\times1} \tag{50}$$

According to Equation (50), columns 2 and 3 are pivot columns, while columns 1, 4, 5, and 6 are free columns. Therefore, R, U, V, and W are the free variables of the action circuit generated by the $C_N = 4$ redundant constraints:

$$\hat{\$}^a = \begin{bmatrix} R & 0 & 0 & U & V & W \end{bmatrix}^T \tag{51}$$

This result is similar to the one obtained when the D4V origami is in unfolded state: the number of pivot and free columns diverge from the order of the screw system that describes the kinematics and statics of a spherical mechanism. Therefore, this configuration corresponds to another singular position of the origami D4V.

4 SINGULARITY ANALYSIS OF MULTICENTER ORIGAMI

This section applies the same analysis to several rectangular multi-loop origami patterns with multiple non-coincident vertices. The order of the screw system used is $\lambda = 6$. Unlike the multi-origami-inspired spherical mechanisms (MOISMs) discussed in subsection 2.3.3, where all vertices coincide at a single point in space, multi-loop origami with multiple non-coincident vertices lack a point where all creases intersect.

When origami structures are partially opened, several important changes occur in their geometric and kinematic properties: (a) Distances between vertices emerge: As the origami unfolds partially, gaps appear between the vertices that were previously coincident in the fully folded state, (b) Non-zero cross products: The separation of vertices leads to a situation where the cross product between the direction vector and the position vector of the folds is no longer zero. This is because the axes of rotation (direction vectors) and the points they pass through (position vectors) are no longer coincident, and (c) Loss of linear independence in motion matrices: The matrices describing the motion of the origami structure cease to have linearly independent rows. This change in the mathematical description reflects the increased complexity of the partially opened state.As a result of these changes, the screw system that describes the origami's motion undergoes a fundamental transformation. Consequently, the screw system ceases to be spherical with order $\lambda = 3$ and becomes a spatial screw system with order $\lambda = 6$.

This section exclusively addresses origamis that meet the "bird's-foot condition" and analyzes them in a partially folded state to avoid singular configurations.

4.1 TWO VERTICES ORIGAMI PATTERN

The first multi-loop origami studied is the two vertices origami pattern shown in Figure 19. It comprises 6 facets ($n = 6$) and 7 folds ($j = 7$).

4.1.1 Schematic Representation of Origami

Figure 20 illustrates the schematic representation of the origami, showing the topology and geometry of the folding pattern and the O_{xyz} coordinate system. The origin O_{xyz} was located at vertex f, noted in Figure 19. In this example, the O_z coordinate axis is perpendicular to the ground plane of the origami (WILCOX, 2014).

4.1.2 Structural representation

Figure 21 depicts the structural representation of the two-vertex origami. It is observed that the kinematic chain of this origami is the Watt chain. Based on the information gathered in chapter 2, and in accordance with Kawasaki's and Maekawa's theorems, we have identified a relationship between the vertices of the origami and the independent circuits of a spherical mechanism. This relationship establishes that the number of independent circuits (ν) of the

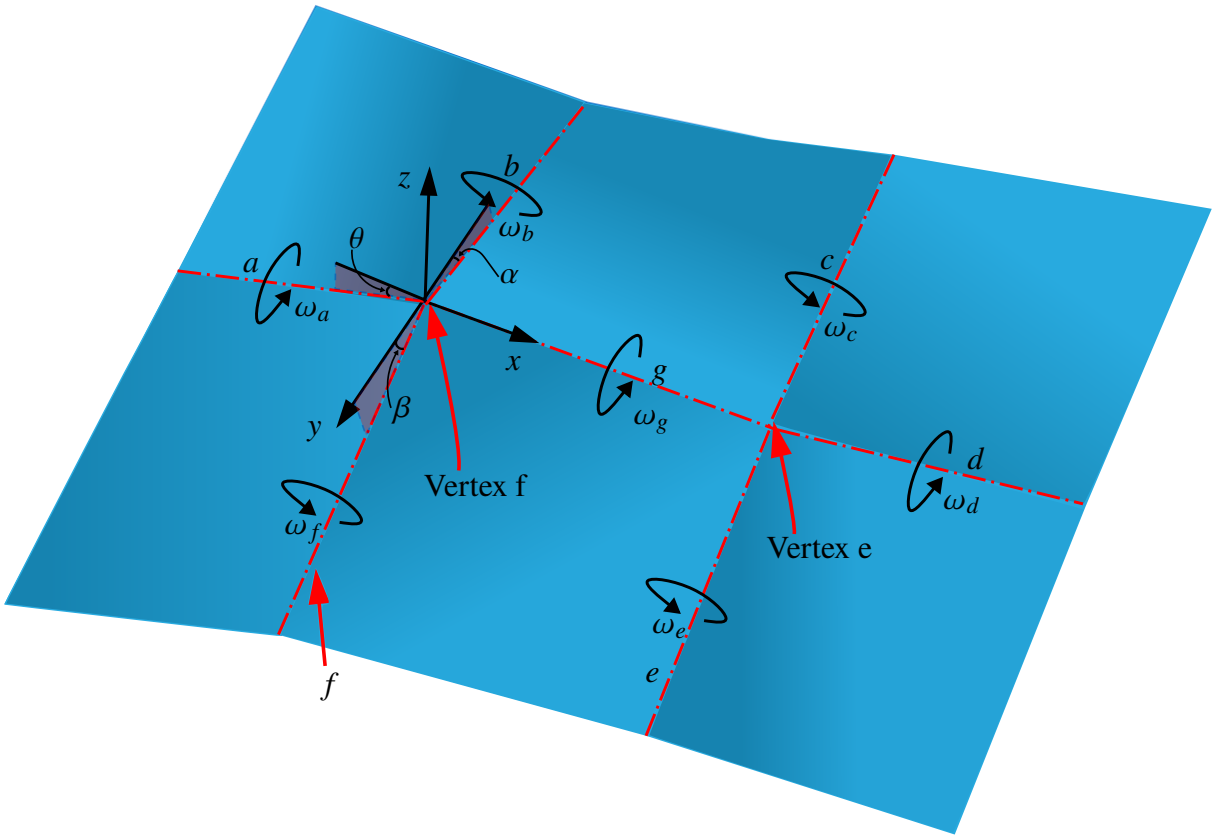

Figure 19 – Two Degree-4 vertices Origami

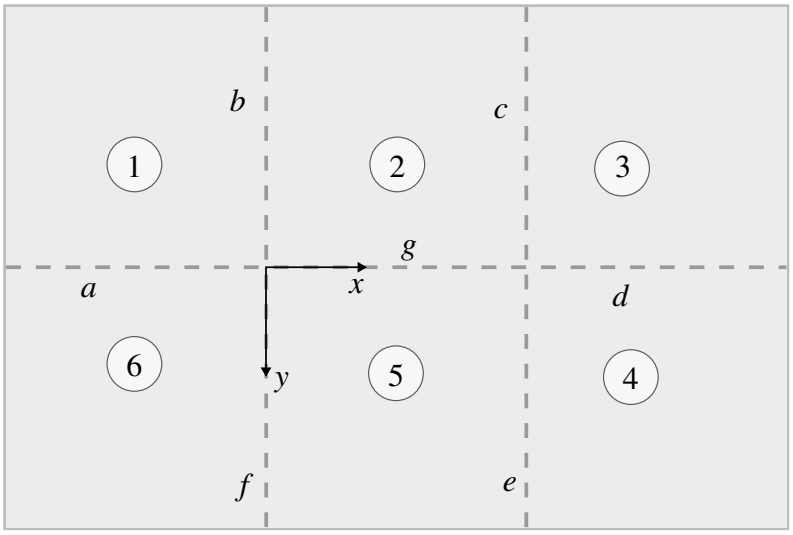

Figure 20 – Squematic representation of Two-D4V origami.

kinematic chain is equal to the number of vertices of the origami. Consequently, this origami has two independent loops (vertices), two ternary links, and four binary links.

4.1.3 Coupling graph

The *coupling graph* G_C is formed from the coupling network. Figure 22 shows the coupling graph G_C of the Two degree-4 origami. The instantaneous kinematic analysis is

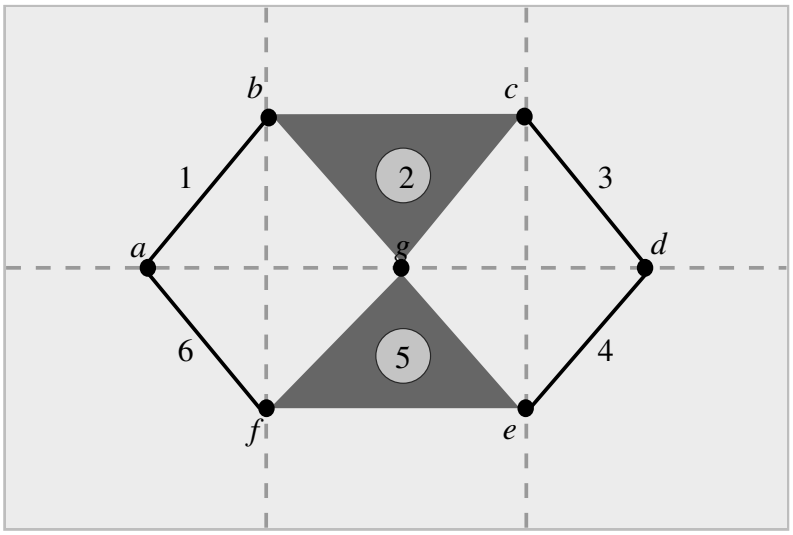

Figure 21 – Structural representation of origami Two-D4V.

performed from this coupling graph.

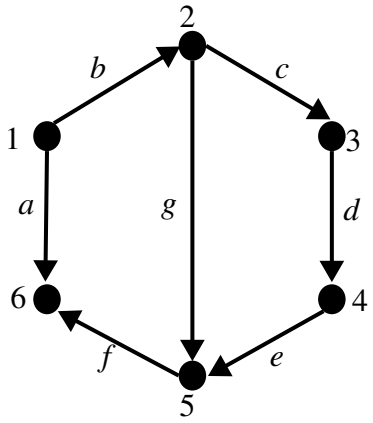

Figure 22 – Coupling graph of two degree-4 vertices Origami .

4.1.4 Coupling characteristics

The kinematic pairs b, c, e, and f have their screw axes lying in the plane composed of the O_y and O_z axes, while the joints a and d have their components along both the O_x and O_z axes. Additionally, the kinematic pair g has its screw axis parallel to the O_x axis, as illustrated in Figure 19. Therefore, the direction vectors of the couplings are as follows:

$$\vec{S}_x^M = \begin{Bmatrix} 1 \\ 0 \\ 0 \end{Bmatrix} \quad ; \quad \vec{S}_{ad}^M = \begin{Bmatrix} \cos\theta \\ \sin\theta \\ 0 \end{Bmatrix} \quad ; \quad \vec{S}_{bc}^M = \begin{Bmatrix} 0 \\ \cos\alpha \\ \sin\alpha \end{Bmatrix} \quad ; \quad \vec{S}_{ef}^M = \begin{Bmatrix} 0 \\ \cos\beta \\ \sin\beta \end{Bmatrix} \tag{52}$$

where the angles α, β, and θ represent the angles between the paper sheet and the coordinate axes, as illustrated in Figure 19. The position vectors of the twist of the kinematic pairs are taken

from the origin O_{xyz} to a point passing through the axis of the twist. Therefore, the position vector for the couplings *a, b, d, f and g* are shown in Equation (53) because all their twists pass through the origin. While for *c and e* the position vector is:

$$\vec{S}_{0_i} = \begin{Bmatrix} 0 \\ 0 \\ 0 \end{Bmatrix} \quad \text{for i= a, b, d, f and g;} \quad \vec{S}_{0_{ii}} = \begin{Bmatrix} x' \\ 0 \\ 0 \end{Bmatrix} \text{for ii= c and e.} \tag{53}$$

where x' represents the distance between vertex f and e, and in this case, $x' = 1$. The $pitch$ of the twist is $h^M = 0$ as they represent pure rotation.

4.1.5 Motion Graph

Once the mechanism's geometry and topology are known, the motion graph G_M shown in Figure 23 can be constructed.

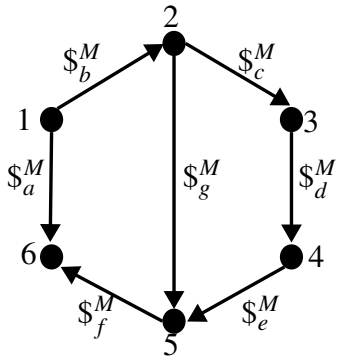

Figure 23 – Motion graph G_M of the two D4V origami.

In this case, the graphs G_C and G_M are identical because all kinematic pairs possess a single unitary motion ($f = 1$). Therefore, the gross degree of freedom (F) is:

$$F = \sum_{i=1}^{7} f_i = 1 + 1 + 1 + 1 + 1 + 1 + 1 = 7 \tag{54}$$

4.1.6 Circuit matrix

The spanning tree is determined by selecting edges *a, b, c, d, and g* as branches (blue color) in Figure 24, and the edges *f and g* as chords (green dashed line) in the same figure. The fundamental circuits are identified in red color, as shown in Figure 24.

From the Figure 24 the circuit matrix is obtained as:

$$[B_M]_{2\times 7} = \begin{array}{c} \begin{matrix} e & f & a & b & c & d & g \end{matrix} \\ \begin{bmatrix} 1 & 0 & 0 & 0 & 1 & 1 & -1 \\ 0 & 1 & -1 & 1 & 0 & 0 & 1 \end{bmatrix} \end{array} \begin{matrix} \nu_e \\ \nu_f \end{matrix} \tag{55}$$

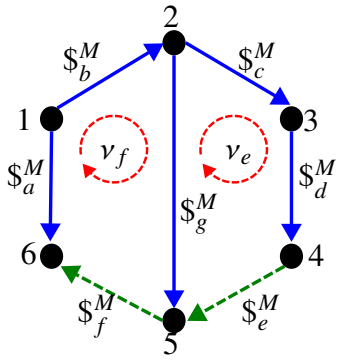

Figure 24 – Two D4V origami spanning tree and fundamental circuits.

4.1.7 Twist´s construction

The twists of the kinematic pairs are shown in Equation (56).

$$\$_a^M = \begin{pmatrix} \omega_a \cos\theta \\ \omega_a \sin\theta \\ 0 \\ \cdots \\ 0 \\ 0 \\ 0 \end{pmatrix}; \quad \$_b^M = \begin{pmatrix} 0 \\ \omega_b \cos\alpha \\ \omega_b \sin\alpha \\ \cdots \\ 0 \\ 0 \\ 0 \end{pmatrix}; \quad \$_c^M = \begin{pmatrix} 0 \\ \omega_c \cos\alpha \\ \omega_c \sin\alpha \\ \cdots \\ 0 \\ -x'\omega_c \sin\alpha \\ x'\omega_c \cos\alpha \end{pmatrix}; \quad \$_d^M = \begin{pmatrix} \omega_d \cos\theta \\ \omega_d \sin\theta \\ 0 \\ \cdots \\ 0 \\ 0 \\ x'\omega_d \sin\theta \end{pmatrix}$$

$$\$_e^M = \begin{pmatrix} 0 \\ \omega_e \cos\beta \\ \omega_e \sin\beta \\ \cdots \\ 0 \\ -x'\omega_e \sin\alpha \\ x'\omega_e \cos\alpha \end{pmatrix}; \quad \$_f^M = \begin{pmatrix} 0 \\ \omega_f \cos\beta \\ \omega_f \sin\beta \\ \cdots \\ 0 \\ 0 \\ 0 \end{pmatrix}; \quad \$_g^M = \begin{pmatrix} \omega_g \\ 0 \\ 0 \\ \cdots \\ 0 \\ 0 \\ 0 \end{pmatrix} \tag{56}$$

4.1.8 Motion Matrix

The Motions matrix $[M_D]_{\lambda \times F}$ gathers all the twists, as shown in Equation (57).

$$[M_D]_{6\times7} = \begin{bmatrix} 0 & 0 & \omega_a\cos\theta & 0 & 0 & \omega_d\cos\theta & \omega_g \\ \omega_e\cos\beta & \omega_f\cos\beta & \omega_a\sin\theta & \omega_b\cos\alpha & \omega_c\cos\alpha & \omega_d\sin\theta & 0 \\ \omega_e\sin\beta & \omega_f\sin\beta & 0 & \omega_b\sin\alpha & \omega_c\sin\alpha & 0 & 0 \\ 0 & 0 & 0 & 0 & 0 & 0 & 0 \\ -x'\omega_e\sin\beta & 0 & 0 & 0 & -x'\omega_c\sin\alpha & 0 & 0 \\ x'\omega_e\cos\beta & 0 & 0 & 0 & x'\omega_c\cos\alpha & x'\omega_d\sin\theta & 0 \end{bmatrix}_{6\times7} \tag{57}$$

By separating the magnitudes of the twists, the motions matrix $[\hat{M}_D]_{\lambda\times F}$ is yield:

$$[M_D]_{6\times7} = \begin{bmatrix} 0 & 0 & \cos\theta & 0 & 0 & \cos\theta & 1 \\ \cos\beta & \cos\beta & \sin\theta & \cos\alpha & \cos\alpha & \sin\theta & 0 \\ \sin\beta & \sin\beta & 0 & \sin\alpha & \sin\alpha & 0 & 0 \\ 0 & 0 & 0 & 0 & 0 & 0 & 0 \\ -x'\sin\beta & 0 & 0 & 0 & -x'\sin\alpha & 0 & 0 \\ x'\cos\beta & 0 & 0 & 0 & x'\cos\alpha & x'\sin\theta & 0 \end{bmatrix}_{6\times7} \tag{58}$$

The magnitude vector of the motions $\{\vec{\psi}\}_{F\times1}$ is shown in Equation (59):

$$\{\vec{\psi}\}_{7\times1} = \begin{Bmatrix} \omega_e \\ \omega_f \\ \omega_a \\ \omega_b \\ \omega_c \\ \omega_d \\ \omega_g \end{Bmatrix}_{7\times1} \tag{59}$$

Thus, we have the kinematic variables of the problem.

4.1.9 Network unit motion matrix

The network unit motion matrix of the two vertices origami $[\hat{M}_N]_{\lambda.\nu\times F}$ is shown in Equation (60).

$$\left[\hat{M}_N\right]_{12\times7} = \begin{bmatrix} 0 & 0 & 0 & 0 & 0 & \cos\theta & -1 \\ \cos\beta & 0 & 0 & 0 & \cos\alpha & \sin\theta & 0 \\ \sin\beta & 0 & 0 & 0 & \sin\alpha & 0 & 0 \\ 0 & 0 & 0 & 0 & 0 & 0 & 0 \\ -x'\sin\beta & 0 & 0 & 0 & -x'\sin\alpha & 0 & 0 \\ x'\cos\beta & 0 & 0 & 0 & x'\cos\alpha & x'\sin\theta & 0 \\ 0 & 0 & -\cos\theta & 0 & 0 & 0 & 1 \\ 0 & \cos\beta & -\sin\theta & \cos\alpha & 0 & 0 & 0 \\ 0 & \sin\beta & 0 & \sin\alpha & 0 & 0 & 0 \\ 0 & 0 & 0 & 0 & 0 & 0 & 0 \\ 0 & 0 & 0 & 0 & 0 & 0 & 0 \\ 0 & 0 & 0 & 0 & 0 & 0 & 0 \end{bmatrix}_{12\times7} \tag{60}$$

4.1.10 System of kinematics equations

Kirchhoff's circuit law is applied, resulting in a system of equations of the kinematics of the two-D4V origami, shown in Equation (61).

$$\left[\hat{M}_N\right]_{12\times7}\{\vec{\Phi}\}_{7\times1} = \{\overrightarrow{0}\}_{12\times1} \quad \therefore$$

$$\begin{bmatrix} 0 & 0 & 0 & 0 & 0 & \cos\theta & -1 \\ \cos\beta & 0 & 0 & 0 & \cos\alpha & \sin\theta & 0 \\ \sin\beta & 0 & 0 & 0 & \sin\alpha & 0 & 0 \\ 0 & 0 & 0 & 0 & 0 & 0 & 0 \\ -x'\sin\beta & 0 & 0 & 0 & -x'\sin\alpha & 0 & 0 \\ x'\cos\beta & 0 & 0 & 0 & x'\cos\alpha & x'\sin\theta & 0 \\ 0 & 0 & -\cos\theta & 0 & 0 & 0 & 1 \\ 0 & \cos\beta & -\sin\theta & \cos\alpha & 0 & 0 & 0 \\ 0 & \sin\beta & 0 & \sin\alpha & 0 & 0 & 0 \\ 0 & 0 & 0 & 0 & 0 & 0 & 0 \\ 0 & 0 & 0 & 0 & 0 & 0 & 0 \\ 0 & 0 & 0 & 0 & 0 & 0 & 0 \end{bmatrix}_{12\times7} \begin{Bmatrix} \omega_e \\ \omega_f \\ \omega_a \\ \omega_b \\ \omega_c \\ \omega_d \\ \omega_g \end{Bmatrix}_{7\times1} = \begin{Bmatrix} 0 \\ 0 \\ 0 \\ 0 \\ 0 \\ 0 \\ 0 \\ 0 \\ 0 \\ 0 \\ 0 \\ 0 \end{Bmatrix}_{12\times1} \tag{61}$$

The rank m of the $\hat{M}_N$ matrix was calculated, resulting in m=6, thus, using the Equation (6) the mobility is determined to be $F_N = 1$.

Also, the number of redundant origami constraints can be determined by applying the Equation (8). In this case, we work with spatial screw system $\lambda = 6$ and consequently the Equation (8) can be written as:

$$\left[\hat{M}_N^T\right]_{F\times\lambda.\nu}\begin{bmatrix} R_1 \\ S_1 \\ T_1 \\ U_1 \\ V_1 \\ W_1 \\ \vdots \\ R_n \\ S_n \\ T_n \\ U_n \\ V_n \\ W_n \end{bmatrix}_{\lambda.\nu\times 1} = \begin{bmatrix} 0 \\ 0 \\ 0 \\ 0 \\ 0 \\ 0 \\ 0 \end{bmatrix}_{F\times 1} \tag{62}$$

where n is the number of independent loops of the origami. Therefore, replacing the values of the Equation (60) in Equation (62) yields a homogeneous linear system with F equations and $\lambda \cdot \nu$ unknowns. Thus, the Equation (62) in origami two-D4V can be written as:

$$\begin{bmatrix} 0 & \cos\beta & \sin\beta & 0 & -x'\sin\beta & x'\cos\beta & 0 & 0 & 0 & 0 & 0 & 0 \\ 0 & 0 & 0 & 0 & 0 & 0 & 0 & \cos\beta & \sin\beta & 0 & 0 & 0 \\ 0 & 0 & 0 & 0 & 0 & 0 & -\cos\theta & -\sin\theta & 0 & 0 & 0 & 0 \\ 0 & 0 & 0 & 0 & 0 & 0 & 0 & \cos\alpha & \sin\alpha & 0 & 0 & 0 \\ 0 & \cos\alpha & \sin\alpha & 0 & -\sin\alpha & \cos\alpha & 0 & 0 & 0 & 0 & 0 & 0 \\ \cos\theta & \sin\theta & 0 & 0 & x'\sin\theta & 0 & 0 & 0 & 0 & 0 & 0 & 0 \\ -1 & 0 & 0 & 0 & 0 & 0 & 1 & 0 & 0 & 0 & 0 & 0 \end{bmatrix}_{7\times 12} \begin{bmatrix} R \\ S \\ T \\ U \\ V \\ W \\ R \\ S \\ T \\ U \\ V \\ W \end{bmatrix}_{12\times 1}$$

$$= \begin{bmatrix} 0 & 0 & 0 & 0 & 0 & 0 & 0 \end{bmatrix}^T_{7\times 1} \tag{63}$$

By finding the rank $m = 6$ of the $[\hat{M}_N^T]$ matrix of the Equation (63), the number of redundant constraints of the origami were computed by applying $C_N = \lambda \cdot \nu - m$. For this origami, in the partially folded configuration, the redundant constraints were $C_N = 6$. On the other hand, by applying reduced row echelon form (rref), the Equation (63) can be rearranged as:

$$\begin{bmatrix} 1 & 0 & 0 & 0 & 0 & 0 & 0 & 0 & 0 & 0 & 0 & 0 \\ 0 & 1 & 0 & 0 & 0 & 2 & 0 & 0 & 0 & 0 & 0 & 0 \\ 0 & 0 & 1 & 0 & -2 & 0 & 0 & 0 & 0 & 0 & 0 & 0 \\ 0 & 0 & 0 & 0 & 0 & 0 & 1 & 0 & 0 & 0 & 0 & 0 \\ 0 & 0 & 0 & 0 & 0 & 0 & 0 & 1 & 0 & 0 & 0 & 0 \\ 0 & 0 & 0 & 0 & 0 & 0 & 0 & 0 & 1 & 0 & 0 & 0 \\ 0 & 0 & 0 & 0 & 0 & 0 & 0 & 0 & 0 & 0 & 0 & 0 \end{bmatrix}_{7\times12} \begin{bmatrix} R_f \\ S_f \\ T_f \\ U_f \\ V_f \\ W_f \\ \cdots \\ R_e \\ S_e \\ T_e \\ U_e \\ V_e \\ W_e \end{bmatrix}_{12\times1} = \begin{bmatrix} 0 \\ 0 \\ 0 \\ 0 \\ 0 \\ 0 \\ 0 \end{bmatrix}_{7\times1} \tag{64}$$

Then columns 1, 2 , 3, 7, 8 and 9 are pivot columns and columns 4, 5, 6, 10, 11 and 12 are free columns. According to the above, U, V and W are the free variables of the action circuit generated by the $C_N = 6$ redundant constraints:

$$\hat{\$}^a = \begin{bmatrix} 0 & 0 & 0 & U_f & V_f & W_f & 0 & 0 & 0 & U_e & V_e & W_e \end{bmatrix}^T \tag{65}$$

Therefore, the screw system of the 2-circuit origami has 3 actions corresponding to forces in x, y, and z axes. As in the previous section, the analysis of the origami in its partially folded configuration shows results that correspond to the screw system of spherical mechanisms. Its mobility is congruent with a spherical Watt mechanism, and the redundant constraints show that the origami is free to perform rotational movements.

4.2 3X3 SHAPED ORIGAMI

Figure 25 illustrates the 3X3-shaped origami. This origami configuration consists of 4 vertices ($\nu = 4$), 12 creases ($j = 12$), and 9 facets ($n = 9$). This configuration was studied using two different spanning trees. It was determined that the distribution of the spanning tree facilitates the identification of redundant constraints.

The origami is presented in a partially folded configuration to avoid singular positions. The angle α denotes the angle between the paper sheet and the x-axis for valley folds, while θ represents the angle between the paper sheet and the x-axis for mountain folds, and β as the angle between the fold and the y-axis. In this example, we assume a distance of 2 units between vertices. The vertices are labeled as illustrated in Figure 25 for easy reference.

Equation (66) presents the direction vectors:

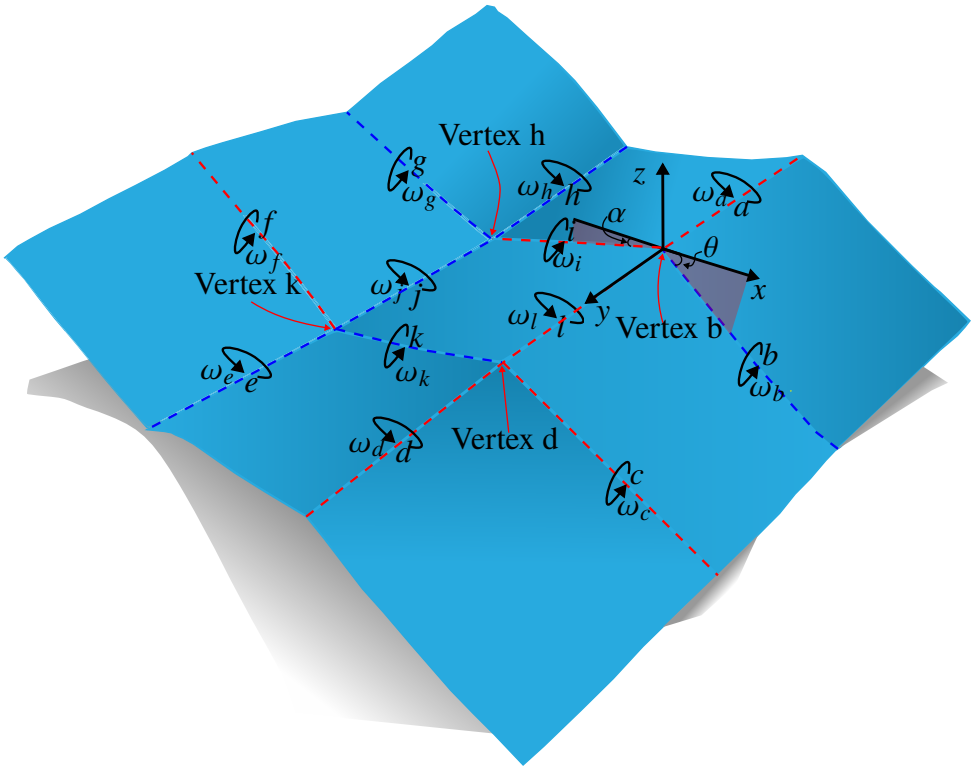

Figure 25 – 3X3-shaped Origami

$$\vec{S}_m^M = \begin{Bmatrix} \cos\alpha \\ 0 \\ \sin\alpha \end{Bmatrix} \quad \textit{for m= i and k;} \quad \vec{S}_n^M = \begin{Bmatrix} \cos\theta \\ 0 \\ -\sin\theta \end{Bmatrix} \quad \textit{for n= b, c, f and g}$$
$$\vec{S}_e^M = \begin{Bmatrix} 0 \\ -\cos\beta \\ \sin\beta \end{Bmatrix} \quad ; \quad \vec{S}_y^M = \begin{Bmatrix} 0 \\ 1 \\ 0 \end{Bmatrix} \quad \textit{for a, d, h, j and l} \tag{66}$$

Equação (67) defines the position vectors:

$$\vec{S}_{0_b} = \begin{Bmatrix} 0 \\ 0 \\ 0 \end{Bmatrix} \quad ; \quad \vec{S}_{0_d} = \begin{Bmatrix} 0 \\ 2 \\ 0 \end{Bmatrix} \quad ; \quad \vec{S}_{0_h} = \begin{Bmatrix} -2\cos\alpha \\ 0 \\ -2\sin\alpha \end{Bmatrix} \quad ; \quad \vec{S}_{0_k} = \begin{Bmatrix} -2\cos\alpha \\ 2 \\ -2\sin\alpha \end{Bmatrix} \tag{67}$$

where $\vec{S}_{0_b}$ is the position of the *a, b, l* and *i*; $\vec{S}_{0_d}$ represents the position of the joints passing through the origami vertex *d*, $\vec{S}_{0_h}$ indicates the position of the kinematic pairs *g, h* and *j*, and the position vector $\vec{S}_{0_k}$ belongs to the couplings *e, f* and *k*.

The gross degree of freedom (F) is calculated as:

$$F = \sum_{i=1}^{12} f_i = 12 \tag{68}$$

Figure 26 illustrates the spanning tree, and Equation (69) presents the circuit matrix:

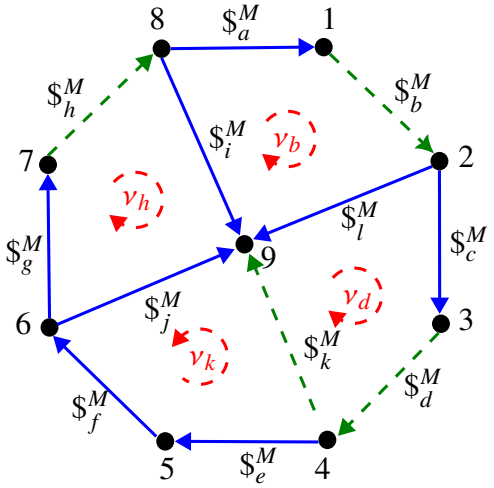

Figure 26 – 3x3-shaped Origami with Asimetric Spanning Tree

$$[B_M]_{4\times 12} = \begin{array}{c} \begin{matrix} b & d & h & k & a & c & e & f & g & i & j & l \end{matrix} \\ \begin{bmatrix} 1 & 0 & 0 & 0 & 1 & 0 & 0 & 0 & 0 & -1 & 0 & 1 \\ 0 & 1 & 0 & 0 & 0 & 1 & 1 & 1 & 0 & 0 & 1 & -1 \\ 0 & 0 & 1 & 0 & 0 & 0 & -1 & -1 & 0 & 0 & -1 & 0 \\ 0 & 0 & 0 & 1 & 0 & 0 & 0 & 0 & 1 & 1 & -1 & 0 \end{bmatrix} \end{array} \begin{matrix} \nu_b \\ \nu_d \\ \nu_h \\ \nu_k \end{matrix} \tag{69}$$

Equation (70) shows the twists of the kinematic pairs:

$$\$_a^M = \begin{pmatrix} 0 \\ \omega_a \\ 0 \\ \cdots \\ 0 \\ 0 \\ 0 \end{pmatrix}; \quad \$_b^M = \begin{pmatrix} \omega_b \cos\theta \\ 0 \\ -\omega_b \sin\theta \\ \cdots \\ 0 \\ 0 \\ 0 \end{pmatrix}; \quad \$_c^M = \begin{pmatrix} \omega_c \cos\theta \\ 0 \\ -\omega_c \sin\theta \\ \cdots \\ -2\omega_c \sin\theta \\ 0 \\ -2\omega_c \cos\theta \end{pmatrix}; \quad \$_f^M = \begin{pmatrix} \omega_f \cos\theta \\ 0 \\ -\omega_f \sin\theta \\ \cdots \\ -2\omega_f s\theta \\ -2\omega_f(s\theta c\alpha + s\alpha c\theta) \\ -2\omega_f c\theta \end{pmatrix}$$

$$\$_d^M = \begin{pmatrix} 0 \\ \omega_d \\ 0 \\ \cdots \\ 0 \\ 0 \\ 0 \end{pmatrix}; \quad \$_e^M = \begin{pmatrix} 0 \\ -\omega_e \cos\beta \\ \omega_e \sin\beta \\ \cdots \\ 2\omega_e(s\beta + c\beta s\alpha) \\ 2\omega_e c\alpha s\beta \\ 2\omega_e c\alpha c\beta \end{pmatrix}; \quad \$_k^M = \begin{pmatrix} \omega_k \cos\alpha \\ 0 \\ \omega_k \sin\alpha \\ \cdots \\ 2\omega_k \sin\alpha \\ 0 \\ -2\omega_k \cos\alpha \end{pmatrix}; \quad \$_i^M = \begin{pmatrix} \omega_i \cos\alpha \\ 0 \\ \omega_i \sin\alpha \\ \cdots \\ 0 \\ 0 \\ 0 \end{pmatrix} \tag{70}$$

$$\$_j^M = \begin{pmatrix} 0 \\ \omega_j \\ 0 \\ \cdots \\ 2\omega_j \sin\alpha \\ 0 \\ -2\omega_j \cos\alpha \end{pmatrix}; \quad \$_g^M = \begin{pmatrix} \omega_g \cos\theta \\ 0 \\ -\omega_g \sin\theta \\ \cdots \\ 0 \\ -2\omega_f(s\theta c\alpha + s\alpha c\theta) \\ 0 \end{pmatrix}; \quad \$_h^M = \begin{pmatrix} 0 \\ 1 \\ 0 \\ \cdots \\ 2\omega_h s\alpha \\ 0 \\ -2\omega_h c\alpha \end{pmatrix}; \quad \$_l^M = \begin{pmatrix} 0 \\ \omega_l \\ 0 \\ \cdots \\ 0 \\ 0 \\ 0 \end{pmatrix}$$

The unit motion matrix is:

$$[\hat{M}_D]_{6\times12} =$$

$$\begin{bmatrix}
c\theta & 0 & 0 & c\alpha & 0 & c\theta & 0 & c\theta & c\theta & c\alpha & 0 & 0 \\
0 & 1 & 1 & 0 & 1 & 0 & -\cos\beta & 0 & 0 & 0 & 1 & 1 \\
-s\theta & 0 & 0 & s\alpha & 0 & -s\theta & \sin\beta & -s\theta & -s\theta & s\alpha & 0 & 0 \\
0 & 0 & 2s\alpha & 2s\alpha & 0 & -2s\theta & 2(s\beta + c\beta s\alpha) & -2s\theta & 0 & 0 & 2s\alpha & 0 \\
0 & 0 & 0 & 0 & 0 & 0 & 2c\alpha s\beta & -2(c\alpha s\theta + s\alpha c\theta) & -2(c\alpha s\theta + s\alpha c\theta) & 0 & 0 & 0 \\
0 & 0 & -2c\alpha & -2c\alpha & 0 & -2c\theta & -2c\alpha c\beta & -2c\theta & 0 & 0 & -2c\alpha & 0
\end{bmatrix} \tag{71}$$

Consequently, the $[\hat{M}_N]$ is:

$$[\hat{M}_N]_{24\times12} =$$

$$\begin{bmatrix}
c\theta & 0 & 0 & 0 & 0 & 0 & 0 & 0 & 0 & -c\alpha & 0 & 0 \\
0 & 0 & 0 & 0 & 1 & 0 & 0 & 0 & 0 & 0 & 0 & 1 \\
s\theta & 0 & 0 & 0 & 0 & 0 & 0 & 0 & 0 & -s\alpha & 0 & 0 \\
0 & 0 & 0 & 0 & 0 & 0 & 0 & 0 & 0 & 0 & 0 & 0 \\
0 & 0 & 0 & 0 & 0 & 0 & 0 & 0 & 0 & 0 & 0 & 0 \\
0 & 0 & 0 & 0 & 0 & 0 & 0 & 0 & 0 & 0 & 0 & 0 \\
0 & 0 & 0 & 0 & 0 & c\theta & 0 & c\theta & 0 & 0 & 0 & 0 \\
0 & 1 & 0 & 0 & 0 & 0 & -c\beta & 0 & 0 & 0 & 1 & -1 \\
0 & 0 & 0 & 0 & 0 & -s\theta & s\beta & -s\theta & 0 & 0 & 0 & 0 \\
0 & 0 & 0 & 0 & 0 & -2s\theta & 2s\beta + 2c\beta s\alpha & -2s\theta & 0 & 0 & 2s\alpha & 0 \\
0 & 0 & 0 & 0 & 0 & 0 & 2c\alpha s\beta & -2(s\alpha c\theta + c\alpha s\theta) & 0 & 0 & 0 & 0 \\
0 & 0 & 0 & 0 & 0 & -2c\theta & 2c\alpha c\beta & -2c\theta & 0 & 0 & -2c\alpha & 0 \\
0 & 0 & 0 & 0 & 0 & 0 & 0 & -c\theta & 0 & 0 & 0 & 0 \\
0 & 0 & 1 & 0 & 0 & 0 & c\beta & 0 & 0 & 0 & -1 & 0 \\
0 & 0 & 0 & 0 & 0 & 0 & -s\beta & s\theta & 0 & 0 & 0 & 0 \\
0 & 0 & 2s\alpha & 0 & 0 & 0 & 2s\beta - 2c\beta s\alpha & 2s\theta & 0 & 0 & -2s\alpha & 0 \\
0 & 0 & 0 & 0 & 0 & 0 & -2c\alpha s\beta & 2(s\alpha c\theta + c\alpha s\theta) & 0 & 0 & 0 & 0 \\
0 & 0 & -2c\alpha & 0 & 0 & 0 & 2c\alpha c\beta & 2c\theta & 0 & 0 & 2c\alpha & 0 \\
0 & 0 & 0 & c\alpha & 0 & 0 & 0 & 0 & c\theta & c\alpha & 0 & 0 \\
0 & 0 & 0 & 0 & 0 & 0 & 0 & 0 & 0 & 0 & 1 & 0 \\
0 & 0 & 0 & s\alpha & 0 & 0 & 0 & 0 & -s\theta & s\alpha & 0 & 0 \\
0 & 0 & 0 & 2s\alpha & 0 & 0 & 0 & 0 & 0 & 0 & 2s\alpha & 0 \\
0 & 0 & 0 & 0 & 0 & 0 & 0 & 0 & -2(c\alpha s\theta + s\alpha c\theta) & 0 & 0 & 0 \\
0 & 0 & 0 & -2c\alpha & 0 & 0 & 0 & 0 & 0 & 0 & -2c\alpha & 0
\end{bmatrix} \tag{72}$$

By calculating the mobility using Equation (72), it was determined that $F_N = 1$, with $C_N = 13$ redundant constraints.

We rearrange the matrix of Equation (72) to its reduced row echelon form, to determine the pivot and free columns, and consequently, to obtain the types of redundant constraints present in each of the vertices.

The $[\hat{M}_N]^T$ in its $rref$ form is:

a	$\frac{-\cos(\beta)\,\cos(\theta)\,\sin(\alpha)^2+\sin(\beta)\,\cos(\theta)\,\sin(\alpha)+\cos(\alpha)\,\sin(\beta)\,\sin(\theta)}{\cos(\beta)\,\sin(\alpha)\,(\cos(\alpha)\,\sin(\theta)+\sin(\alpha)\,\cos(\theta))}$	f	$\frac{-\sin(\theta)}{2\,(\cos(\alpha)\,\sin(\theta)+\sin(\alpha)\,\cos(\theta))}$
b	$\frac{\cos(\alpha)\,\sin(\theta)}{\cos(\alpha)\,\sin(\theta)+\sin(\alpha)\,\cos(\theta)}$	g	$\frac{2\,\sin(\alpha)\,\sin(\theta)}{\cos(\alpha)\,\sin(\theta)+\cos(\alpha)\,\cos(\theta)}$
c	$\frac{\cos(\alpha)\,\cos(\theta)}{\cos(\alpha)\,\sin(\theta)+\sin(\alpha)\,\cos(\theta)}$	h	$\frac{2\,\sin(\alpha)\,\cos(\theta)}{\cos(\alpha)\,\sin(\theta)+\sin(\alpha)\,\cos(\theta)}$
d	$\frac{\cos(\theta)}{2\,(\cos(\alpha)\,\sin(\theta)+\sin(\alpha)\,\cos(\theta))}$	i	$-\frac{2\,c(\alpha)\,s(\theta)}{c(\alpha)\,s(\theta)+s(\alpha)\,c(\theta)}$
e	$\frac{-\sin(\alpha)\,\sin(\theta)}{\cos(\alpha)\,\sin(\theta)+\sin(\alpha)\,\cos(\theta)}$	j	$\frac{-2\,c(\alpha)\,c(\theta)}{c(\alpha)\,s(\theta)+s(\alpha)\,c(\theta)}$

Table 1 – Summary rref 3x3-Shaped

$$
\begin{bmatrix}
1 & 0 & 0 & 0 & 0 & 0 & 0 & 0 & 0 & 0 & 0 & 0 & 0 & 0 & 0 & 0 \\
0 & 1 & 0 & 0 & 0 & 0 & 0 & 0 & 0 & 0 & 0 & 0 & 0 & 0 & 0 & 0 \\
0 & 0 & 1 & 0 & 0 & 0 & 0 & 0 & 0 & 0 & 0 & 0 & 0 & 0 & 0 & 0 \\
0 & 0 & 0 & 0 & 0 & 0 & 1 & 0 & 0 & 0 & 0 & -2 & -b & 0 & e & 2e \\
0 & 0 & 0 & 0 & 0 & 0 & 0 & 1 & 0 & 0 & 0 & 0 & 0 & 0 & 0 & 0 \\
0 & 0 & 0 & 0 & 0 & 0 & 0 & 0 & 1 & 0 & 0 & \frac{2\,c(\alpha)}{s(\alpha)} & -c & 0 & a & \frac{-2\,s(\alpha)\,c(\theta)}{c(\alpha)\,s(\theta)+s(\alpha)\,c(\theta)} \\
0 & 0 & 0 & 0 & 0 & 0 & 0 & 0 & 0 & 1 & 0 & \frac{-c(\alpha)}{s(\alpha)} & 0 & 0 & \frac{-s(\beta)}{2\,c(\beta)\,s(\alpha)} & 0 \\
0 & 0 & 0 & 0 & 0 & 0 & 0 & 0 & 0 & 0 & 1 & 0 & d & 0 & f & 2f \\
0 & 0 & 0 & 0 & 0 & 0 & 0 & 0 & 0 & 0 & 0 & 0 & 0 & 1 & -\frac{s(\beta)}{c(\beta)} & 2\,s\,(\alpha) \\
0 & 0 & 0 & 0 & 0 & 0 & 0 & 0 & 0 & 0 & 0 & 0 & 0 & 0 & 0 & 0 \\
0 & 0 & 0 & 0 & 0 & 0 & 0 & 0 & 0 & 0 & 0 & 0 & 0 & 0 & 0 & 0 \\
0 & 0 & 0 & 0 & 0 & 0 & 0 & 0 & 0 & 0 & 0 & 0 & 0 & 0 & 0 & 0
\end{bmatrix}
\cdots
$$

$$
\cdots
\begin{bmatrix}
0 & 0 & 0 & 0 & 0 & g & 0 & i \\
0 & 0 & 0 & 0 & 0 & 0 & 0 & 0 \\
0 & 0 & 0 & 0 & 0 & h & 0 & j \\
0 & 2b & 0 & \frac{c(\beta)\,s(\theta)}{s(\beta)\,c(\theta)} & 0 & \frac{2\,c(\beta)\,s(\alpha)\,s(\theta)}{s(\beta)\,c(\theta)} & 0 & \frac{-2\,c(\alpha)\,c(\beta)\,s(\theta)}{s(\beta)\,c(\theta)} \\
0 & 0 & 0 & 0 & 0 & 0 & 0 & 0 \\
\frac{2\,c(\alpha)\,s(\beta)}{c(\beta)\,s(\alpha)} & 2c & 0 & \frac{s(\beta)+c(\beta)\,s(\alpha)}{s(\alpha)\,s(\beta)} & 0 & \frac{2\,(s(\beta)+c(\beta)\,s(\alpha))}{s(\beta)} & 0 & -\frac{2\,c(\alpha)\,(s(\beta)+c(\beta)\,s(\alpha))}{s(\alpha)\,s(\beta)} \\
\frac{-c(\alpha)\,s(\beta)}{c(\beta)\,s(\alpha)} & 0 & 0 & \frac{-1}{2\,s(\alpha)} & 0 & -1 & 0 & \frac{c(\alpha)}{s(\alpha)} \\
-1 & -2d & 0 & 0 & 0 & 0 & 0 & 0 \\
\frac{-2\,c(\alpha)\,s(\beta)}{c(\beta)} & -2\,c\,(\alpha) & 0 & 0 & 0 & 0 & 0 & 0 \\
0 & 0 & 1 & 0 & 0 & g & -2\,s\,(\alpha) & i \\
0 & 0 & 0 & 0 & 1 & h & 2\,c\,(\alpha) & j \\
0 & 0 & 0 & 0 & 0 & 0 & 0 & 0
\end{bmatrix}
\begin{bmatrix}
R_b \\ S_b \\ T_b \\ U_b \\ V_b \\ W_b \\ \cdots \\ R_d \\ S_d \\ T_d \\ U_d \\ V_d \\ W_d \\ \cdots \\ R_k \\ S_k \\ T_k \\ U_k \\ V_k \\ W_k \\ \cdots \\ R_h \\ S_h \\ T_h \\ U_h \\ V_h \\ W_h
\end{bmatrix}
$$

$$
= \begin{bmatrix} 0 & 0 & 0 & 0 & 0 & 0 & 0 & 0 & 0 & 0 & 0 & 0 \end{bmatrix}^T_{12\times 1} \tag{73}
$$

For practicality, the Table 1 was elaborated. the symbols are indicated in Table 1.

The constraints per loop are:

$$\hat{\$}^a = \begin{bmatrix} 0 & 0 & 0 & U_b & V_b & W_b & 0 & 0 & 0 & 0 & 0 & W_d & R_k & 0 & T_k & U_k & V_k & W_k & 0 & S_h & 0 & U_h & V_h & W_h \end{bmatrix}^T \tag{74}$$

The redundant constraints acting on the 3×3-shaped origami are illustrated in Figure 27. Vertices *b, d*, and *k* are subjected to force constraints along all three principal axes. Conversely, vertex *h* experiences force constraints along the O_y and O_z axes but retains translational freedom along the O_x axis. This translational freedom induces a torsional moment about the O_z axis, which is counterbalanced at vertex *k*. Moreover, at vertex *h*, a torsion constraint is evident, representing the redundant constraint in this configuration.

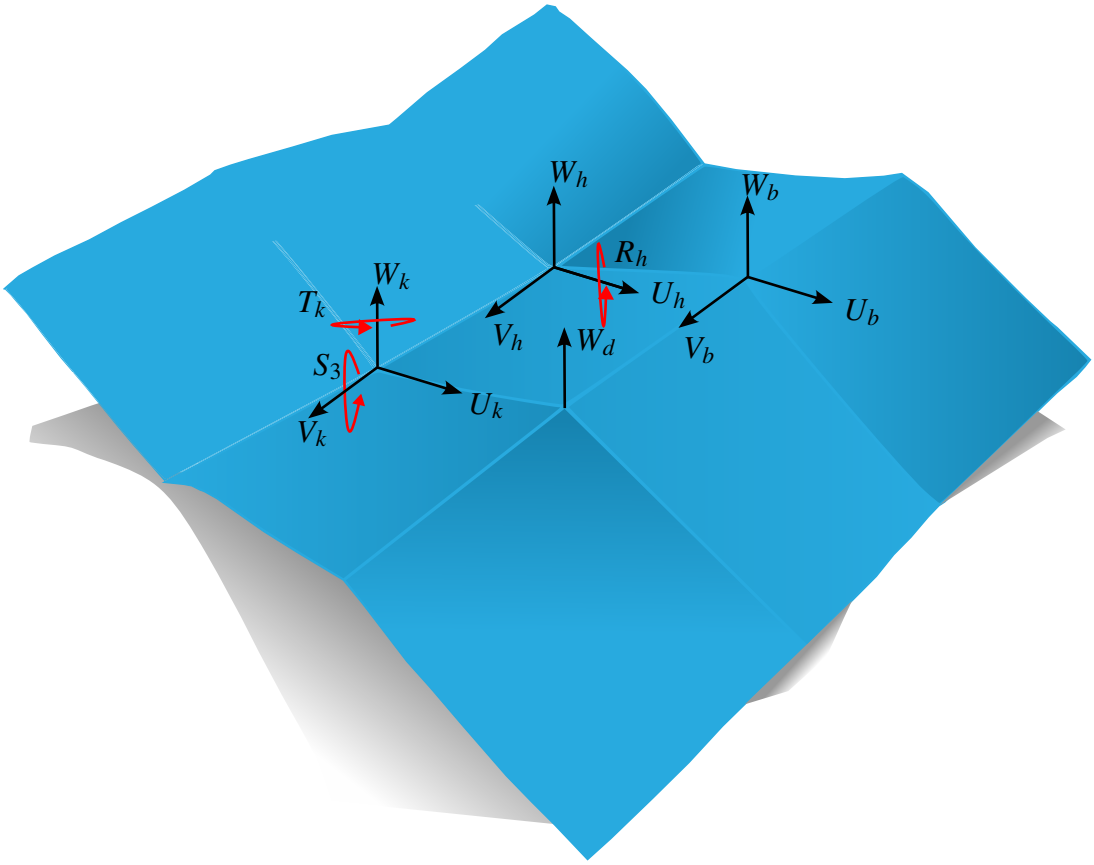

Figure 27 – Actions of 3x3-shaped Origami with Asimetric Spanning Tree

This model attempts to depict the constraints of the 3×3-Shaped origami, but it fails to align with the expected constraints of a spherical mechanism studied in three-dimensional space ($\lambda = 6$). There are translational freedoms at vertex 2 and rotational constraints along the crease directions, which contradicts physical expectations. As a result, a new spanning tree was designed, presented in Figure 28, along with its circuit matrix in Equation (75). Unlike the previous one, this new spanning tree is symmetric.

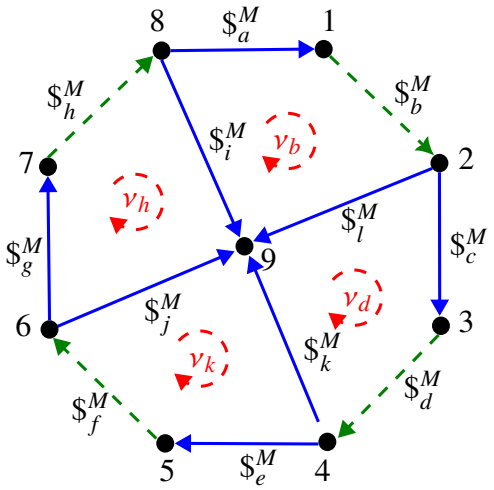

Figure 28 – 3x3-shaped Origami with Simetric Spanning Tree

$$[B_M]_{4\times12} = \begin{array}{c} \begin{matrix} b & d & f & h & a & c & e & g & i & j & k & l \end{matrix} \\ \begin{bmatrix} 1 & 0 & 0 & 0 & 1 & 0 & 0 & 0 & -1 & 0 & 0 & 1 \\ 0 & 1 & 0 & 0 & 0 & 1 & 0 & 0 & 0 & 0 & 1 & -1 \\ 0 & 0 & 1 & 0 & 0 & 0 & 1 & 0 & 0 & 1 & -1 & 0 \\ 0 & 0 & 0 & 1 & 0 & 0 & 0 & 1 & 1 & -1 & 0 & 0 \end{bmatrix} \end{array} \begin{matrix} \nu_b \\ \nu_d \\ \nu_f \\ \nu_h \end{matrix} \tag{75}$$

Consequently, the $[\hat{M}_N]$ is

$$[\hat{M}_N]_{24\times12} = \begin{bmatrix}
c\theta & 0 & 0 & 0 & 0 & 0 & 0 & 0 & -c\alpha & 0 & 0 & 0 \\
0 & 0 & 0 & 0 & 1 & 0 & 0 & 0 & 0 & 0 & 0 & 1 \\
-s\theta & 0 & 0 & 0 & 0 & 0 & 0 & 0 & s\alpha & 0 & 0 & 0 \\
0 & 0 & 0 & 0 & 0 & 0 & 0 & 0 & 0 & 0 & 0 & 0 \\
0 & 0 & 0 & 0 & 0 & 0 & 0 & 0 & 0 & 0 & 0 & 0 \\
0 & 0 & 0 & 0 & 0 & 0 & 0 & 0 & 0 & 0 & 0 & 0 \\
0 & 0 & 0 & 0 & 0 & c\theta & 0 & 0 & 0 & 0 & c\alpha & 0 \\
0 & 1 & 0 & 0 & 0 & 0 & 0 & 0 & 0 & 0 & 0 & -1 \\
0 & 0 & 0 & 0 & 0 & -s\theta & 0 & 0 & 0 & 0 & s\alpha & 0 \\
0 & 0 & 0 & 0 & 0 & -2s\theta & 0 & 0 & 0 & 0 & 2s\alpha & 0 \\
0 & 0 & 0 & 0 & 0 & 0 & 0 & 0 & 0 & 0 & 0 & 0 \\
0 & 0 & 0 & 0 & 0 & -2c\theta & 0 & 0 & 0 & 0 & -2c\alpha & 0 \\
0 & 0 & c\theta & 0 & 0 & 0 & 0 & 0 & 0 & 0 & -c\alpha & 0 \\
0 & 0 & 0 & 0 & 0 & 0 & c\beta & 0 & 0 & 1 & 0 & 0 \\
0 & 0 & -s\theta & 0 & 0 & 0 & s\beta & 0 & 0 & 0 & -s\alpha & 0 \\
0 & 0 & -2s\theta & 0 & 0 & 0 & 2(s\alpha + c\beta s\alpha) & 0 & 0 & 2s\alpha & -2s\alpha & 0 \\
0 & 0 & -2(c\alpha s\theta + s\alpha c\theta) & 0 & 0 & 0 & 2c\alpha s\beta & 0 & 0 & 0 & 0 & 0 \\
0 & 0 & -2c\theta & 0 & 0 & 0 & -2c\alpha c\beta & 0 & 0 & -2c\alpha & 2c\alpha & 0 \\
0 & 0 & 0 & 0 & 0 & 0 & 0 & c\theta & c\alpha & 0 & 0 & 0 \\
0 & 0 & 0 & -c\beta & 0 & 0 & 0 & 0 & 0 & -1 & 0 & 0 \\
0 & 0 & 0 & s\alpha & 0 & 0 & 0 & -s\theta & s\alpha & 0 & 0 & 0 \\
0 & 0 & 0 & -2s\alpha c\beta) & 0 & 0 & 0 & 0 & 0 & -2s\alpha & 0 & 0 \\
0 & 0 & 0 & 2c\alpha s\beta & 0 & 0 & 0 & -2(c\alpha s\theta + s\alpha c\theta) & 0 & 0 & 0 & 0 \\
0 & 0 & 0 & 2c\alpha c\beta & 0 & 0 & 0 & 0 & 0 & 2c\alpha & 0 & 0
\end{bmatrix} \tag{76}$$

Obtaining mobility from Equation (76), we find that $F_N = 1$, and there are 13 redundant constraints, as represented by $C_N = 13$.

We applied rref to the $[\hat{M}_N]^T$ to determine the pivot and free columns, and consequently, to obtain the types of redundant constraints present in each of the spherical centers.

The $[\hat{M}_N]^T$ in its $rref$ form is:

$$\begin{bmatrix}
1 & 0 & 0 & 0 & 0 & 0 & 0 & 0 & 0 & 0 & 0 & 0 & 0 & 0 & 0 & 0 & 0 & 0 & 0 & 0 & \frac{-s\alpha}{c\alpha} & 0 & -2s\alpha & 0 \\
0 & 1 & 0 & 0 & 0 & 0 & 0 & 0 & 0 & 0 & 0 & 0 & 0 & 0 & 0 & 0 & 0 & 0 & 0 & 0 & 0 & 0 & 0 & 0 \\
0 & 0 & 1 & 0 & 0 & 0 & 0 & 0 & 0 & 0 & 0 & 0 & 0 & 0 & 0 & 0 & 0 & 0 & 0 & 0 & -1 & 0 & -2c\alpha & 0 \\
0 & 0 & 0 & 0 & 0 & 0 & 1 & 0 & 0 & 0 & 0 & -2 & 0 & 0 & 0 & 0 & 0 & 0 & 0 & 0 & 0 & 0 & 0 & 0 \\
0 & 0 & 0 & 0 & 0 & 0 & 0 & 1 & 0 & 0 & 0 & 0 & 0 & 0 & 0 & 0 & 0 & 0 & 0 & 0 & 0 & 0 & 0 & 0 \\
0 & 0 & 0 & 0 & 0 & 0 & 0 & 0 & 1 & 2 & 0 & 0 & 0 & 0 & 0 & 0 & 0 & 0 & 0 & 0 & 0 & 0 & 0 & 0 \\
0 & 0 & 0 & 0 & 0 & 0 & 0 & 0 & 0 & 0 & 0 & 0 & 1 & 0 & 0 & 2s\alpha & -2s\alpha & -2 & 0 & 0 & 0 & 0 & 0 & 0 \\
0 & 0 & 0 & 0 & 0 & 0 & 0 & 0 & 0 & 0 & 0 & 0 & 0 & 1 & 0 & 2 & 0 & -2c\alpha & 0 & 0 & 0 & 0 & 0 & 0 \\
0 & 0 & 0 & 0 & 0 & 0 & 0 & 0 & 0 & 0 & 0 & 0 & 0 & 0 & 1 & 0 & 2c\alpha & 0 & 0 & 0 & 0 & 0 & 0 & 0 \\
0 & 0 & 0 & 0 & 0 & 0 & 0 & 0 & 0 & 0 & 0 & 0 & 0 & 0 & 0 & 0 & 0 & 0 & 1 & 0 & \frac{-s\alpha}{c\alpha} & 0 & -4s\alpha & 0 \\
0 & 0 & 0 & 0 & 0 & 0 & 0 & 0 & 0 & 0 & 0 & 0 & 0 & 0 & 0 & 0 & 0 & 0 & 0 & 1 & 0 & 2s\alpha & 0 & -2c\alpha \\
0 & 0 & 0 & 0 & 0 & 0 & 0 & 0 & 0 & 0 & 0 & 0 & 0 & 0 & 0 & 0 & 0 & 0 & 0 & 0 & 0 & 0 & 0 & 0
\end{bmatrix}$$

$$\begin{bmatrix} R_b & S_b & T_b & U_b & V_b & W_b & R_d & S_d & T_d & U_d & V_d & W_d & R_k & S_k & T_k & U_k & V_k & W_k & R_h & S_h & T_h & U_h & V_h & W_h \end{bmatrix}^T$$
$$= \begin{bmatrix} 0 & 0 & 0 & 0 & 0 & 0 & 0 & 0 & 0 & 0 & 0 & 0 \end{bmatrix}^T_{12\times 1} \tag{77}$$

The constraints per loop are:

$$\hat{\$}^a =$$
$$\begin{bmatrix} 0 & 0 & 0 & U_b & V_b & W_b & 0 & 0 & 0 & U_d & V_d & W_d & 0 & 0 & 0 & U_k & V_k & W_k & 0 & 0 & T_h & U_h & V_h & W_h \end{bmatrix}^T \tag{78}$$

The redundant constraints acting on the 3×3-shaped origami can be seen in Figure 29. The vertices *b, d, k and h* are subject to force constraints on all three principal axes. On the other hand, vertex h has torque constraints on the O_z. This result shows that symmetry in spanning tree provides better outcomes and facilitates the calculation of origami kinematics. As can be observed in this section and Appendix A, arrays with symmetric spanning trees impose linear displacement constraints in all three axes and rotation constraints along the O_z axis direction at certain vertices. Conversely, asymmetric spanning trees yield responses with varied effects on displacement restrictions along the O_x, O_y and O_z axes, as well as O_z-axis rotations. It should be noted that symmetry in the organization of the spanning tree must exist both topologically and in the direction of the arrows. Due to the nature of origami joint types, rotation freedoms are only permitted in all three axes, and the presence of facets contained within four spherical centers (which can be seen as four spherical joints) generates a redundant constraint, preventing rotation around the z-axis.

4.3 COMPARISON WITH OTHER RESULTS FROM THE LITERATURE

Some researchers have investigated the mobility of origamis, and the findings of this study align with theirs. For instance, Tachi (2010) computes the mobility of origamis using his formulated equations. For mesh array origamis like the Miura-Ori, he suggests considering singularity in their application and notes they typically have exactly 1 degree of freedom, with a redundant structure.

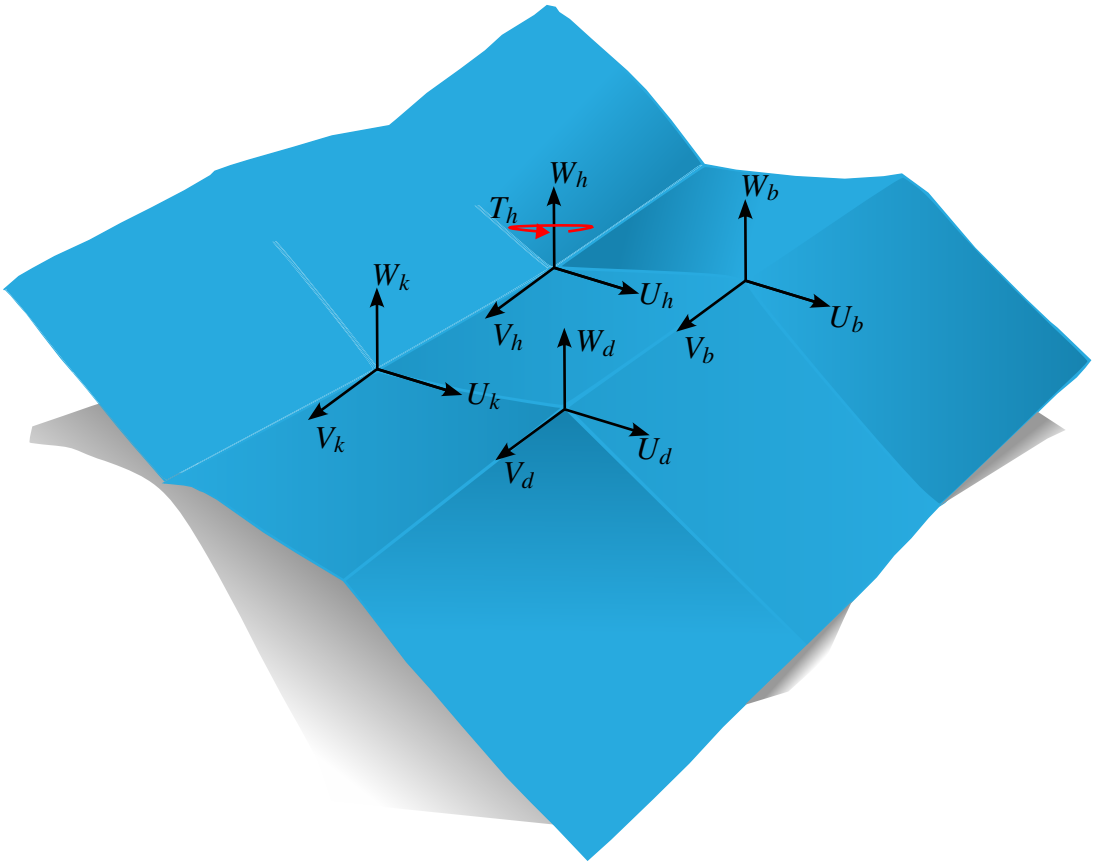

Figure 29 – Actions of 3X3-shaped Origami with Simetric Spanning Tree

Similarly, Yu, Guo, and Wang (2018) determine the mobility of various origami types using the adjacency matrix. One of the origamis they analyze is the 3×3-Shaped origami, as examined in the previous subsection. They confirm that Miura-Ori patterns have a mobility of 1 and classify this origami as a special case within a group they term "Cross-crease vertex". They highlight that cross-crease vertex characteristics may introduce potential errors when assessing the degree of freedom using the adjacency matrix method.

It is important to note that the Davies method does not have the issues associated with the adjacency matrix, and the calculation of mobility and redundant constraints proves effective.

5 MOBILITY EQUATION OF ORIGAMI-INSPIRED MECHANISMS WITH MULTIPLE CENTERS

After conducting kinematic analysis of various origami patterns, a equation to define their mobility was proposed, considering the structural characteristics of the equivalent spherical mechanisms, theorems, and geometric characteristics of origami. We start from the modified Chebychev-Glubber-Kutzbach mobility criterion (HUANG; LIU; ZENG, 2009), expressed as:

$$F_N = (n - j - 1)\lambda + j + C_N \tag{79}$$

where F_N represents the mobility of the origami, n denotes the number of facets of the origami, j signifies the number creases of the origami pattern, λ characterizes the screw system of the origami (for this equation were considered $\lambda = 6$) and C_N quantifies the number of redundant constraints.

Literature shows that determining the value of redundant constraints C_N in origamis (BROWN et al., 2022; YU; GUO; WANG, 2018) is challenging. However, this research has revealed that for origamis satisfying the bird's foot condition, this value can be calculated using the Equation (80).

$$C_N = 3\nu + C'_N \tag{80}$$

where ν is the number of vertices of the origami (which is equivalent to the number of independent loops of the spherical mechanisms) and C'_N is the number of additional redundant constraints. The first term (3ν) relates to the spherical screw system (LANG, 2017), recognizing that each vertex contributes 3 redundant constraints. While the second term (C'_N) derives from observations of various patterns studied in chapter 4 and Appendix A.

To calculate C'_N, each of the origami configurations presented in chapter 4 was studied. Initially, the D4V origami presented in Figure 30 was analyzed.

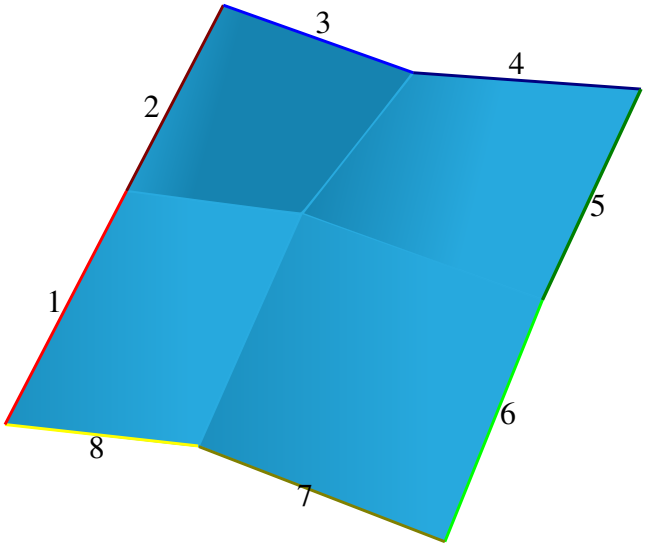

Figure 30 – Edges of D4V Origami pattern

It can be observed that the origami in Figure 30 exhibits 4 facets ($n = 4$), 4 creases ($j = 4$), 1 vertex ($\nu = 1$), and 8 external edges, with edges 1, 2, 5, and 6 being lateral edges, and edges 3, 4, 7, and 8 being vertical edges. This configuration can be considered a 2x2 origami. Substituting these values into Equation (79), and recalling that the mobility $F_N = 1$, yields:

$$C_N = 3$$

Substituting this into Equation (80) with $\nu = 1$ gives:

$$3 = 3(1) + C'_N$$

Therefore:

$$C'_N = 0$$

This configuration's redundant constraints stem solely from the 3 constraints per vertex, with no additional constraints.

The two-vertex origami pattern shown in Figure 31 was studied. In this case, the origami has 2 vertices ($\nu = 2$), 6 faces ($n = 6$), 7 creases ($j = 7$), and 10 folds at the boundary. Applying Equation (79), reveals $C_N = 6$ redundant constraints, indicating no additional redundant constraints beyond those corresponding to the vertices.

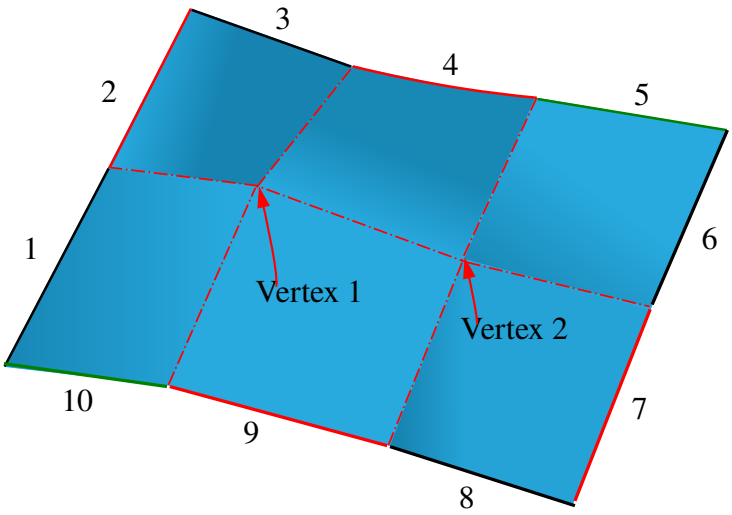

Figure 31 – Edges of Two-D4V Origami pattern

Analysis of the 3x3 origami in Figure 32 yielded $C_N = 13$ redundant constraints, with 12 corresponding to vertex constraints and an additional $C'_N = 1$.

For the 3x4 origami in Figure 33, we found $C_N = 20$ redundant constraints, including 18 vertex-related constraints and 2 additional redundant constraints ($C'_N = 2$).

After applying the Davies method to other origami patterns, such as Figure 34, it was observed that the number of redundant constraints aligns with the proposal in Equation (80). The first term corresponds to three constraints per vertex, while the second term represents additional redundant constraints.

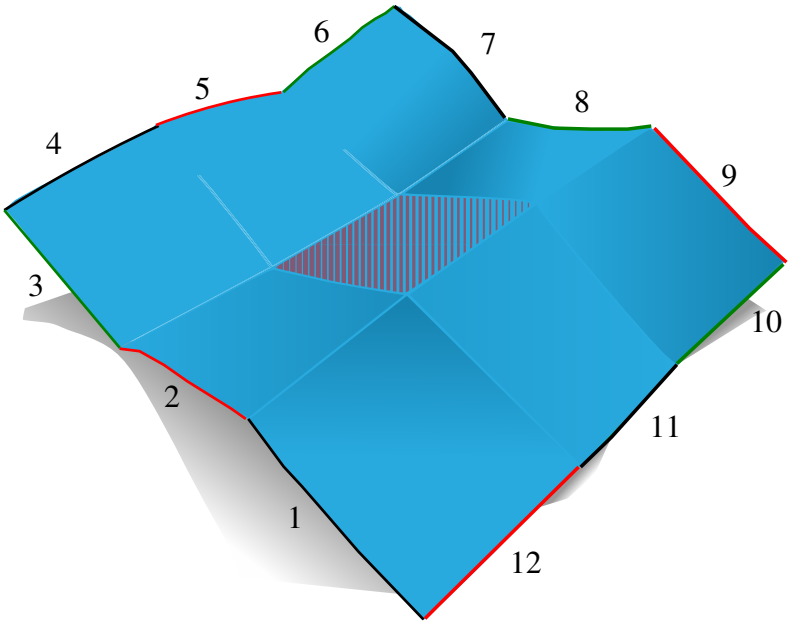

Figure 32 – 3x3 origami with an intermediate face highlighted and lateral edges

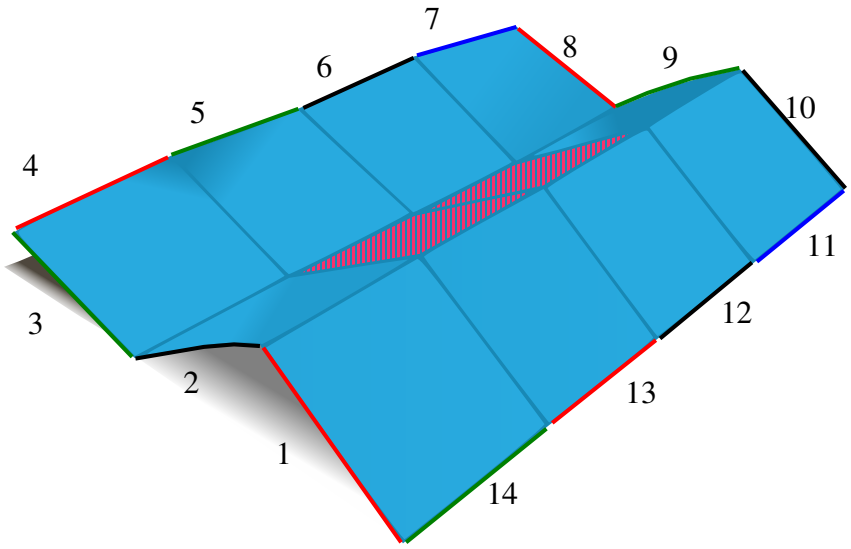

Figure 33 – 3x4 origami with an intermediate face highlighted and lateral edges

By observation, it was discovered that the number of additional redundant constraints directly relate to the number of faces that are enclosed within at least four vertices of the origami pattern. For instance, in Figure 32, it is highlighted that the origami has one face contained within 4 vertices (face shaded in red), and its additional redundant constraints were $C'_N = 1$. Meanwhile, in the origami shown in Figure 33, the additional redundant constraints were $C'_N = 2$, and the number of faces contained within 4 vertices was 2.

Similarly, when the number of faces contained within 4 vertices increased, as in the origami shown in Figure 34, which has 12 faces, the number of additional redundant constraints also increased to $C'_N = 12$.

To determine the number of faces contained within a least 4 vertices for any origami pattern size, we considered a 3X3 origami with vertical sides m_{ei} and lateral sides l_{ei}, as shown

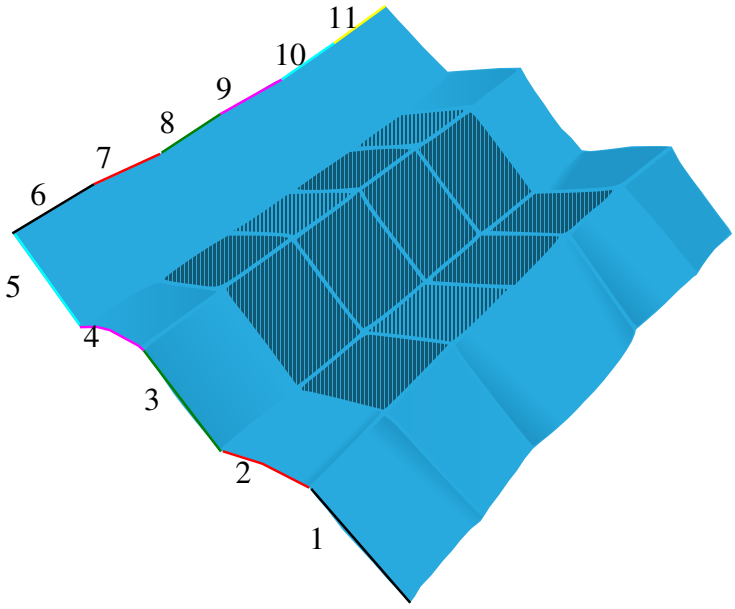

Figure 34 – 6x5 origami with an intermediate face highlighted and lateral edges

in Figure 35.

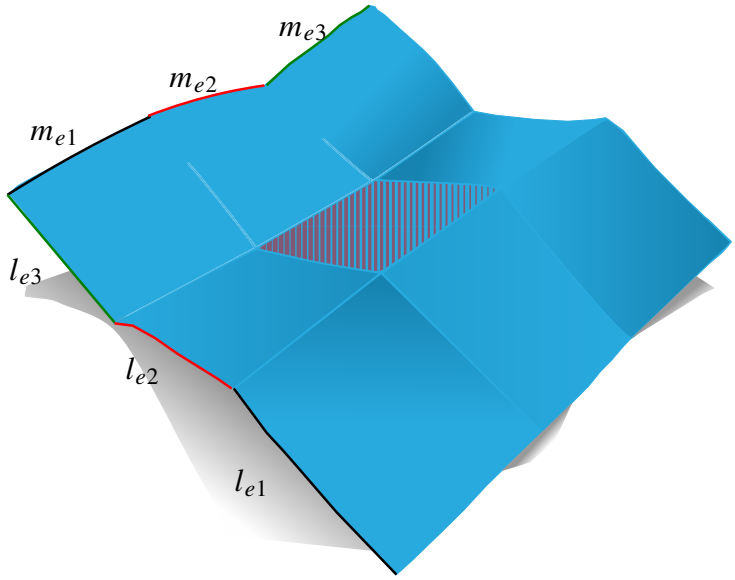

Figure 35 – 3x3 Origami pattern with vertical sides m_{ei} and lateral sides l_{ei}

The shaded face is the only one contained within at least 4 vertices of the origami. To calculate this value, the peripheral faces were subtracted, in this case, those located on columns m_{e1} and m_{e3} (Figure 36a), and rows l_{e1} and l_{e3} (Figure 36b).

Applying this procedure to other origami patterns, such as the 3x4 origami pattern shown in Figure 37a, it can be observed that it is necessary to subtract the sides m_{e1}, m_{e4}, l_{e1}, and l_{e3}. In the case of the 6x5 origami shown in Figure 37b, it is necessary to subtract the faces on rows l_{e1} and l_{e5}, and the faces on columns m_{e1} and m_{e6}.

In general, to determine the number of faces contained within at least 4 vertices of the origami, it is necessary to subtract 2 rows and 2 columns. Consequently, This leads to the general

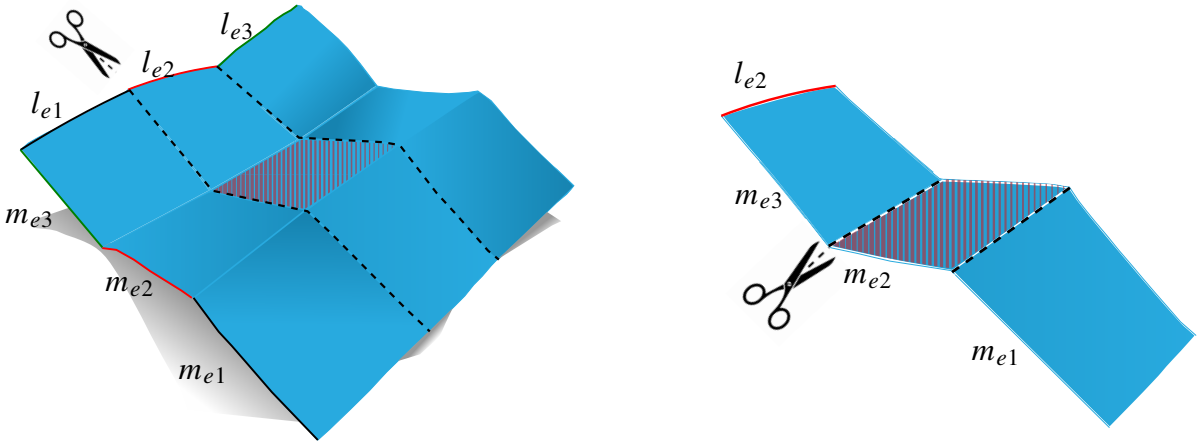

(a) (b)

Figure 36 – 3X3 Shaped Origami:(a) m_i columns and (b) l_i rows subtracted

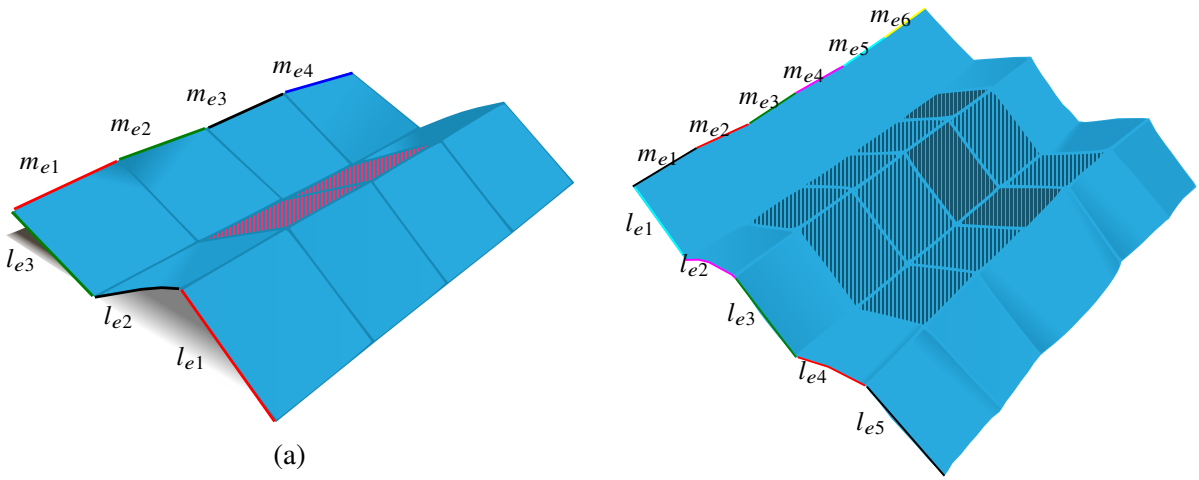

(a) (b)

Figure 37 – patterns with vertical sides m_{ei} and lateral sides l_{ei}: (a) 3X4 Shaped Origami and (b) 6X5 Shaped Origami

expression:

$$C'_N = (m-2)(l-2) \tag{81}$$

where l_e is the number of lateral edges and m_e is the number of vertices edges.

Substituting Equation (81) into Equation (80) yields a general equation that describes the redundant constraints present in an origami pattern with rectangular faces, as shown:

$$C_N = 3v + (l-2)(m-2) \tag{82}$$

Incorporating (82) into Equation (79), results in proposed conjecture of mobility equation for origami patterns obeying the bird´s foot condition:

$$F_N = (n-j-1)\lambda + j + 3v + (l-2)(m-2) \tag{83}$$

Equations (82) and (83) apply exclusively to origamis that satisfy the bird's foot condition or possess at least one spherical center. For serial origamis where m or l is equal to 1, as shown in Figure 38, the Equation (80) generates negative values, potentially leading to erroneous mobility calculations for such origamis.

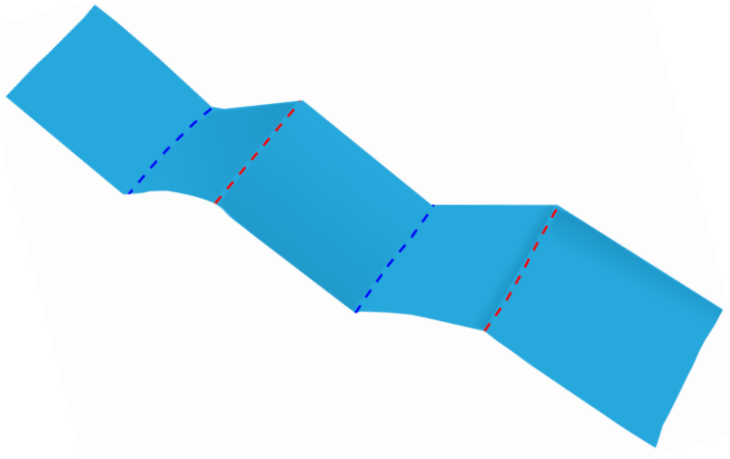

Figure 38 – Serial Origami Example

Figure 39 depicts an origami with $l_e = 2$ lateral edges, $m_e = 3$ vertices edges, and $\nu = 2$. Applying Equation (80), yields $C_N = 6$, aligning with the calculation using the Davies method in chapter 4 for the two-vertex origami. Given that $n = 6$, $j = 7$, and $\lambda = 6$ for this origami, substituting into Equation (83) results $F_N = 1$.

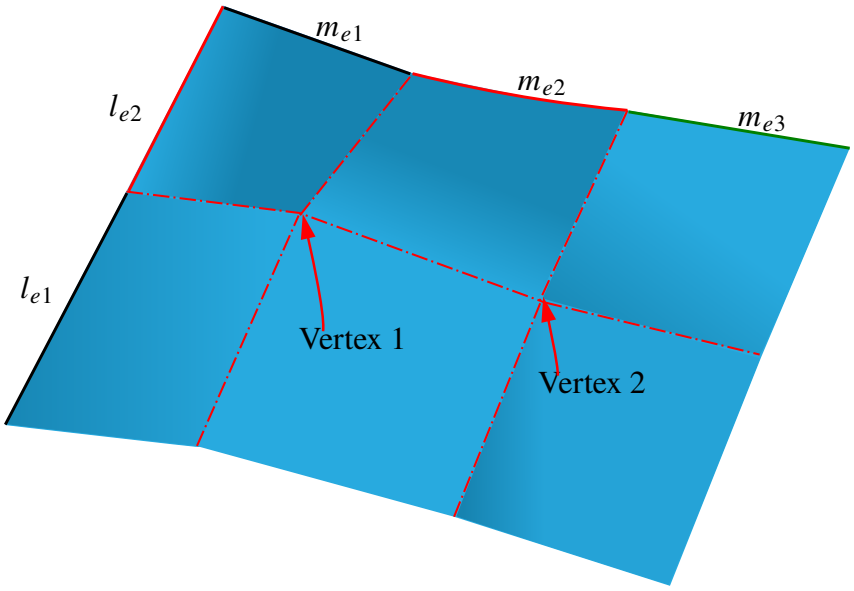

Figure 39 – l_e and m_e Edges in Two Vertices Origami pattern

We can extend this analysis to origami patterns with higher number of facets, creases, and vertices. Consider the 3x3-shaped origami in Figure 40, characterized by $l_e = 3$, $m_e = 3$, and $\nu = 4$. Equation (80), yields $C_N = 13$, and its mobility can be calculated by noting that $n = 9$, $j = 12$, and $\lambda = 6$. Substituting these values into Equation (83) yields $F_N = 1$.

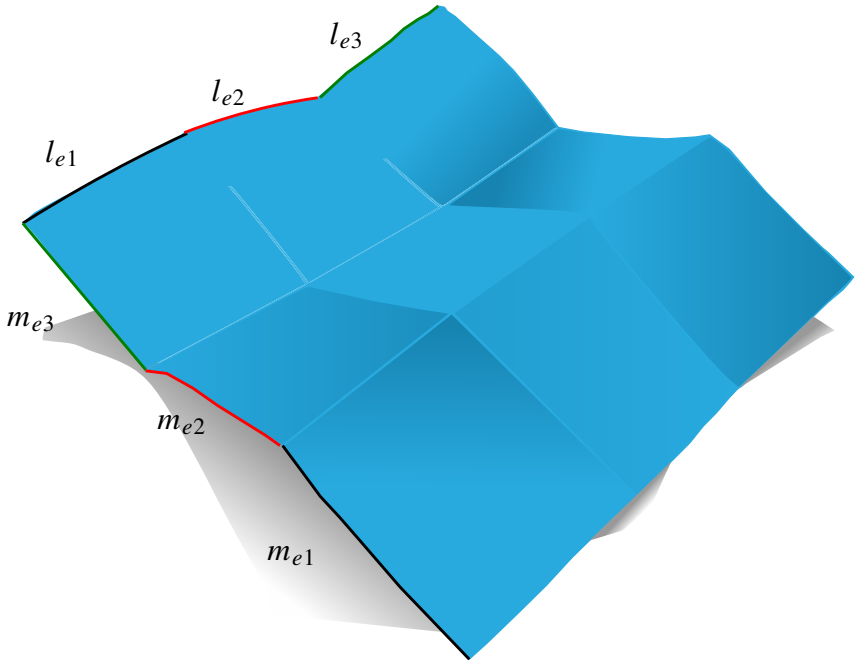

Figure 40 – l_e and m_e Edges in 3x3 Origami Pattern

Applying Equation (80) and Equation (83) to the pattern in Figure 41, which exhibits $m_e = 5$, $l_e = 6$, and $\nu = 20$, it is found that its redundant constraints are $C_N = 72$, and its mobility is $F_N = 1$.

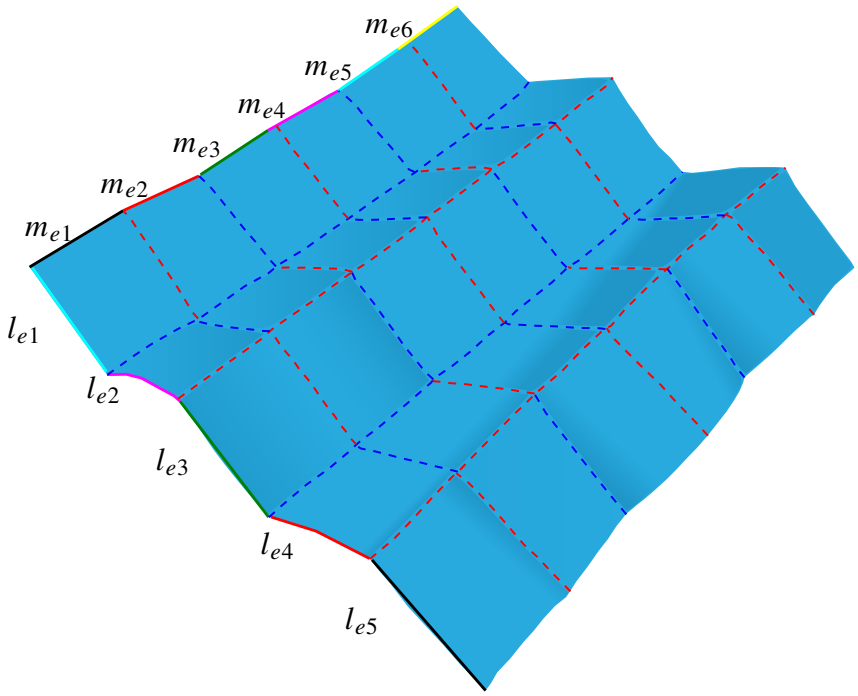

Figure 41 – l_e and m_e Edges in 6x5 Origami Pattern

All multi-loop origami with multiple vertices analyzed in this section using Equation (80) and Equation (83), produce results consistent with those obtained through the Davies Method. While these findings corroborate our proposed equations, it remains crucial to employ the Davies

method for origami analysis, as it provides proven results and offers insights into the behavior and distribution of redundant constraints.

The equation presented in this dissertation offers a precise method for calculating redundant constraints. This contribution provides a valuable tool for the field of origamis and origami-inspired mechanisms, particularly in mobility calculations.

6 CONCLUSIONS

This dissertation introduces a systematic methodology for analyzing the mobility and redundant constraints of origami using Davies' method. Unlike existing methods in the literature, this analysis identifies positions where the origami enters singular configurations, thereby impacting its mobility. Drawing upon screw theory, graph theory, and the principle of virtual work, the analysis is applied to a single degree-4-vertex origami in three fundamental states: fully open, partially open, and fully closed. The study accurately identifies specific singular positions of origami patterns, crucial for enhancing the understanding of their kinematic behavior. Moreover, for the first time, the Davies method has been adapted for origami analysis, facilitated by a novel methodology presented herein. This adaptation extends the method's applicability, allowing for the calculation of mobility and the number of redundant constraints. This advancement significantly augments the method's utility and versatility in the domain of origami-based mechanisms. Taken together, these findings provide a robust foundation for designing origami-inspired mechanisms, deepening the understanding of their characteristics, and opening up new avenues for their application across diverse fields.

The application of the Davies method to multi-loop origamis with multiple vertices allowed for the calculation of their mobility and redundant constraints. Notably, it was observed that while the screw system for each vertex is spherical, patterns with more than one vertex necessitate analysis with the spatial screw system. Moreover, this investigation revealed that all vertices exhibit similar kinematic behavior, with constraints per vertex comprising forces in the three rectangular components. In instances of redundant constraints, these manifest as a moment around the O_z axis.

The study also revealed that the sequence in which facets are named in the functional representation of origamis influences the direction of arrows in the spanning tree and, consequently, its symmetry. Combined with appropriate edge selection in the motion graph, this influence leads to more organized responses. In essence, Symmetric spanning trees, both in terms of topology and orientation, yield more structured results compared to asymmetric graphs. This observation also led to the identification of equivalent systems, highlighting the possibility of rearranging joint types in origami structures to achieve varied mechanical behaviors.

In chapter 5, two equations are proposed: one for calculating redundant constraints and another for defining the mobility of rectangular origamis with multi-loops and multiple vertices. The origami pattern must obey the bird´s foot condition. These equations were explained and validated using examples of origami patterns.

6.1 FUTURE WORK

Future works on this dissertation include:

- In this work, we analyzed the origami patterns with rectangular shape, the same method can be used to analyze other patterns such as Water Bomb, Tachi-Miura, etc.

- Use the equations proposed in this work to perform number synthesis of origami-inspired mechanisms.
- Analyzing the kinematics of rectangular origamis using the Davies method, but with a different approach, now considering the vertices as spherical joints.
- Carry out the dimensional synthesis of origami, investigating how origami structures with specific properties can be designed and manufactured through the manipulation of their dimensions.

6.2 PUBLISHED AND SUBMITTED PAPERS

This work yielded a paper for a conference:

- PINZON CUTA, Carlos; NUÑEZ, Neider Nadid Romero; de SOUZA, Marina Baldissera; ZHAO, Jing-Shan: MARTINS, Daniel. On the Singularity Analysis of Origami Using Graph and Screw Theories. 6th IEEE/IFToMM International Conference on Reconfigurable Mechanisms and Robots ReMAR, [S. l.], p. 1-8, 23 Jun. 2024.

REFERENCES

BALL, Robert Stawell. **A Treatise on the Theory of Screws**. [S.l.]: Cambridge university press, 1998.

BARRETO, Rodrigo Luis Pereira et al. Multiloop origami inspired spherical mechanisms. **Mechanism and Machine Theory**, v. 155, p. 104063, Jan. 2021. DOI: 10.1016/j.mechmachtheory.2020.104063.

BLANDING, Douglass L. Using exact constraint to design flexure mechanisms. In: AMERICAN SOCIETY OF MECHANICAL ENGINEERS. ASME International Mechanical Engineering Congress and Exposition. [S.l.: s.n.], 2000. P. 849–854.

BOWEN, Landen A. et al. A classification of action origami as systems of spherical mechanisms. **Journal of Mechanical Design, Transactions of the ASME**, v. 135, 11 2013. ISSN 10500472. DOI: 10.1115/1.4025379.

BROWN, Nathan C. et al. Approaches for Minimizing Joints in Single-Degree-of-Freedom Origami-Based Mechanisms. **Journal of Mechanical Design**, ASME International, v. 144, 10 Oct. 2022. ISSN 1050-0472. DOI: 10.1115/1.4054633.

CARBONI, Andrea Piga et al. Análise de mecanismos com restrições redundantes através da aplicação da teoria de matroides, 2015.

CAZANGI, Humberto Reder et al. Aplicação do método de Davies para análise cinemática e estática de mecanismos com múltiplos graus de liberdade. Florianópolis, SC, 2008.

CHEN, Yao; FENG, Jian; LIU, Yangqing. A group-theoretic approach to the mobility and kinematic of symmetric over-constrained structures. **Mechanism and Machine Theory**, Elsevier Ltd, v. 105, p. 91–107, Nov. 2016. ISSN 0094114X. DOI: 10.1016/j.mechmachtheory.2016.06.004.

DAI, J. S.; JONES, J. Rees. Mobility in Metamorphic Mechanisms of Foldable/Erectable Kinds. **Journal of Mechanical Design**, v. 121, p. 375–382, 3 Sept. 1999. ISSN 1050-0472. DOI: 10.1115/1.2829470.

DAI, Jian S. Euler-Rodrigues formula variations, quaternion conjugation and intrinsic connections. **Mechanism and Machine Theory**, Elsevier Ltd, v. 92, p. 144–152, May 2015. ISSN 0094114X. DOI: 10.1016/j.mechmachtheory.2015.03.004.

DAVIES, TH. Freedom and constraint in coupling networks. **Proceedings of the Institution of Mechanical Engineers, Part C: Journal of Mechanical Engineering Science**, SAGE Publications Sage UK: London, England, v. 220, n. 7, p. 989–1010, 2006.

DUREISSEIX, David. An overview of mechanisms and patterns with origami. **International Journal of Space Structures**, SAGE Publications Sage UK: London, England, v. 27, n. 1, p. 1–14, 2012.

HATORI, Koshiro. History of Origami in the East and the West before Interfusion. **Origami**, v. 5, p. 3–11, 2011.

HOPKINS, Jonathan Brigham. **Design of parallel flexure systems via freedom and constraint topologies (FACT)**. 2007. PhD thesis – Massachusetts Institute of Technology.

HUANG, Zhen; LIU, JingFang; ZENG, DaXing. A general methodology for mobility analysis of mechanisms based on constraint screw theory. **Science in China Series E: Technological Sciences**, Springer, v. 52, n. 5, p. 1337–1347, 2009.

HULL, Thomas. The combinatorics of flat folds: a survey. In: THIRD International Meeting of Origami Science. [S.l.: s.n.], 2002. P. 29–38.

HUNT, Kenneth Henderson. Kinematic geometry of mechanisms, 1978.

KIM, Woongbae; EOM, Jaemin; CHO, Kyu-Jin. A Dual-Origami Design that Enables the Quasisequential Deployment and Bending Motion of Soft Robots and Grippers. **Advanced Intelligent Systems**, v. 4, p. 2100176, 3 Mar. 2022. ISSN 2640-4567. DOI: 10.1002/aisy.202100176.

LANG, Robert J. **Twists, tilings, and tessellations: Mathematical methods for geometric origami**. [S.l.]: AK Peters/CRC Press, 2017.

LANG, Robert J et al. A review of thickness-accommodation techniques in origami-inspired engineering. **Applied Mechanics Reviews**, American Society of Mechanical Engineers Digital Collection, v. 70, n. 1, 2018.

LIMA, Taynah Barbosa Brandão et al. Conceptual design of origami endoprosthesis and its delivery system, 2021.

LIU, Chenying; YOU, Zhong; MAIOLINO, Perla. Kinematics of an Origami Inspired Millipede Robot. **Volume 7: 46th Mechanisms and Robotics Conference (MR)**, 2022.

MARTINS, Daniel; MURAI, Estevan Hideki. **Mecanismos: síntese e análise com aplicações em robótica**. [S.l.: s.n.], June 2020. P. 59–60. ISBN 9788532808462.

MELONI, Marco M. et al. Engineering Origami: A Comprehensive Review of Recent Applications, Design Methods, and Tools. **Advanced Science**, v. 8, 2021.

PENG, Rui; MA, Jiayao; CHEN, Yan. The effect of mountain-valley folds on the rigid foldability of double corrugated pattern. **Mechanism and Machine Theory**, Elsevier Ltd, v. 128, p. 461–474, Oct. 2018. ISSN 0094114X. DOI: 10.1016/j.mechmachtheory.2018.06.012.

PERAZA-HERNANDEZ, Edwin A et al. Origami-inspired active structures: a synthesis and review. **Smart Materials and Structures**, IOP Publishing, v. 23, n. 9, p. 094001, 2014.

SAREH, Pooya; GUEST, Simon D. Design of isomorphic symmetric descendants of the Miura-ori. **Smart Materials and Structures**, IOP Publishing, v. 24, n. 8, p. 085001, 2015. DOI: doi.org/10.1088/0964-1726/24/8/085001.

SIMONI, R.; CARBONI, A. P.; MARTINS, D. Enumeration of kinematic chains and mechanisms. **Proceedings of the Institution of Mechanical Engineers, Part C: Journal of Mechanical Engineering Science**, v. 223, p. 1017–1024, 4 Apr. 2009. ISSN 09544062. DOI: 10.1243/09544062JMES1071.

SOUZA, Marina Baldissera de et al. Powertrain optimization of hybrid and electric vehicles, 2023.

TACHI, Tomohiro. Generalization of rigid-foldable quadrilateral-mesh origami. **Journal of the International Association for Shell and Spatial Structures**, International Association for Shell and Spatial Structures (IASS), v. 50, n. 3, p. 173–179, 2009.

TACHI, Tomohiro. Geometric considerations for the design of rigid origami structures. In: ELSEVIER LTD SHANGHAI, CHINA, 10. PROCEEDINGS of the International Association for Shell and Spatial Structures (IASS) Symposium. [S.l.: s.n.], 2010. P. 458–460.

WEI, Guowu; CHEN, Yao; DAI, Jian S. Synthesis, mobility, and multifurcation of deployable polyhedral mechanisms with radially reciprocating motion. **Journal of Mechanical Design, Transactions of the ASME**, American Society of Mechanical Engineers (ASME), v. 136, 9 2014. ISSN 10500472. DOI: 10.1115/1.4027638.

WEI, Guowu; DING, Xilun; DAI, Jian S. Mobility and geometric analysis of the Hoberman switch-pitch ball and its variant. **Journal of Mechanisms and Robotics**, v. 2, 3 Aug. 2010. ISSN 19424302. DOI: 10.1115/1.4001730.

WILCOX, Eric W. **Design Considerations in the Development and Actuation of Origami-Based Mechanisms**. [S.l.]: Brigham Young University, 2014.

YU, Hongying; GUO, Zhen; WANG, Junru. A method of calculating the degree of freedom of foldable plate rigid origami with adjacency matrix. **Advances in Mechanical Engineering**, SAGE Publications Sage UK: London, England, v. 10, n. 6, p. 1687814018779696, 2018.

YUE, Songlin. A Review of Origami-Based Deployable Structures in Aerospace Engineering. v. 2459, n. 1, p. 012137, 2023.

Appendix

APPENDIX A – ORIGAMI PATTERNS

A.1 3X4 SHAPED ORIGAMI

The origami array composed of 3 rows and 4 columns is shown in Figure 42. This pattern has 12 facets, 17 creases, and 6 vertices.

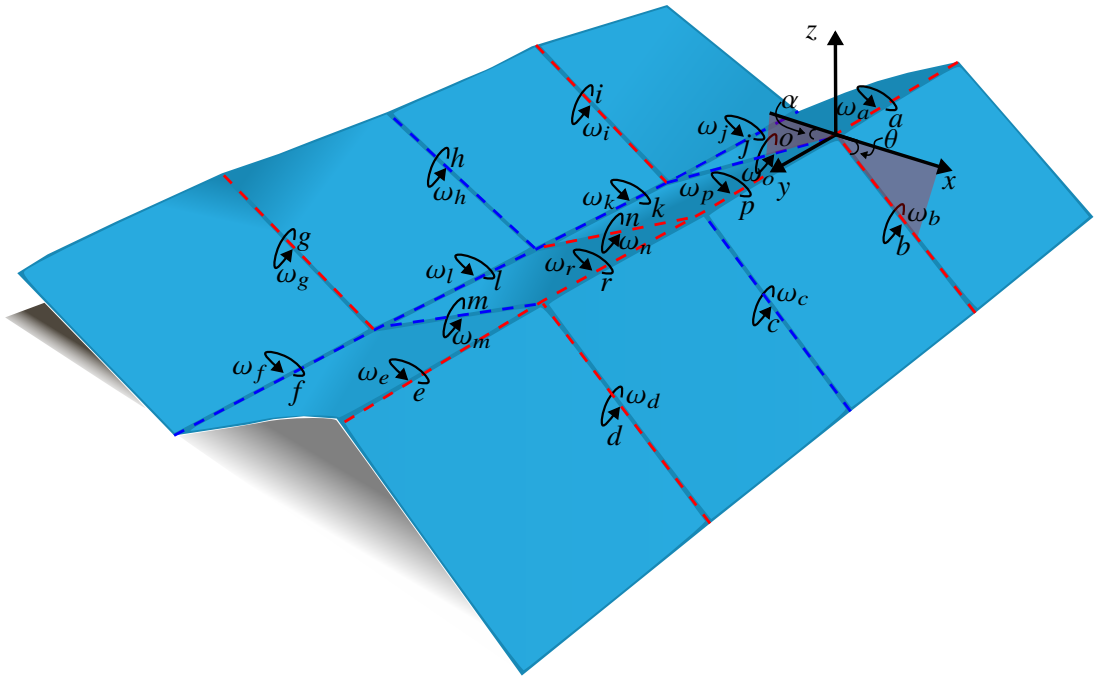

Figure 42 – 3x4 Shaped Origami

The direction vectors of this array are shown in the Equation (84).

$$\vec{S}_m^M = \begin{Bmatrix} \cos\alpha \\ 0 \\ \sin\alpha \end{Bmatrix} \quad \textit{for t= m, n and o;} \quad \vec{S}_n^M = \begin{Bmatrix} \cos\theta \\ 0 \\ -\sin\theta \end{Bmatrix} \quad \textit{for n= b, c, d, g, h and i}$$
$$\vec{S}_y^M = \begin{Bmatrix} 0 \\ 1 \\ 0 \end{Bmatrix} \quad \textit{for a, e, f, j, k, l p and r} \tag{84}$$

The distance between origami vertices was considered to be 2 units, and the position vectors are:

$$\vec{S}_{0_b} = \begin{Bmatrix} 0 \\ 0 \\ 0 \end{Bmatrix} \quad ; \quad \vec{S}_{0_c} = \begin{Bmatrix} 0 \\ 2 \\ 0 \end{Bmatrix} \quad ; \quad \vec{S}_{0_d} = \begin{Bmatrix} 0 \\ 4 \\ 0 \end{Bmatrix} \quad ; \quad \vec{S}_{0_i} = \begin{Bmatrix} -2\cos\alpha \\ 0 \\ -2\sin\alpha \end{Bmatrix}$$
$$\vec{S}_{0_h} = \begin{Bmatrix} -2\cos\alpha \\ 2 \\ -2\sin\alpha \end{Bmatrix} \quad ; \quad \vec{S}_{0_g} = \begin{Bmatrix} -2\cos\alpha \\ 4 \\ -2\sin\alpha \end{Bmatrix} \tag{85}$$

where $\vec{S}_{0_b}$ is the position of the *a, b and p*; $\vec{S}_{0_c}$ represents the position of the joints passing through the spherical center *c*, while the $\vec{S}_{0_d}$ is the position vector of *d and e*; $\vec{S}_{0_g}$ indicates the position of the kinematic pairs *f, g and m*, for other hand, *h, k, l and n* Couplings are through $\vec{S}_{0_h}$ position vector, and the position vector $\vec{S}_{0_i}$ belongs to the couplings *i, j and o*.

Coupling twist are shown in Equation (86)

$$\$_a^M = \begin{pmatrix} 0 \\ \omega_a \\ 0 \\ \cdots \\ 0 \\ 0 \\ 0 \end{pmatrix}; \quad \$_b^M = \begin{pmatrix} \omega_b\cos\theta \\ 0 \\ -\omega_b\sin\theta \\ \cdots \\ 0 \\ 0 \\ 0 \end{pmatrix}; \quad \$_c^M = \begin{pmatrix} \omega_c\cos\theta \\ 0 \\ -\omega_c\sin\theta \\ \cdots \\ -2\omega_c\sin\theta \\ 0 \\ -2\omega_c\cos\theta \end{pmatrix}; \quad \$_d^M = \begin{pmatrix} \omega_d\cos\theta \\ 0 \\ \omega_d\sin\theta \\ \cdots \\ -4\omega_d\sin\theta \\ 0 \\ -4\omega_d\cos\theta \end{pmatrix}; \quad \$_e^M = \begin{pmatrix} 0 \\ \omega_e \\ 0 \\ \cdots \\ 0 \\ 0 \\ 0 \end{pmatrix}$$
$$\$_f^M = \begin{pmatrix} 0 \\ \omega_f \\ 0 \\ \cdots \\ 2\omega_f\sin\alpha \\ 0 \\ -2\omega_f\cos\alpha \end{pmatrix}; \quad \$_g^M = \begin{pmatrix} \omega_g\cos\theta \\ 0 \\ -\omega_g\sin\theta \\ \cdots \\ -4\omega_g\sin\theta \\ -2\omega(\cos\alpha\sin\theta + \sin\alpha\cos\theta) \\ -4\omega_g\cos\alpha \end{pmatrix}; \quad \$_h^M = \begin{pmatrix} \omega_h\cos\theta \\ 0 \\ -\omega_h\sin\theta \\ \cdots \\ -2\omega_h\sin\theta \\ -2\omega_h(\cos\alpha\sin\theta + \sin\alpha\cos\theta) \\ -2\omega_h\cos\theta \end{pmatrix}$$
$$\$_i^M = \begin{pmatrix} \omega_i\cos\theta \\ 0 \\ -\omega_i\sin\theta \ \cdots \\ 0 \\ -2\omega_i(\cos\alpha\sin\theta + \sin\alpha\cos\theta) \\ 0 \end{pmatrix}; \quad \$_j^M = \begin{pmatrix} 0 \\ \omega_j \\ 0 \\ \cdots \\ 2\omega_j\sin\alpha \\ 0 \\ -2\omega_j\cos\alpha \end{pmatrix}; \quad \$_k^M = \begin{pmatrix} 0 \\ \omega_k \\ 0 \\ \cdots \\ 2\omega_k\sin\alpha \\ 0 \\ -2\omega_k\cos\alpha \end{pmatrix} \tag{86}$$
$$\$_l^M = \begin{pmatrix} 0 \\ \omega_l \\ 0 \\ \cdots \\ 2\omega_l\sin\alpha \\ 0 \\ -2\omega_l\cos\alpha \end{pmatrix}; \quad \$_m^M = \begin{pmatrix} \omega_m\cos\alpha \\ 0 \\ \omega_m\sin\alpha \\ \cdots \\ 4\omega_m\sin\alpha \\ 0 \\ -4\omega_m\cos\alpha \end{pmatrix}; \quad \$_n^M = \begin{pmatrix} \omega_n\cos\alpha \\ 0 \\ \omega_n\sin\alpha \\ \cdots \\ 2\omega_n\sin\alpha \\ 0 \\ -2\omega_n\cos\alpha \end{pmatrix}; \quad \$_o^M = \begin{pmatrix} \omega_o\cos\alpha \\ 0 \\ \omega_o\sin\alpha \\ \cdots \\ 0 \\ 0 \\ 0 \end{pmatrix}$$
$$\$_p^M = \begin{pmatrix} 0 \\ \omega_p \\ 0 \\ \cdots \\ 0 \\ 0 \\ 0 \end{pmatrix}; \quad \$_r^M = \begin{pmatrix} 0 \\ \omega_r \\ 0 \\ \cdots \\ 0 \\ 0 \\ 0 \end{pmatrix}$$

The spanning tree is:

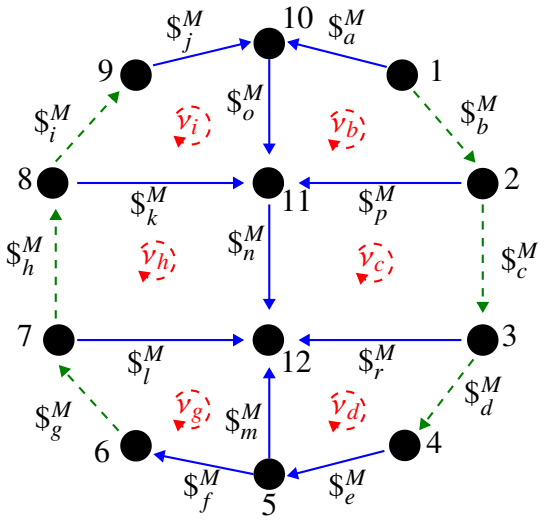

Figure 43 – Spanning Tree 3x4-shaped Origami-hold

Then, the circuit matrix for this pattern is:

$$[B_M]_{6\times 17} =$$

$$\begin{array}{c} \begin{matrix} b & c & d & g & h & i & a & e & f & j & k & l & m & n & o & p & r \end{matrix} \\ \begin{bmatrix} 1 & 0 & 0 & 0 & 0 & 0 & -1 & 0 & 0 & 0 & 0 & 0 & 0 & 0 & -1 & 1 & 0 \\ 0 & 1 & 0 & 0 & 0 & 0 & 0 & 0 & 0 & 0 & 0 & 0 & 0 & -1 & 0 & -1 & 1 \\ 0 & 0 & 1 & 0 & 0 & 0 & 0 & 1 & 0 & 0 & 0 & 0 & -1 & 0 & 0 & 0 & -1 \\ 0 & 0 & 0 & 1 & 0 & 0 & 0 & 0 & 1 & 0 & 0 & 1 & -1 & 0 & 0 & 0 & 0 \\ 0 & 0 & 0 & 0 & 1 & 0 & 0 & 0 & 0 & 0 & 1 & -1 & 0 & 1 & 0 & 0 & 0 \\ 0 & 0 & 0 & 0 & 0 & 1 & 0 & 0 & 0 & 1 & -1 & 0 & 0 & 0 & 1 & 0 & 0 \end{bmatrix} \end{array} \begin{matrix} v_b \\ v_c \\ v_d \\ v_g \\ v_h \\ v_i \end{matrix} \tag{87}$$

The $[\hat{M}_N]$ is:

$$[\hat{M}_N]_{36\times12} =$$

$$\begin{bmatrix}
c\theta & 0 & 0 & 0 & 0 & 0 & 0 & 0 & 0 & 0 & 0 & 0 & 0 & 0 & -c\theta & 0 & 0 \\
0 & 0 & 0 & 0 & 0 & 0 & -1 & 0 & 0 & 0 & 0 & 0 & 0 & 0 & 0 & 1 & 0 \\
-s\theta & 0 & 0 & 0 & 0 & 0 & 0 & 0 & 0 & 0 & 0 & 0 & 0 & 0 & -s\theta & 0 & 0 \\
0 & 0 & 0 & 0 & 0 & 0 & 0 & 0 & 0 & 0 & 0 & 0 & 0 & 0 & 0 & 0 & 0 \\
0 & 0 & 0 & 0 & 0 & 0 & 0 & 0 & 0 & 0 & 0 & 0 & 0 & 0 & 0 & 0 & 0 \\
0 & 0 & 0 & 0 & 0 & 0 & 0 & 0 & 0 & 0 & 0 & 0 & 0 & 0 & 0 & 0 & 0 \\
0 & c\theta & 0 & 0 & 0 & 0 & 0 & 0 & 0 & 0 & 0 & 0 & 0 & -c\theta & 0 & 0 & 0 \\
0 & 0 & 0 & 0 & 0 & 0 & 0 & 0 & 0 & 0 & 0 & 0 & 0 & 0 & 0 & -1 & 1 \\
0 & -s\theta & 0 & 0 & 0 & 0 & 0 & 0 & 0 & 0 & 0 & 0 & 0 & -s\theta & 0 & 0 & 0 \\
0 & -2\,s\theta & 0 & 0 & 0 & 0 & 0 & 0 & 0 & 0 & 0 & 0 & 0 & -2\,s\theta & 0 & 0 & 0 \\
0 & 0 & 0 & 0 & 0 & 0 & 0 & 0 & 0 & 0 & 0 & 0 & 0 & 0 & 0 & 0 & 0 \\
0 & -2\,c\theta & 0 & 0 & 0 & 0 & 0 & 0 & 0 & 0 & 0 & 0 & 0 & 2\,c\theta & 0 & 0 & 0 \\
0 & 0 & c\theta & 0 & 0 & 0 & 0 & 0 & 0 & 0 & 0 & 0 & -c\theta & 0 & 0 & 0 & 0 \\
0 & 0 & 0 & 0 & 0 & 0 & 0 & 1 & 0 & 0 & 0 & 0 & 0 & 0 & 0 & 0 & -1 \\
0 & 0 & -s\theta & 0 & 0 & 0 & 0 & 0 & 0 & 0 & 0 & 0 & -s\theta & 0 & 0 & 0 & 0 \\
0 & 0 & -4\,s\theta & 0 & 0 & 0 & 0 & 0 & 0 & 0 & 0 & 0 & -4\,s\theta & 0 & 0 & 0 & 0 \\
0 & 0 & 0 & 0 & 0 & 0 & 0 & 0 & 0 & 0 & 0 & 0 & 0 & 0 & 0 & 0 & 0 \\
0 & 0 & -4\,c\theta & 0 & 0 & 0 & 0 & 0 & 0 & 0 & 0 & 0 & 4\,c\theta & 0 & 0 & 0 & 0 \\
0 & 0 & 0 & c\theta & 0 & 0 & 0 & 0 & 0 & 0 & 0 & 0 & -c\theta & 0 & 0 & 0 & 0 \\
0 & 0 & 0 & 0 & 0 & 0 & 0 & 0 & -c\beta & 0 & 0 & 1 & 0 & 0 & 0 & 0 & 0 \\
0 & 0 & 0 & -s\theta & 0 & 0 & 0 & 0 & s\beta & 0 & 0 & 0 & -s\theta & 0 & 0 & 0 & 0 \\
0 & 0 & 0 & -4\,s\theta & 0 & 0 & 0 & 0 & 4\,s\beta - 2\,c\beta\,s\theta & 0 & 0 & 2\,stheta & -4\,s\theta & 0 & 0 & 0 & 0 \\
0 & 0 & 0 & -4\,c\theta\,s\theta & 0 & 0 & 0 & 0 & 2\,s\beta\,c\theta & 0 & 0 & 0 & 0 & 0 & 0 & 0 & 0 \\
0 & 0 & 0 & -4\,c\theta & 0 & 0 & 0 & 0 & 2\,c\beta\,c\theta & 0 & 0 & -2\,c\theta & 4\,c\theta & 0 & 0 & 0 & 0 \\
0 & 0 & 0 & 0 & c\theta & 0 & 0 & 0 & 0 & 0 & 0 & 0 & 0 & c\theta & 0 & 0 & 0 \\
0 & 0 & 0 & 0 & 0 & 0 & 0 & 0 & 0 & 0 & 1 & -1 & 0 & 0 & 0 & 0 & 0 \\
0 & 0 & 0 & 0 & -s\theta & 0 & 0 & 0 & 0 & 0 & 0 & 0 & 0 & s\theta & 0 & 0 & 0 \\
0 & 0 & 0 & 0 & -2\,s\theta & 0 & 0 & 0 & 0 & 0 & 2\,s\theta & -2\,s\theta & 0 & 2\,s\theta & 0 & 0 & 0 \\
0 & 0 & 0 & 0 & -4\,c\theta\,s\theta & 0 & 0 & 0 & 0 & 0 & 0 & 0 & 0 & 0 & 0 & 0 & 0 \\
0 & 0 & 0 & 0 & -2\,c\theta & 0 & 0 & 0 & 0 & 0 & -2\,c\theta & 2\,c\theta & 0 & -2\,c\theta & 0 & 0 & 0 \\
0 & 0 & 0 & 0 & 0 & c\theta & 0 & 0 & 0 & 0 & 0 & 0 & 0 & 0 & c\theta & 0 & 0 \\
0 & 0 & 0 & 0 & 0 & 0 & 0 & 0 & 0 & c\beta & -1 & 0 & 0 & 0 & 0 & 0 & 0 \\
0 & 0 & 0 & 0 & 0 & -s\theta & 0 & 0 & 0 & s\beta & 0 & 0 & 0 & 0 & s\theta & 0 & 0 \\
0 & 0 & 0 & 0 & 0 & 0 & 0 & 0 & 0 & 2\,c\beta\,stheta & -2\,s\theta & 0 & 0 & 0 & 0 & 0 & 0 \\
0 & 0 & 0 & 0 & 0 & -4\,c\theta\,s\theta & 0 & 0 & 0 & 2\,s\beta\,c\theta & 0 & 0 & 0 & 0 & 0 & 0 & 0 \\
0 & 0 & 0 & 0 & 0 & 0 & 0 & 0 & 0 & -2\,c\beta\,c\theta & 2\,\theta & 0 & 0 & 0 & 0 & 0 & 0
\end{bmatrix} \tag{88}$$

It is obtained that the mobility is ($F_N = 1$) and the array has ($C_N = 20$) redundant constraints.

On the other hand, the pivot columns and free columns of the rref of M_N were found and the result was

$$
\begin{bmatrix}
1&0&0&0&0&0&0&0&0&0&0&0&0&0&0&0&0&0\\
0&1&0&0&0&0&0&0&0&0&0&0&0&0&0&0&0&0\\
0&0&1&0&0&0&0&0&0&0&0&0&0&0&0&0&0&0\\
0&0&0&0&0&0&1&0&0&0&0&-2&0&0&0&0&0&0\\
0&0&0&0&0&0&0&1&0&0&0&0&0&0&0&0&0&0\\
0&0&0&0&0&0&0&0&1&2&0&0&0&0&0&0&0&0\\
0&0&0&0&0&0&0&0&0&0&0&0&1&0&0&0&0&-4\\
0&0&0&0&0&0&0&0&0&0&0&0&0&1&0&0&0&0\\
0&0&0&0&0&0&0&0&0&0&0&0&0&0&1&4&0&0\\
0&0&0&0&0&0&0&0&0&0&0&0&0&0&0&0&0&0\\
0&0&0&0&0&0&0&0&0&0&0&0&0&0&0&0&0&0\\
0&0&0&0&0&0&0&0&0&0&0&0&0&0&0&0&0&0\\
0&0&0&0&0&0&0&0&0&0&0&0&0&0&0&0&0&0\\
0&0&0&0&0&0&0&0&0&0&0&0&0&0&0&0&0&0\\
0&0&0&0&0&0&0&0&0&0&0&0&0&0&0&0&0&0\\
0&0&0&0&0&0&0&0&0&0&0&0&0&0&0&0&0&0
\end{bmatrix}
\begin{bmatrix}
0&0&0&0&0&0&0&0&0&0&0&0&0&0&-\frac{s\theta}{c\theta}&0&-2s\theta&0\\
0&0&0&0&0&0&0&0&0&0&0&0&0&0&0&0&0&0\\
0&0&0&0&0&0&0&0&0&0&0&0&0&0&-1&0&-2c\theta&0\\
0&0&0&0&0&0&0&0&-\frac{s\theta}{c\theta}&-\frac{2s\theta}{c\theta}&-2s\theta&0&0&0&0&0&0&0\\
0&0&0&0&0&0&0&0&0&0&0&0&0&0&0&0&0&0\\
0&0&0&0&0&0&0&0&-1&-2&-2c\theta&0&0&0&0&0&0&0\\
0&0&0&0&0&0&0&0&0&0&0&0&0&0&-\frac{s\theta}{c\theta}&0&-2s\theta&0\\
0&0&0&0&0&0&0&0&0&0&0&0&0&0&0&0&0&0\\
0&0&0&0&0&0&0&0&0&0&0&0&0&0&-1&0&-2c\theta&0\\
1&0&0&0&-2s\theta&-4&0&0&0&0&0&0&0&0&\frac{s\theta}{c\theta}&0&2s\theta&0\\
0&1&0&2s\theta&0&-2c\theta&0&0&0&0&0&0&0&0&\frac{s\beta}{c\beta}&0&\frac{2s\beta c\theta}{c\beta}&0\\
0&0&1&4&2c\theta&0&0&0&0&0&0&0&0&0&1&0&2c\theta&0\\
0&0&0&0&0&0&1&0&-\frac{s\theta}{c\theta}&-\frac{2s\theta}{c\theta}&-4s\theta&-2&0&0&0&0&0&0\\
0&0&0&0&0&0&0&1&0&2s\theta&0&-2c\theta&0&0&\frac{s\beta}{c\beta}&0&\frac{2s\beta c\theta}{c\beta}&0\\
0&0&0&0&0&0&0&0&0&0&0&0&1&0&-\frac{s\theta}{c\theta}&0&-4s\theta&0\\
0&0&0&0&0&0&0&0&0&0&0&0&0&1&\frac{s\beta}{c\beta}&2s\theta&\frac{2s\beta c\theta}{c\beta}&-2c\theta\\
0&0&0&0&0&0&0&0&0&0&0&0&0&0&0&0&0&0
\end{bmatrix}
\begin{bmatrix}
R_1&S_1&T_1&U_1&V_1&W_1&\cdots&R_6&S_6&T_6&U_6&V_6&W_6
\end{bmatrix}^T_{36\times1}
= \begin{bmatrix} 0&0&0&0&\cdots&0&0&0&0&0 \end{bmatrix}^T_{17\times1}
\tag{89}
$$

The restrictions per loop are:

$$
\begin{aligned}
\hat{\$}^a = \Big[\ & 0\ \ 0\ \ 0\ \ U_1\ \ V_1\ \ W_1\ \ 0\ \ 0\ \ 0\ \ U_2\ \ V_2\ \ W_2\ \ 0\ \ 0\ \ 0\ \ U_3\ \ V_3\ \ W_3\ \ \dots \\
& \dots\ 0\ \ 0\ \ T_4\ \ U_4\ \ V_4\ \ W_4\ \ 0\ \ 0\ \ T_5\ \ U_5\ \ V_5\ \ W_5\ \ 0\ \ 0\ \ T_6\ \ U_6\ \ V_6\ \ W_6\ \Big]
\end{aligned}
\tag{90}
$$

The redundant constraints acting on the 3x4 Origami are shown in Figure 44 .

A.2 4X4 ORIGAMI

4X4 origami is a arrangement that has 16 faces (n=16), 24 creases and 9 vertex. This is shown in Figure 45. Thenmore, is we can obtain the direction vector of screw, as is seen in Equation (91).

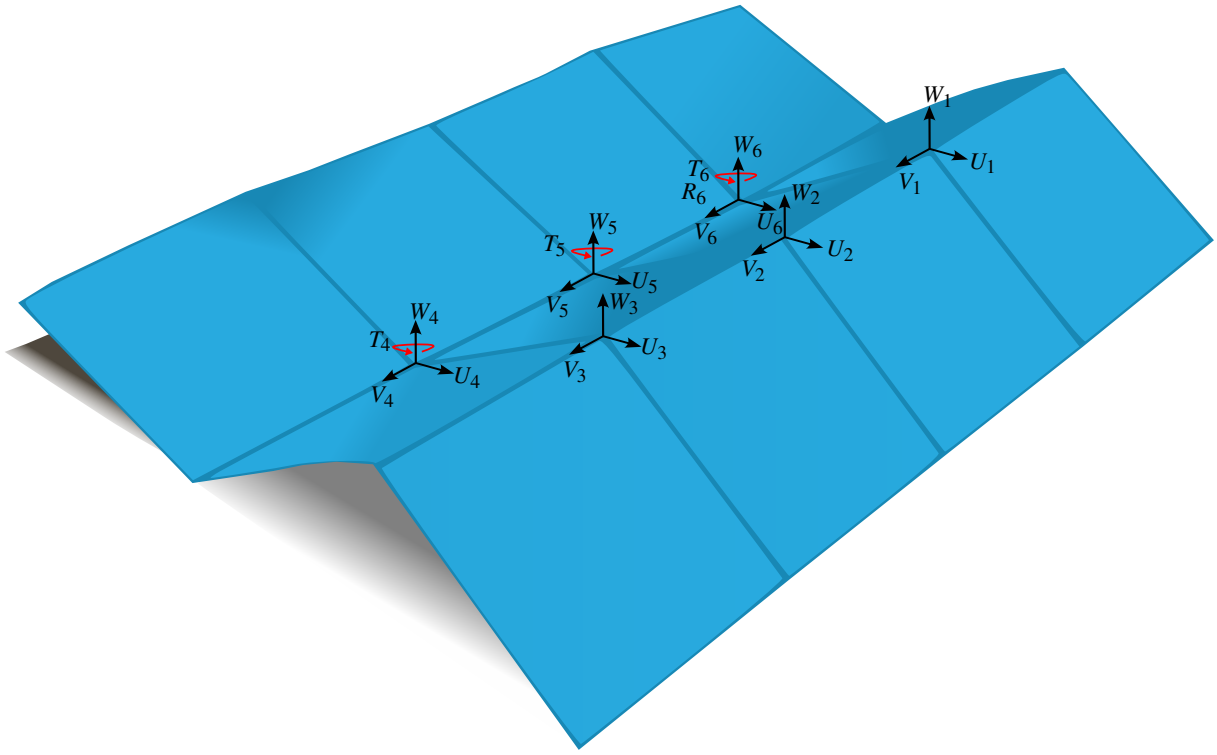

Figure 44 – 3x4 Shaped Origami actions

$$\vec{S}_m^M = \begin{Bmatrix} \cos\alpha \\ 0 \\ \sin\alpha \end{Bmatrix} \quad \textit{for t= m, n, o, t, v and x;} \quad \vec{S}_n^M = \begin{Bmatrix} \cos\theta \\ 0 \\ -\sin\theta \end{Bmatrix} \quad \textit{for n= b, c, d, g, h and i}$$
$$\vec{S}_y^M = \begin{Bmatrix} 0 \\ 1 \\ 0 \end{Bmatrix} \quad \textit{for a, e, f, j, k, l p, r, s, u, w and y} \tag{91}$$

For other hand, The position vector are:

$$\vec{S}_{0_b} = \begin{Bmatrix} 0 \\ 0 \\ 0 \end{Bmatrix} \; ; \quad \vec{S}_{0_c} = \begin{Bmatrix} 0 \\ 2 \\ 0 \end{Bmatrix} \; ; \quad \vec{S}_{0_d} = \begin{Bmatrix} 0 \\ 4 \\ 0 \end{Bmatrix} \; ; \quad \vec{S}_{0_i} = \begin{Bmatrix} -2\cos\alpha \\ 0 \\ -2\sin\alpha \end{Bmatrix}$$
$$\vec{S}_{0_h} = \begin{Bmatrix} -2\cos\alpha \\ 2 \\ -2\sin\alpha \end{Bmatrix} \; ; \quad \vec{S}_{0_g} = \begin{Bmatrix} -2\cos\alpha \\ 4 \\ -2\sin\alpha \end{Bmatrix} ; \quad \vec{S}_{0_t} = \begin{Bmatrix} -2(\cos\alpha + \cos\theta) \\ 0 \\ 0 \end{Bmatrix} \tag{92}$$
$$\vec{S}_{0_v} = \begin{Bmatrix} -2(\cos\alpha + \cos\theta) \\ 2 \\ 0 \end{Bmatrix} ; \quad \vec{S}_{0_x} = \begin{Bmatrix} -2(\cos\alpha + \cos\theta) \\ 4 \\ 0 \end{Bmatrix}$$

The spanning tree is shown in Figure 46. Consequently, the circuit matrix for this patron is:

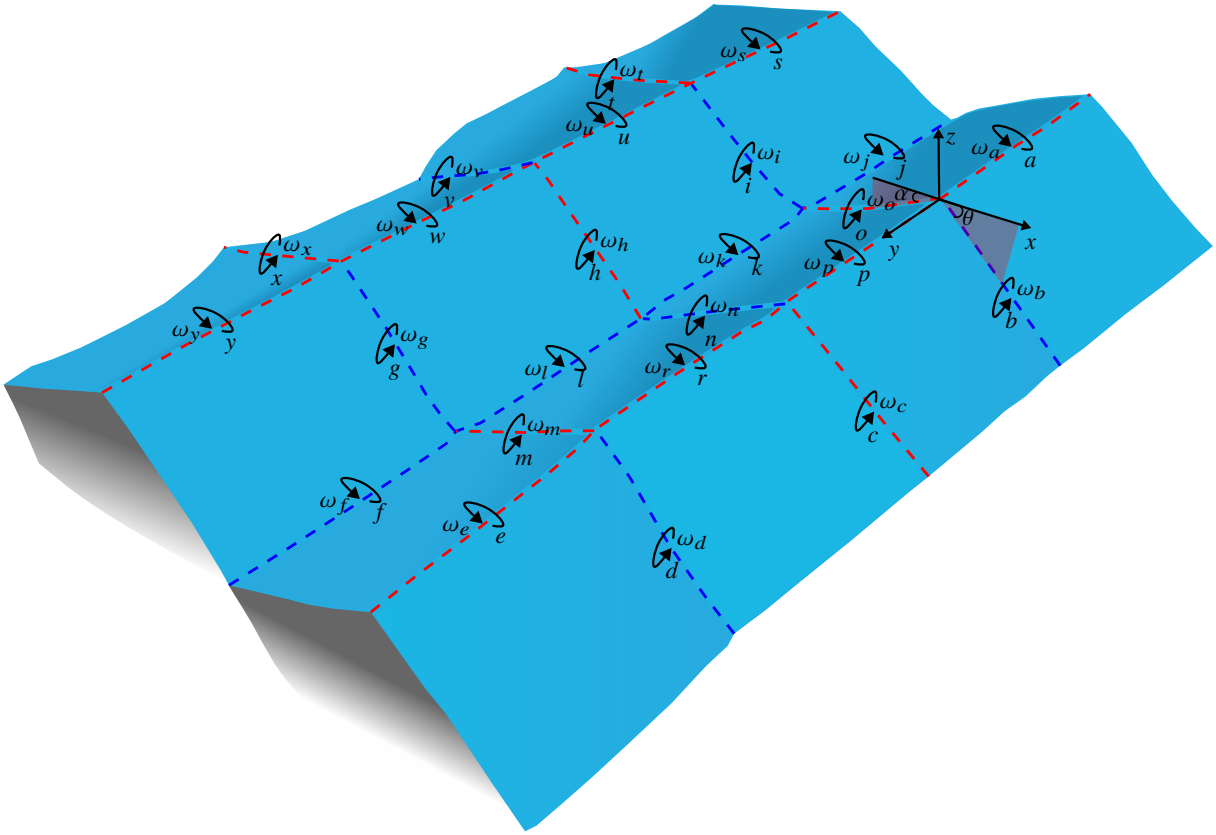

Figure 45 – 4x4 Shaped Origami

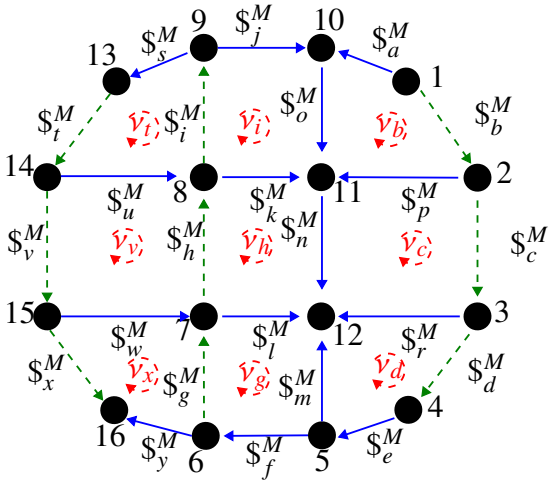

Figure 46 – Spanning Tree 4x4-shaped Origami-hold

$$
[B_M]_{6\times 24} =
$$

	b	c	d	g	h	i	t	v	x	a	e	f	j	k	l	m	n	o	p	r	s	u	w	y	
	1	0	0	0	0	0	0	0	0	−1	0	0	0	0	0	0	0	−1	1	0	0	0	0	0	b
	0	1	0	0	0	0	0	0	0	0	0	0	0	0	0	0	−1	0	−1	1	0	0	0	0	c
	0	0	1	0	0	0	0	0	0	0	1	0	0	0	0	−1	0	0	0	−1	0	0	0	0	d
	0	0	0	1	0	0	0	0	0	0	0	1	0	0	1	−1	0	0	0	0	0	0	0	0	g
	0	0	0	0	1	0	0	0	0	0	0	0	0	1	−1	0	1	0	0	0	0	0	0	0	h
	0	0	0	0	0	1	0	0	0	0	0	0	1	−1	0	0	0	1	0	0	0	0	0	0	i
	0	0	0	0	0	0	1	0	0	0	0	0	−1	1	0	0	0	−1	0	0	1	1	0	0	t
	0	0	0	0	1	0	0	0	0	0	0	0	0	−1	1	0	−1	0	0	0	0	−1	1	0	v
	0	0	0	1	0	0	0	0	0	0	0	−1	0	0	−1	1	0	0	0	0	0	0	−1	−1	x

(93)

The twist per joint are shown in Equation (94).

$$
\$_a^M = \begin{pmatrix} 0 \\ \omega_a \\ 0 \\ \cdots \\ 0 \\ 0 \\ 0 \end{pmatrix}; \quad \$_b^M = \begin{pmatrix} \omega_b \cos\theta \\ 0 \\ -\omega_b \sin\theta \\ \cdots \\ 0 \\ 0 \\ 0 \end{pmatrix}; \quad \$_c^M = \begin{pmatrix} \omega_c \cos\theta \\ 0 \\ -\omega_c \sin\theta \\ \cdots \\ -2\omega_c \sin\theta \\ 0 \\ -2\omega_c \cos\theta \end{pmatrix}; \quad \$_d^M = \begin{pmatrix} \omega_d \cos\theta \\ 0 \\ \omega_d \sin\theta \\ \cdots \\ -4\omega_d \sin\theta \\ 0 \\ -4\omega_d \cos\theta \end{pmatrix}; \quad \$_e^M = \begin{pmatrix} 0 \\ \omega_e \\ 0 \\ \cdots \\ 0 \\ 0 \\ 0 \end{pmatrix}
$$

$$
\$_f^M = \begin{pmatrix} 0 \\ -\omega_f \cos\beta \\ \omega_f \sin\beta \\ \cdots \\ 2\omega_f(2\sin\beta - \cos\beta\sin\theta) \\ 2\omega_f \sin\beta\cos\theta \\ 2\omega_f \cos\beta\cos\theta \end{pmatrix}; \quad \$_g^M = \begin{pmatrix} \omega_g \cos\theta \\ 0 \\ -\omega_g \sin\theta \\ \cdots \\ -4\omega_g \sin\theta \\ -4\omega_g \cos\theta\sin\theta \\ -4\omega_g \cos\theta \end{pmatrix}; \quad \$_h^M = \begin{pmatrix} \omega_h \cos\theta \\ 0 \\ -\omega_h \sin\theta \\ \cdots \\ -2\omega_h \sin\theta \\ -4\omega_h \cos\theta\sin\theta \\ -2\omega_h \cos\theta \end{pmatrix}
$$

$$
\$_i^M = \begin{pmatrix} \omega_i \cos\theta \\ 0 \\ -\omega_i \sin\theta \ \cdots \\ 0 \\ -4\omega_i \cos\theta\sin\theta \\ 0 \end{pmatrix}; \quad \$_j^M = \begin{pmatrix} 0 \\ \omega_j \cos\beta \\ \omega_j \sin\beta \\ \cdots \\ 2\omega_j \sin\theta\cos\beta \\ 2\omega_j \cos\theta\sin\beta \\ -2\omega_j \cos\theta\cos\beta \end{pmatrix}; \quad \$_k^M = \begin{pmatrix} 0 \\ \omega_k \\ 0 \\ \cdots \\ 2\omega_k \sin\theta \\ 0 \\ -2\omega_k \cos\theta \end{pmatrix}
$$

$$
\$_l^M = \begin{pmatrix} 0 \\ \omega_l \\ 0 \\ \cdots \\ 2\omega_l \sin\theta \\ 0 \\ -2\omega_l \cos\theta \end{pmatrix}; \quad \$_m^M = \begin{pmatrix} \omega_m \cos\theta \\ 0 \\ \omega_m \sin\theta \\ \cdots \\ 4\omega_m \sin\theta \\ 0 \\ -4\omega_m \cos\theta \end{pmatrix}; \quad \$_n^M = \begin{pmatrix} \omega_n \cos\theta \\ 0 \\ \omega_n \sin\theta \\ \cdots \\ 2\omega_n \sin\theta \\ 0 \\ -2\omega_n \cos\theta \end{pmatrix}; \quad \$_o^M = \begin{pmatrix} \omega_o \cos\theta \\ 0 \\ \omega_o \sin\theta \\ \cdots \\ 0 \\ 0 \\ 0 \end{pmatrix}
$$

$$
\$_p^M = \begin{pmatrix} 0 \\ \omega_p \\ 0 \\ \cdots \\ 0 \\ 0 \\ 0 \end{pmatrix}; \quad \$_r^M = \begin{pmatrix} 0 \\ \omega_r \\ 0 \\ \cdots \\ 0 \\ 0 \\ 0 \end{pmatrix}; \quad \$_s^M = \begin{pmatrix} 0 \\ \omega_s \\ 0 \\ \cdots \\ 0 \\ 0 \\ -4\omega_s \cos\theta \end{pmatrix}; \quad \$_t^M = \begin{pmatrix} \omega_t \cos\theta \\ 0 \\ \omega_t \sin\theta \\ \cdots \\ 0 \\ 4\omega_t \cos\theta\sin\theta \\ 0 \end{pmatrix}; \quad \$_u^M = \begin{pmatrix} 0 \\ \omega_u \\ 0 \\ \cdots \\ 0 \\ 0 \\ -4\omega_u \cos\theta \end{pmatrix}
$$

$$
\$_v^M = \begin{pmatrix} \omega_v \cos\theta \\ 0 \\ \omega_v \sin\theta \\ \cdots \\ 2\omega_v \sin\theta \\ 4\omega_v \cos\theta\sin\theta \\ -2\omega_v \cos\theta \end{pmatrix}; \quad \$_w^M = \begin{pmatrix} 0 \\ \omega_w \\ 0 \\ \cdots \\ 0 \\ 0 \\ -4\omega_w \cos\theta \end{pmatrix}; \quad \$_x^M = \begin{pmatrix} \omega_x \cos\theta \\ 0 \\ \omega_x \sin\theta \\ \cdots \\ 4\omega_x \sin\theta \\ 4\omega_x \cos\theta\sin\theta \\ -4\omega_x \cos\theta \end{pmatrix}; \quad \$_y^M = \begin{pmatrix} 0 \\ -\omega_y \cos\beta \\ \omega_y \sin\beta \\ \cdots \\ 4\sin\beta \\ 4\sin\beta\cos\theta \\ 4\cos\beta\cos\theta \end{pmatrix}
$$

(94)

The screws were used to generate the M_D and M_N matrices, and the mobility $F_N = 1$ and the redundant constraints $C_N = 31$ were calculated. Also, by employing $rref$ on the M_N matrix, the pivot columns and free columns were found and finally, the redundant constraints per circuit were determined to be as shown in Equation (96) and Figure 47.

The restrictions per loop are:

$$
\begin{aligned}
\hat{\$}^a = \big[\ & 0\ \ 0\ \ 0\ \ U_1\ \ V_1\ \ W_1\ \ 0\ \ 0\ \ 0\ \ U_2\ \ V_2\ \ W_2\ \ 0\ \ 0\ \ 0\ \ U_3\ \ V_3\ \ W_3\ \ \ldots \\
& \ldots\ 0\ \ 0\ \ 0\ \ U_4\ \ V_4\ \ W_4\ \ 0\ \ 0\ \ T_5\ \ U_5\ \ V_5\ \ W_5\ \ 0\ \ 0\ \ T_6\ \ U_6\ \ V_6\ \ W_6\ \ \ldots \\
& \ldots\ 0\ \ 0\ \ T_7\ \ U_7\ \ V_7\ \ W_7\ \ 0\ \ 0\ \ T_8\ \ U_8\ \ V_8\ \ W_8\ \ 0\ \ 0\ \ 0\ \ U_9\ \ V_9\ \ W_9\ \big]
\end{aligned}
\tag{95}
$$

$$
\left[\begin{array}{cccccccccccccccccccccccc}
1&0&0&0&0&0&0&0&0&0&0&0&0&0&0&0&0&0&0&0&0&0&0&0\\
0&1&0&0&0&0&0&0&0&0&0&0&0&0&0&0&0&0&0&0&0&0&0&0\\
0&0&1&0&0&0&0&0&0&0&0&0&0&0&0&0&0&0&0&0&0&0&0&0\\
0&0&0&0&0&0&1&0&0&0&0&-2&0&0&0&0&0&0&0&0&0&0&0&0\\
0&0&0&0&0&0&0&1&0&0&0&0&0&0&0&0&0&0&0&0&0&0&0&0\\
0&0&0&0&0&0&0&0&1&2&0&0&0&0&0&0&0&0&0&0&0&0&0&0\\
0&0&0&0&0&0&0&0&0&0&0&0&1&0&0&0&0&-4&0&0&0&0&0&0\\
0&0&0&0&0&0&0&0&0&0&0&0&0&1&0&0&0&0&0&0&0&0&0&0\\
0&0&0&0&0&0&0&0&0&0&0&0&0&0&1&4&0&0&0&0&0&0&0&0\\
0&0&0&0&0&0&0&0&0&0&0&0&0&0&0&0&0&0&1&0&0&0&-2s\theta&-4\\
0&0&0&0&0&0&0&0&0&0&0&0&0&0&0&0&0&0&0&1&0&2s\theta&0&-2c\theta\\
0&0&0&0&0&0&0&0&0&0&0&0&0&0&0&0&0&0&0&0&1&4&2c\theta&0\\
0&0&0&0&0&0&0&0&0&0&0&0&0&0&0&0&0&0&0&0&0&0&0&0\\
0&0&0&0&0&0&0&0&0&0&0&0&0&0&0&0&0&0&0&0&0&0&0&0\\
0&0&0&0&0&0&0&0&0&0&0&0&0&0&0&0&0&0&0&0&0&0&0&0\\
0&0&0&0&0&0&0&0&0&0&0&0&0&0&0&0&0&0&0&0&0&0&0&0\\
0&0&0&0&0&0&0&0&0&0&0&0&0&0&0&0&0&0&0&0&0&0&0&0\\
0&0&0&0&0&0&0&0&0&0&0&0&0&0&0&0&0&0&0&0&0&0&0&0\\
0&0&0&0&0&0&0&0&0&0&0&0&0&0&0&0&0&0&0&0&0&0&0&0\\
0&0&0&0&0&0&0&0&0&0&0&0&0&0&0&0&0&0&0&0&0&0&0&0\\
0&0&0&0&0&0&0&0&0&0&0&0&0&0&0&0&0&0&0&0&0&0&0&0\\
0&0&0&0&0&0&0&0&0&0&0&0&0&0&0&0&0&0&0&0&0&0&0&0\\
0&0&0&0&0&0&0&0&0&0&0&0&0&0&0&0&0&0&0&0&0&0&0&0\\
0&0&0&0&0&0&0&0&0&0&0&0&0&0&0&0&0&0&0&0&0&0&0&0
\end{array}\right.\cdots
$$

$$
\cdots\begin{array}{ccccccccccccccc}
0&0&0&0&0&0&0&0&0&0&-2s\theta&0&0&0&0\\
0&0&0&0&0&0&0&0&0&0&0&0&0&0&0\\
0&0&0&0&0&0&0&0&-1&0&-2c\theta&0&0&0&0\\
0&0&-\frac{s\theta}{c\theta}&-\frac{2s\theta}{c\theta}&-2s\theta&0&0&0&0&0&0&0&0&0&0\\
0&0&0&0&0&0&0&0&0&0&0&0&0&0&0\\
0&0&-1&-2&-2c\theta&0&0&0&0&0&0&0&0&0&0\\
0&0&0&0&0&0&0&0&-\frac{s\theta}{c\theta}&0&-2s\theta&0&0&0&\frac{s\theta}{c\theta}\\
0&0&0&0&0&0&0&0&0&0&0&0&0&0&0\\
0&0&0&0&0&0&0&0&-1&0&-2c\theta&0&0&0&1\\
0&0&0&0&0&0&0&0&\frac{s\theta}{c\theta}&0&2s\theta&0&0&0&-\frac{s\theta}{c\theta}\\
0&0&0&0&0&0&0&0&\frac{s\beta}{c\beta}&0&\frac{2s\beta c\theta}{c\beta}&0&0&0&-\frac{s\beta}{c\beta}\\
0&0&0&0&0&0&0&0&1&0&2c\theta&0&0&0&-1\\
1&0&-\frac{s\theta}{c\theta}&-\frac{2s\theta}{c\theta}&-4s\theta&-2&0&0&0&0&0&0&0&0&0\\
0&1&0&2s\theta&0&-2c\theta&0&0&\frac{s\beta}{c\beta}&0&\frac{2s\beta c\theta}{c\beta}&0&0&0&-\frac{s\beta}{c\beta}\\
0&0&0&0&0&0&1&0&-\frac{s\theta}{c\theta}&0&-4s\theta&0&0&0&0\\
0&0&0&0&0&0&0&1&\frac{s\beta}{c\beta}&2s\theta&\frac{2s\beta c\theta}{c\beta}&-2c\theta&0&0&-\frac{s\beta}{c\beta}\\
0&0&0&0&0&0&0&0&0&0&0&0&1&0&\frac{s\theta}{c\theta}\\
0&0&0&0&0&0&0&0&0&0&0&0&0&1&0\\
0&0&0&0&0&0&0&0&0&0&0&0&0&0&0\\
0&0&0&0&0&0&0&0&0&0&0&0&0&0&0\\
0&0&0&0&0&0&0&0&0&0&0&0&0&0&0\\
0&0&0&0&0&0&0&0&0&0&0&0&0&0&0\\
0&0&0&0&0&0&0&0&0&0&0&0&0&0&0\\
0&0&0&0&0&0&0&0&0&0&0&0&0&0&0
\end{array}\cdots \tag{96}
$$

$$
\cdots\left.\begin{array}{ccccccccccccccc}
0&-2s\theta&0&0&0&0&0&0&0&0&0&0&0&0&0\\
0&0&0&0&0&0&0&0&0&0&0&0&0&0&0\\
0&-2c\theta&0&0&0&0&0&0&0&0&0&0&0&0&0\\
0&0&0&0&0&0&0&0&0&0&0&0&0&0&0\\
0&0&0&0&0&0&0&0&0&0&0&0&0&0&0\\
0&0&0&0&0&0&0&0&0&0&0&0&0&0&0\\
0&2s\theta&0&0&0&0&0&0&0&0&0&0&\frac{2s\theta\,2s\beta-c\beta s\theta}{s\beta c\theta}&2s\theta&-\frac{2c\beta s\theta}{s\beta}\\
0&0&0&0&0&0&0&0&0&0&0&0&0&0&0\\
0&2c\theta&0&0&0&0&0&0&0&0&0&0&\frac{2(2s\beta-c\beta s\theta)}{s\beta}&2c\theta&-\frac{2c\beta c\theta}{s\beta}\\
0&-2s\theta&0&0&0&0&0&0&0&0&0&0&-\frac{2s\theta\,2s\beta-c\beta s\theta}{s\beta c\theta}&0&\frac{2c\beta s\theta}{s\beta}\\
0&-\frac{2s\beta c\theta}{c\beta}&0&0&0&0&0&0&0&0&0&0&-\frac{4s\beta}{c\beta}&-\frac{2s\beta c\theta}{c\beta}&0\\
0&-2c\theta&0&0&0&0&0&0&0&0&0&0&-\frac{2(2s\beta-c\beta s\theta)}{s\beta}&0&\frac{2c\beta c\theta}{s\beta}\\
0&0&0&0&0&0&0&0&0&0&0&0&0&0&0\\
0&-\frac{2s\beta c\theta}{c\beta}&0&0&0&0&-2s\theta&0&-2c\theta&0&0&0&-\frac{2(2s\beta-c\beta s\theta)}{c\beta}&-\frac{2s\beta c\theta}{c\beta}&2c\theta\\
0&0&0&0&0&0&0&0&0&0&0&0&0&0&0\\
0&-\frac{2s\beta c\theta}{c\beta}&-2c\theta&0&0&0&0&0&0&0&0&0&-\frac{2(2s\beta-c\beta s\theta)}{c\beta}&-\frac{2s\beta c\theta}{c\beta}&2c\theta\\
0&4s\theta&0&0&0&0&0&0&0&0&0&0&0&0&0\\
-2s\theta&0&-4c\theta&0&0&0&0&0&0&0&0&0&0&0&0\\
0&0&0&1&0&\frac{s\theta}{c\theta}&\frac{2s\theta}{c\theta}&4s\theta&-2&0&0&0&0&0&0\\
0&0&0&0&1&0&0&0&-4c\theta&0&0&0&0&0&0\\
0&0&0&0&0&0&0&0&0&1&0&0&0&0&-4\\
0&0&0&0&0&0&0&0&0&0&1&0&0&0&-4c\theta\\
0&0&0&0&0&0&0&0&0&0&0&1&0&4c\theta&0\\
0&0&0&0&0&0&0&0&0&0&0&0&0&0&0
\end{array}\right]
$$

$$
\left[\begin{array}{ccccccccccccc} R_1 & S_1 & T_1 & U_1 & V_1 & W_1 & \cdots & R_6 & S_6 & T_6 & U_6 & V_6 & W_6 \end{array}\right]^T_{36\times 1}
$$

$$
= \left[\begin{array}{ccccccccc} 0 & 0 & 0 & 0 & \cdots & 0 & 0 & 0 & 0 & 0 \end{array}\right]^T_{17\times 1}
$$

The redundant constraints acting on the 4x4 Origami are shown in Figure 47 .

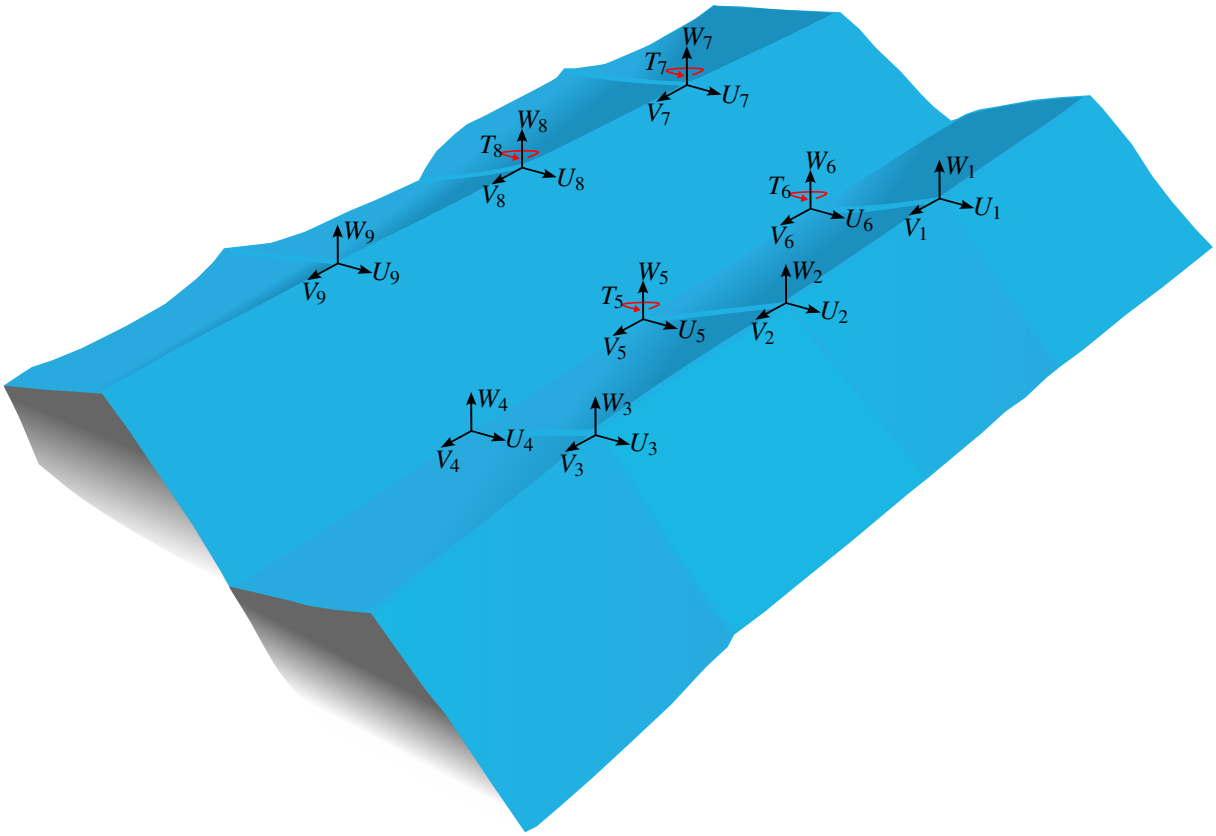

Figure 47 – 4x4 Shaped Origami actions

A.3 5X5 SHAPED ORIGAMI

Davis' method was applied to the 5x5 shaped origami shown in Figure 48, in an attempt to determine its mobility and redundant constraints. This origami pattern has 25 facets, 40 folds, and 16 spherical centers. In the Figure 48 the above information can be seen. From this same figure, the information needed to construct the direction vectors is extracted, as seen in the Equation (97).

$$\vec{S}_m^M = \begin{Bmatrix} \cos\alpha \\ 0 \\ \sin\alpha \end{Bmatrix} \quad \textit{for t= m, n, o, t, v, x, z, and ab ;} \quad \vec{S}_n^M = \begin{Bmatrix} \cos\theta \\ 0 \\ -\sin\theta \end{Bmatrix} \quad \textit{for n= b, c, d, g, h, i, aa, ac, ah, aj, al, am}$$

$$\vec{S}_y^M = \begin{Bmatrix} 0 \\ 1 \\ 0 \end{Bmatrix} \quad \textit{for y=a, e, f, j, k, l p, r, s, u, w, y, ad, ae, af, ag, ai, ak, an, ao} \tag{97}$$

For other hand, The position vector are:

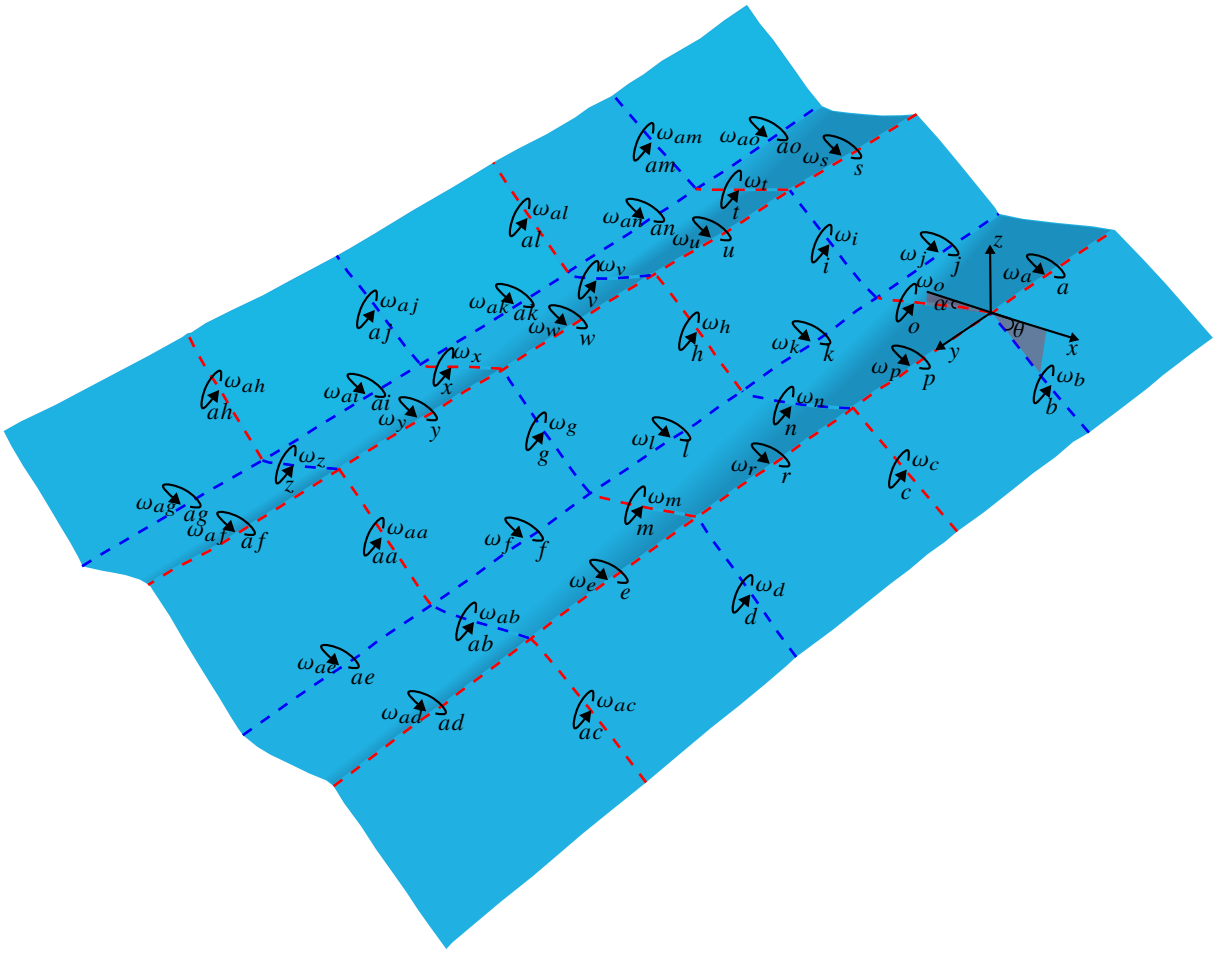

Figure 48 – 5x5 Shaped Origami

$$\vec{S}_{0_b} = \begin{Bmatrix} 0 \\ 0 \\ 0 \end{Bmatrix}; \quad \vec{S}_{0_c} = \begin{Bmatrix} 0 \\ 2 \\ 0 \end{Bmatrix}; \quad \vec{S}_{0_d} = \begin{Bmatrix} 0 \\ 4 \\ 0 \end{Bmatrix}; \quad \vec{S}_{0_{ac}} = \begin{Bmatrix} 0 \\ 6 \\ 0 \end{Bmatrix}; \quad \vec{S}_{0_i} = \begin{Bmatrix} -2\cos\alpha \\ 0 \\ -2\sin\alpha \end{Bmatrix}; \quad \vec{S}_{0_h} = \begin{Bmatrix} -2\cos\alpha \\ 2 \\ -2\sin\alpha \end{Bmatrix}$$

$$\vec{S}_{0_g} = \begin{Bmatrix} -2\cos\alpha \\ 4 \\ -2\sin\alpha \end{Bmatrix}; \quad \vec{S}_{0_{aa}} = \begin{Bmatrix} -2\cos\alpha \\ 6 \\ -2\sin\alpha \end{Bmatrix} \quad \vec{S}_{0_t} = \begin{Bmatrix} -2(\cos\alpha+\cos\theta) \\ 0 \\ 0 \end{Bmatrix}; \quad \vec{S}_{0_v} = \begin{Bmatrix} -2(\cos\alpha+\cos\theta) \\ 2 \\ 0 \end{Bmatrix}$$

$$\vec{S}_{0_x} = \begin{Bmatrix} -2(\cos\alpha+\cos\theta) \\ 4 \\ 0 \end{Bmatrix}; \quad \vec{S}_{0_z} = \begin{Bmatrix} -2(\cos\alpha+\cos\theta) \\ 6 \\ 0 \end{Bmatrix}; \quad \vec{S}_{0_{am}} = \begin{Bmatrix} -2(2\cos\alpha+\cos\theta) \\ 0 \\ -2\sin\alpha \end{Bmatrix}$$

$$\vec{S}_{0_{al}} = \begin{Bmatrix} -2(2\cos\alpha+\cos\theta) \\ 2 \\ -2\sin\alpha \end{Bmatrix}; \quad \vec{S}_{0_{aj}} = \begin{Bmatrix} -2(2\cos\alpha+\cos\theta) \\ 4 \\ -2\sin\alpha \end{Bmatrix}; \quad \vec{S}_{0_{ah}} = \begin{Bmatrix} -2(2\cos\alpha+\cos\theta) \\ 6 \\ -2\sin\alpha \end{Bmatrix} \tag{98}$$

Where the subscripts $(b, c, d, ac...., ah)$ refer to the position of the spherical centers to which each of the folds named with the same name belongs.

The spanning tree is:

Then, the circuit matrix can be written as Equation (99):

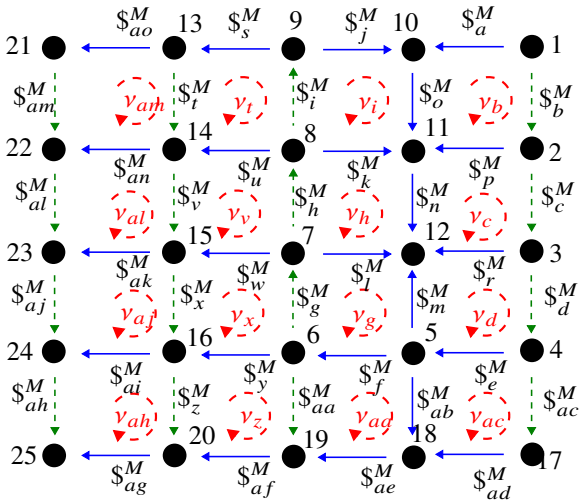

Figure 49 – Spanning Tree 5x5-shaped Origami-hold

$$[B_M]_{16\times 40} =$$

b	c	d	g	h	i	t	v	x	z	aa	ac	ah	aj	al	am	a	e	f	j
1	0	0	0	0	0	0	0	0	0	0	0	0	0	0	0	−1	0	0	0
0	1	0	0	0	0	0	0	0	0	0	0	0	0	0	0	0	0	0	0
0	0	1	0	0	0	0	0	0	0	0	0	0	0	0	0	0	1	0	0
0	0	0	1	0	0	0	0	0	0	0	0	0	0	0	0	0	0	1	0
0	0	0	0	1	0	0	0	0	0	0	0	0	0	0	0	0	0	0	0
0	0	0	0	0	1	0	0	0	0	0	0	0	0	0	0	0	0	0	1
0	0	0	0	0	0	1	0	0	0	0	0	0	0	0	0	0	0	0	−1
0	0	0	0	0	0	0	1	0	0	0	0	0	0	0	0	0	0	0	0
0	0	0	0	0	0	0	0	1	0	0	0	0	0	0	0	0	0	−1	0
0	0	0	0	0	0	0	0	0	1	0	0	0	0	0	0	0	0	1	0
0	0	0	0	0	0	0	0	0	0	1	0	0	0	0	0	0	0	1	0
0	0	0	0	0	0	0	0	0	0	0	1	0	0	0	0	0	−1	0	0
0	0	0	0	0	0	0	0	0	0	0	0	1	0	0	0	0	0	1	0
0	0	0	0	0	0	0	0	0	0	0	0	0	1	0	0	0	0	−1	0
0	0	0	0	0	0	0	0	0	0	0	0	0	0	1	0	0	0	0	0
0	0	0	0	0	0	0	0	0	0	0	0	0	0	0	1	0	0	0	−1

k	l	m	n	o	p	r	s	u	w	y	ab	ad	ae	af	ag	ai	ak	an	ao	
0	0	0	0	−1	1	0	0	0	0	0	0	0	0	0	0	0	0	0	0	b
0	0	0	−1	0	−1	1	0	0	0	0	0	0	0	0	0	0	0	0	0	c
0	0	−1	0	0	0	−1	0	0	0	0	0	0	0	0	0	0	0	0	0	d
0	1	−1	0	0	0	0	0	0	0	0	0	0	0	0	0	0	0	0	0	g
1	−1	0	1	0	0	0	0	0	0	0	0	0	0	0	0	0	0	0	0	h
−1	0	0	0	1	0	0	0	0	0	0	0	0	0	0	0	0	0	0	0	i
1	0	0	0	−1	0	0	1	−1	0	0	0	0	0	0	0	0	0	0	0	t
−1	1	0	−1	0	0	0	0	1	−1	0	0	0	0	0	0	0	0	0	0	v
0	−1	1	0	0	0	0	0	0	1	−1	0	0	0	0	0	0	0	0	0	x
0	0	0	0	0	0	0	0	0	0	1	−1	0	−1	−1	0	0	0	0	0	z
0	0	0	0	0	0	0	0	0	0	0	−1	0	−1	0	0	0	0	0	0	aa
0	0	0	0	0	0	0	0	0	0	0	−	1	0	0	0	0	0	0	0	ac
0	0	0	0	0	0	0	0	0	0	1	−1	0	−1	−1	−1	1	0	0	0	ah
0	−1	1	0	0	0	0	0	0	1	−1	0	0	0	0	0	−1	1	0	0	aj
−1	1	0	−1	0	0	0	0	1	−1	0	0	0	0	0	0	0	−1	1	0	al
1	0	0	0	−1	0	0	1	−1	0	0	0	0	0	0	0	0	0	−1	1	am

(99)

The twist per joint are shown in Equation (100).

$$\$_a^M = \begin{pmatrix} 0 \\ \omega_a \\ 0 \\ 0 \\ 0 \\ 0 \end{pmatrix}; \quad \$_b^M = \begin{pmatrix} \omega_b \cos\theta \\ 0 \\ -\omega_b \sin\theta \\ 0 \\ 0 \\ 0 \end{pmatrix}; \quad \$_c^M = \begin{pmatrix} \omega_c \cos\theta \\ 0 \\ -\omega_c \sin\theta \\ -2\omega_c \sin\theta \\ 0 \\ -2\omega_c \cos\theta \end{pmatrix}; \quad \$_d^M = \begin{pmatrix} \omega_d \cos\theta \\ 0 \\ \omega_d \sin\theta \\ -4\omega_d \sin\theta \\ 0 \\ -4\omega_d \cos\theta \end{pmatrix}; \quad \$_e^M = \begin{pmatrix} 0 \\ \omega_e \\ 0 \\ 0 \\ 0 \\ 0 \end{pmatrix}$$

$$\$_f^M = \begin{pmatrix} 0 \\ \omega_f \\ \\ 2\omega_f \sin\theta) \\ 0 \\ 2\omega_f \cos\theta \end{pmatrix}; \quad \$_g^M = \begin{pmatrix} \omega_g \cos\theta \\ 0 \\ -\omega_g \sin\theta \\ -4\omega_g \sin\theta \\ -4\omega_g \cos\theta \sin\theta \\ -4\omega_g \cos\theta \end{pmatrix}; \quad \$_h^M = \begin{pmatrix} \omega_h \cos\theta \\ 0 \\ -\omega_h \sin\theta \\ -2\omega_h \sin\theta \\ -4\omega_h \cos\theta \sin\theta \\ -2\omega_h \cos\theta \end{pmatrix}; \quad \$_i^M = \begin{pmatrix} \omega_i \cos\theta \\ 0 \\ -\omega_i \sin\theta\, 0 \\ -4\omega_i \cos\theta \sin\theta \\ 0 \end{pmatrix}$$

$$\$_j^M = \begin{pmatrix} 0 \\ \omega_j \cos\beta \\ \omega_j \sin\beta \\ 2\omega_j \sin\theta \cos\beta \\ 2\omega_j \cos\theta \sin\beta \\ -2\omega_j \cos\theta \cos\beta \end{pmatrix}; \quad \$_k^M = \begin{pmatrix} 0 \\ \omega_k \\ 0 \\ 2\omega_k \sin\theta \\ 0 \\ -2\omega_k \cos\theta \end{pmatrix}; \quad \$_l^M = \begin{pmatrix} 0 \\ \omega_l \\ 0 \\ 2\omega_l \sin\theta \\ 0 \\ -2\omega_l \cos\theta \end{pmatrix}; \quad \$_m^M = \begin{pmatrix} \omega_m \cos\theta \\ 0 \\ \omega_m \sin\theta \\ 4\omega_m \sin\theta \\ 0 \\ -4\omega_m \cos\theta \end{pmatrix}$$

$$\$_n^M = \begin{pmatrix} \omega_n \cos\theta \\ 0 \\ \omega_n \sin\theta \\ 2\omega_n \sin\theta \\ 0 \\ -2\omega_n \cos\theta \end{pmatrix}; \quad \$_o^M = \begin{pmatrix} \omega_o \cos\theta \\ 0 \\ \omega_o \sin\theta \\ 0 \\ 0 \\ 0 \end{pmatrix}; \quad \$_p^M = \begin{pmatrix} 0 \\ \omega_p \\ 0 \\ 0 \\ 0 \\ 0 \end{pmatrix}; \quad \$_r^M = \begin{pmatrix} 0 \\ \omega_r \\ 0 \\ 0 \\ 0 \\ 0 \end{pmatrix}; \quad \$_s^M = \begin{pmatrix} 0 \\ \omega_s \\ 0 \\ 0 \\ 0 \\ -4\omega_s \cos\theta \end{pmatrix}$$

$$\$_t^M = \begin{pmatrix} \omega_t \cos\theta \\ 0 \\ \omega_t \sin\theta \\ 0 \\ 4\omega_t \cos\theta \sin\theta \\ 0 \end{pmatrix}; \quad \$_u^M = \begin{pmatrix} 0 \\ \omega_u \\ 0 \\ 0 \\ 0 \\ -4\omega_u \cos\theta \end{pmatrix}; \quad \$_v^M = \begin{pmatrix} \omega_v \cos\theta \\ 0 \\ \omega_v \sin\theta \\ 2\omega_v \sin\theta \\ 4\omega_v \cos\theta \sin\theta \\ -2\omega_v \cos\theta \end{pmatrix}; \quad \$_w^M = \begin{pmatrix} 0 \\ \omega_w \\ 0 \\ 0 \\ 0 \\ -4\omega_w \cos\theta \end{pmatrix}$$

$$\$_x^M = \begin{pmatrix} \omega_x \cos\theta \\ 0 \\ \omega_x \sin\theta \\ 4\omega_x \sin\theta \\ 4\omega_x \cos\theta \sin\theta \\ -4\omega_x \cos\theta \end{pmatrix}; \quad \$_y^M = \begin{pmatrix} 0 \\ \omega_y \\ 0 \\ 0 \\ 0 \\ -4\cos\theta \end{pmatrix}; \quad \$_z^M = \begin{pmatrix} \omega_z \cos\theta \\ 0 \\ \omega_z \sin\theta \\ 6\omega_z \sin\theta \\ 4\omega_z \cos\theta \sin\theta \\ -6\omega_z \cos\theta \end{pmatrix}; \quad \$_{aa}^M = \begin{pmatrix} \omega_{aa} \cos\theta \\ 0 \\ \omega_{aa} \sin\theta \\ 6\omega_{aa} \sin\theta \\ 0 \\ -6\omega_{aa} \cos\theta \end{pmatrix}$$

$$\$_{ab}^M = \begin{pmatrix} \omega_{ab} \cos\theta \\ 0 \\ \omega_{ab} \sin\theta \\ 6\omega_{ab} \sin\theta \\ 0 \\ -6\omega_{ab} \cos\theta \end{pmatrix}: \quad \$_{ac}^M = \begin{pmatrix} \omega_{ac} \cos\theta \\ 0 \\ -\omega_{ac} \sin\theta \\ -6\omega_{ac} \sin\theta \\ 0 \\ -6\omega_{ac} \cos\theta \end{pmatrix}; \quad \$_{ad}^M = \begin{pmatrix} 0 \\ \omega_{ad} \\ 0 \\ 0 \\ 0 \\ 0 \end{pmatrix}; \quad \$_{ae}^M = \begin{pmatrix} 0 \\ \omega_{ae} \cos\beta \\ \omega_{ae} \sin\beta \\ \omega_{ae}(6\sin\beta - 2\sin\theta\cos\beta) \\ 2\omega_{ae} \cos\theta \sin\beta \\ 2\omega_{ae} \cos\theta \cos\beta \end{pmatrix}$$

$$\$_{af}^M = \begin{pmatrix} 0 \\ \omega_{af} \cos\beta \\ \omega_{af} \sin\beta \\ -6\omega_{af} \sin\beta \\ -4\omega_{af} \cos\theta \sin\beta \\ -4\omega_{af} \cos\theta \cos\beta \end{pmatrix}; \quad \$_{ag}^M = \begin{pmatrix} 0 \\ \omega_{ag} \cos\beta \\ \omega_{ag} \sin\beta \\ \omega_{ag}(6\sin\beta - 2\sin\theta\cos\beta) \\ 6\omega_{ag} \cos\theta \sin\beta \\ 6\omega_{ag} \cos\theta \cos\beta \end{pmatrix}; \quad \$_{ah}^M = \begin{pmatrix} \omega_{ah} \cos\theta \\ 0 \\ -\omega_{ah} \sin\theta \\ -6\omega_{ah} \sin\theta \\ -8\omega_{ah} \cos\theta \sin\theta \\ -6\omega_{ah} \cos\theta \end{pmatrix}; \quad \$_{ai}^M = \begin{pmatrix} 0 \\ \omega_{ai} \\ 0 \\ 2\omega_{ai} \sin\theta \\ 0 \\ -6\omega_{ai} \cos\theta \end{pmatrix}$$

$$\$_{aj}^M = \begin{pmatrix} \omega_{aj} \cos\theta \\ 0 \\ -\omega_{aj} \sin\theta \\ -4\omega_{aj} \sin\theta \\ -8\omega_{aj} \cos\theta \sin\theta \\ -4\omega_{aj} \cos\theta \end{pmatrix}; \quad \$_{ak}^M = \begin{pmatrix} 0 \\ \omega_{ak} \\ 0 \\ 2\omega_{ak} \sin\theta \\ 0 \\ -6\omega_{ak} \cos\theta \end{pmatrix}; \quad \$_{al}^M = \begin{pmatrix} \omega_{al} \cos\theta \\ 0 \\ -\omega_{al} \sin\theta \\ -2\omega_{al} \sin\theta \\ -8\omega_{al} \cos\theta \sin\theta \\ -2\omega_{al} \cos\theta \end{pmatrix}; \quad \$_{am}^M = \begin{pmatrix} \omega_{am} \cos\theta \\ 0 \\ -\omega_{am} \sin\theta \\ 0 \\ -8\omega_a \cos\theta \sin\theta \\ 0 \end{pmatrix}$$

$$\$_{an}^M = \begin{pmatrix} 0 \\ \omega_{an} \\ 0 \\ 2\omega_{an} \sin\theta \\ 0 \\ -6\omega_{an} \cos\theta \end{pmatrix}; \quad \$_{ao}^M = \begin{pmatrix} 0 \\ -\omega_{ao} \cos\beta \\ \omega_{ao} \sin\beta \\ -2\omega_{ao} \sin\theta \cos\beta) \\ 6\omega_{ao} \cos\theta \sin\beta \\ 6\omega_{ao} \cos\theta \cos\beta \end{pmatrix}$$

(100)

By replacing the screw in the M_D matrix, subsequently in M_N, it is possible to calculate the rank of the M_N matrix and finally it is determined that the mobility of this origami array is $F_N = 1$. On the other hand, it is found that this pattern has $C_N = 57$ redundant constraints, which are distributed as shown in Equation (101) and Figure 50 .

$$
\begin{aligned}
\hat{\$}^a = [\ & 0\ \ 0\ \ 0\ \ U_1\ \ V_1\ \ W_1\ \ 0\ \ 0\ \ 0\ \ U_2\ \ V_2\ \ W_2\ \ 0\ \ 0\ \ 0\ \ U_3\ \ V_3\ \ W_3\ \ 0\ \ 0\ \ T_4\ \ U_4\ \ V_4\ \ W_4\ \ \dots \\
& \dots\ \ 0\ \ 0\ \ T_5\ \ U_5\ \ V_5\ \ W_5\ \ 0\ \ 0\ \ 0\ \ U_6\ \ V_6\ \ W_6\ \ 0\ \ 0\ \ 0\ \ U_7\ \ V_7\ \ W_7\ \ \dots \\
& \dots\ 0\ \ 0\ \ T_8\ \ U_8\ \ V_8\ \ W_8\ \ 0\ \ 0\ \ T_9\ \ U_9\ \ V_9\ \ W_9\ \ 0\ \ 0\ \ T_{10}\ \ 0\ \ 0\ \ W_{10}\ \ \dots \\
& \dots\ 0\ \ S_{11}\ \ T_{11}\ \ U_{11}\ \ V_{11}\ \ W_{11}\ \ 0\ \ 0\ \ T_{12}\ \ U_{12}\ \ V_{12}\ \ W_{12}\ \ 0\ \ 0\ \ 0\ \ U_{13}\ \ V_{13}\ \ W_{13}\ \ \dots \\
& \dots\ \ 0\ \ 0\ \ T_{14}\ \ U_{14}\ \ V_{14}\ \ W_{14}\ \ 0\ \ 0\ \ T_{15}\ \ U_{15}\ \ V_{15}\ \ W_{15}\ \ 0\ \ 0\ \ T_{16}\ \ U_{16}\ \ V_{16}\ \ W_{16}\ ]
\end{aligned}
\tag{101}
$$

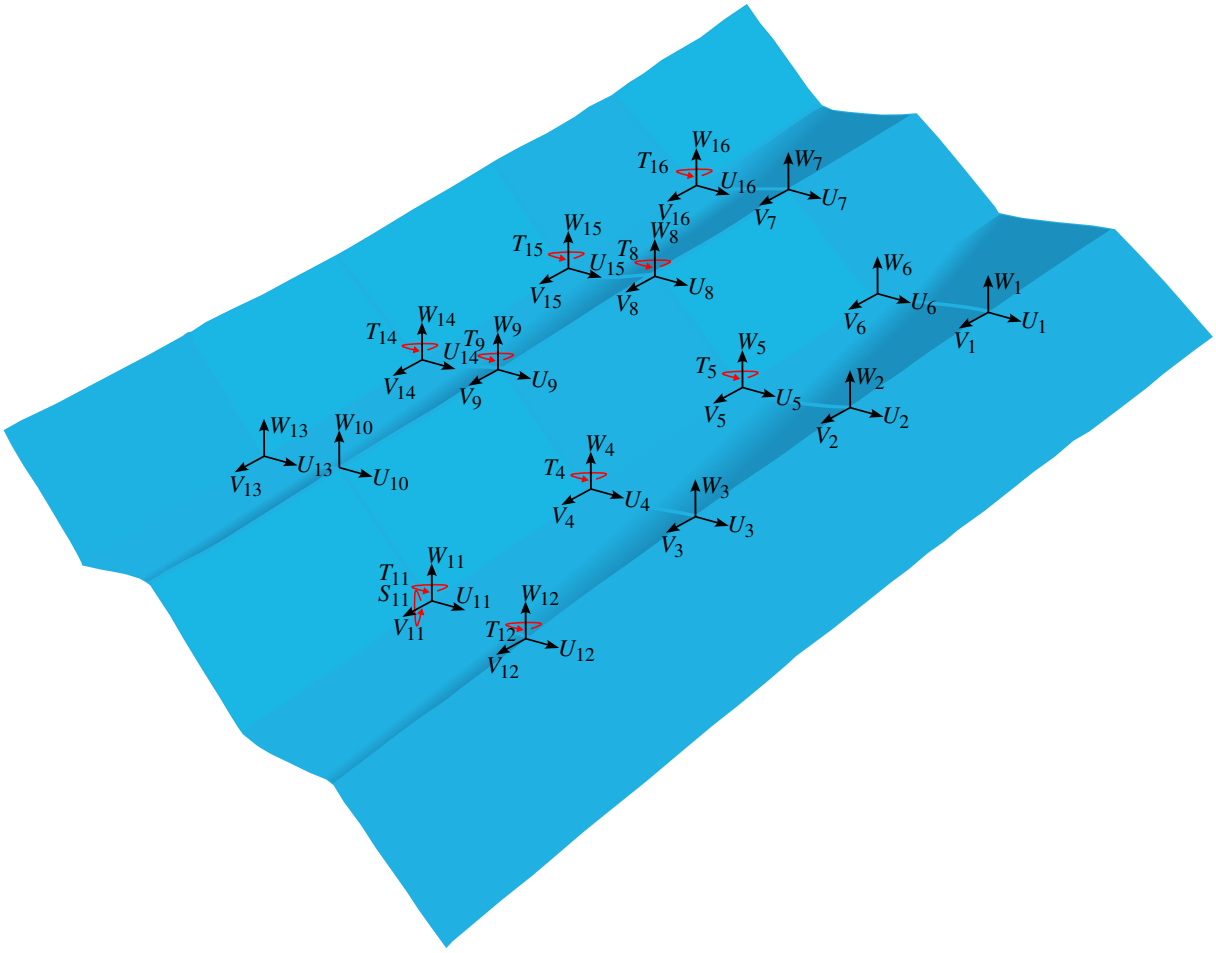

Figure 50 – 5x5 Shaped Origami

The 5x5 origami pattern has 57 redundant constraints that correspond to 48 constraints coming from the 3 constraints per spherical center and 9 additional constraints.

A.4 6X5 SHAPED ORIGAMI

The mobility and redundant constraints of the 6x5 origami pattern shown in the figure were determined by applying Davies' method. This origami pattern has 30 facets, 49 folds and 20 spherical centers. In Figure 48 the previous information can be seen. From this same figure, the information needed to construct the direction vectors is extracted, as seen in the Equation (97).

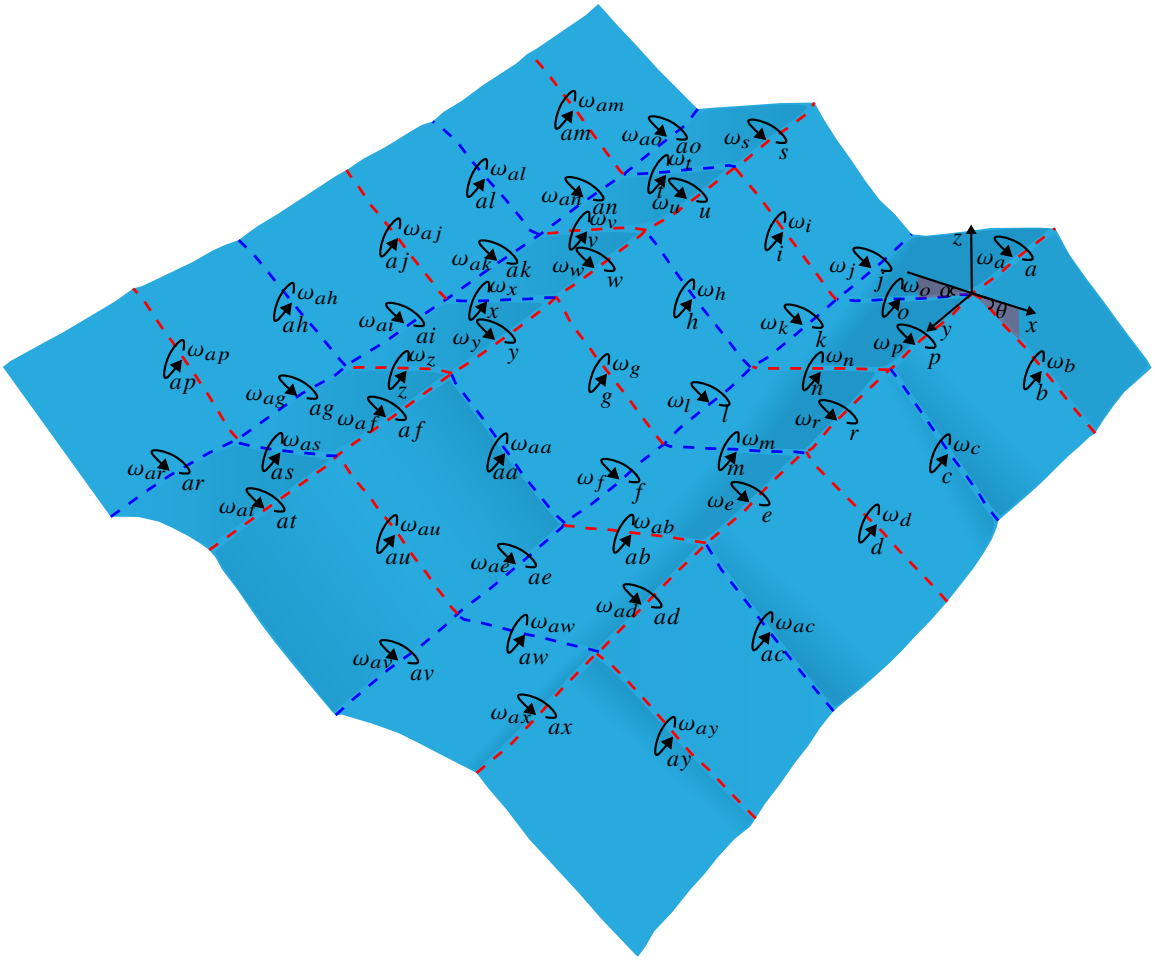

Figure 51 – 6x5 Shaped Origami

$$\vec{S}_m^M = \begin{Bmatrix} \cos\alpha \\ 0 \\ \sin\alpha \end{Bmatrix} \quad \textit{for t= m, n, o, t, v, x, z, ab, as, aw}$$

$$\vec{S}_n^M = \begin{Bmatrix} \cos\theta \\ 0 \\ -\sin\theta \end{Bmatrix} \quad \textit{for n= b, c, d, g, h, i, aa, ac, ah, aj, al, am, ap, ay and ay} \tag{102}$$

$$\vec{S}_y^M = \begin{Bmatrix} 0 \\ 1 \\ 0 \end{Bmatrix} \quad \textit{for y=a, e, f, j, k, l p, r, s, u, w, y, ad, ae, af, ag, ai, ak, an, ao}$$

For other hand, The position vector are:

$$
\begin{aligned}
&\vec{S}_{0_b} = \begin{Bmatrix} 0 \\ 0 \\ 0 \end{Bmatrix}; \quad \vec{S}_{0_c} = \begin{Bmatrix} 0 \\ 2 \\ 0 \end{Bmatrix}; \quad \vec{S}_{0_d} = \begin{Bmatrix} 0 \\ 4 \\ 0 \end{Bmatrix}; \quad \vec{S}_{0_{ac}} = \begin{Bmatrix} 0 \\ 6 \\ 0 \end{Bmatrix}; \quad \vec{S}_{0_{ay}} = \begin{Bmatrix} 0 \\ 8 \\ 0 \end{Bmatrix}; \quad \vec{S}_{0_i} = \begin{Bmatrix} -2\cos\alpha \\ 0 \\ -2\sin\alpha \end{Bmatrix} \\
&\vec{S}_{0_h} = \begin{Bmatrix} -2\cos\alpha \\ 2 \\ -2\sin\alpha \end{Bmatrix}; \quad \vec{S}_{0_g} = \begin{Bmatrix} -2\cos\alpha \\ 4 \\ -2\sin\alpha \end{Bmatrix}; \quad \vec{S}_{0_{aa}} = \begin{Bmatrix} -2\cos\alpha \\ 6 \\ -2\sin\alpha \end{Bmatrix}; \quad \vec{S}_{0_{au}} = \begin{Bmatrix} -2\cos\alpha \\ 8 \\ -2\sin\alpha \end{Bmatrix} \\
&\vec{S}_{0_t} = \begin{Bmatrix} -2(\cos\alpha+\cos\theta) \\ 0 \\ 0 \end{Bmatrix}; \quad \vec{S}_{0_v} = \begin{Bmatrix} -2(\cos\alpha+\cos\theta) \\ 2 \\ 0 \end{Bmatrix}; \quad \vec{S}_{0_x} = \begin{Bmatrix} -2(\cos\alpha+\cos\theta) \\ 4 \\ 0 \end{Bmatrix} \\
&\vec{S}_{0_z} = \begin{Bmatrix} -2(\cos\alpha+\cos\theta) \\ 6 \\ 0 \end{Bmatrix}; \quad \vec{S}_{0_{as}} = \begin{Bmatrix} -2(\cos\alpha+\cos\theta) \\ 8 \\ 0 \end{Bmatrix}; \quad \vec{S}_{0_{am}} = \begin{Bmatrix} -2(2\cos\alpha+\cos\theta) \\ 0 \\ -2\sin\alpha \end{Bmatrix} \\
&\vec{S}_{0_{al}} = \begin{Bmatrix} -2(2\cos\alpha+\cos\theta) \\ 2 \\ -2\sin\alpha \end{Bmatrix}; \quad \vec{S}_{0_{aj}} = \begin{Bmatrix} -2(2\cos\alpha+\cos\theta) \\ 4 \\ -2\sin\alpha \end{Bmatrix}; \quad \vec{S}_{0_{ah}} = \begin{Bmatrix} -2(2\cos\alpha+\cos\theta) \\ 6 \\ -2\sin\alpha \end{Bmatrix} \\
&\vec{S}_{0_{ap}} = \begin{Bmatrix} -2(2\cos\alpha+\cos\theta) \\ 8 \\ -2\sin\alpha \end{Bmatrix}
\end{aligned}
\tag{103}
$$

Where the subscripts $(b, c, d, ac...., ap)$ refer to the position of the spherical centers to which each of the folds named with the same name belongs.

Thenfore, the spaning tree is:

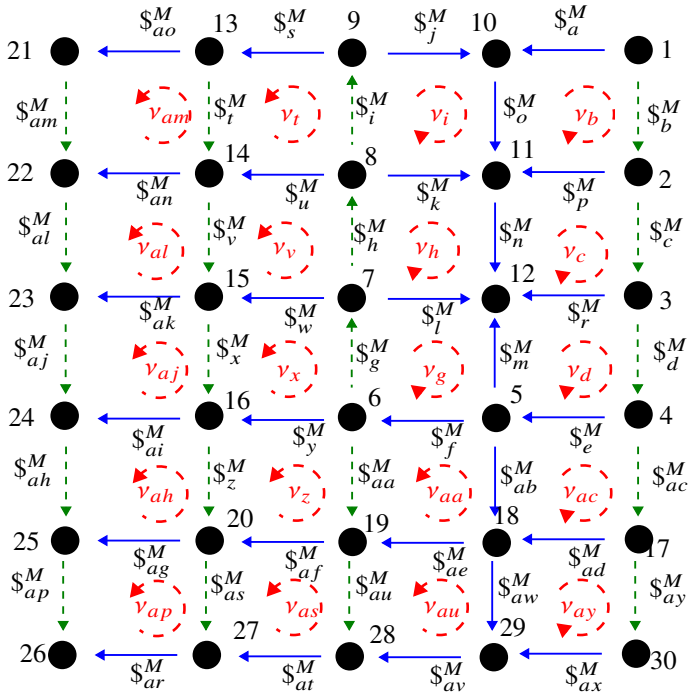

Figure 52 – Spanning Tree 6x5-shaped Origami-hold

Then, the circuit matrix is:

$$[B_M]_{16\times 40} =$$

b	c	d	g	h	i	t	v	x	z	aa	ac	ah	aj	al	am	ap
1	0	0	0	0	0	0	0	0	0	0	0	0	0	0	0	0
0	1	0	0	0	0	0	0	0	0	0	0	0	0	0	0	0
0	0	1	0	0	0	0	0	0	0	0	0	0	0	0	0	0
0	0	0	1	0	0	0	0	0	0	0	0	0	0	0	0	0
0	0	0	0	1	0	0	0	0	0	0	0	0	0	0	0	0
0	0	0	0	0	1	0	0	0	0	0	0	0	0	0	0	0
0	0	0	0	0	0	1	0	0	0	0	0	0	0	0	0	0
0	0	0	0	0	0	0	1	0	0	0	0	0	0	0	0	0
0	0	0	0	0	0	0	0	1	0	0	0	0	0	0	0	0
0	0	0	0	0	0	0	0	0	1	0	0	0	0	0	0	0
0	0	0	0	0	0	0	0	0	0	1	0	0	0	0	0	0
0	0	0	0	0	0	0	0	0	0	0	1	0	0	0	0	0
0	0	0	0	0	0	0	0	0	0	0	0	1	0	0	0	0
0	0	0	0	0	0	0	0	0	0	0	0	0	1	0	0	0
0	0	0	0	0	0	0	0	0	0	0	0	0	0	1	0	0
0	0	0	0	0	0	0	0	0	0	0	0	0	0	0	1	0
0	0	0	0	0	0	0	0	0	0	0	0	0	0	0	0	1
0	0	0	0	0	0	0	0	0	0	0	0	0	0	0	0	0
0	0	0	0	0	0	0	0	0	0	0	0	0	0	0	0	0
0	0	0	0	0	0	0	0	0	0	0	0	0	0	0	0	0

as	au	ay	a	e	f	j	k	l	m	n	o	p	r	s	u	w
0	0	0	−1	0	0	0	0	0	0	0	−1	1	0	0	0	0
0	0	0	0	0	0	0	0	0	0	−1	0	−1	1	0	0	0
0	0	0	0	1	0	0	0	0	−1	0	0	0	−1	0	0	0
0	0	0	0	0	1	0	0	1	−1	0	0	0	0	0	0	0
0	0	0	0	0	0	0	1	−1	0	1	0	0	0	0	0	0
0	0	0	0	0	0	1	−1	0	0	0	1	0	0	0	0	0
0	0	0	0	0	0	−1	1	0	0	0	−1	0	0	1	−1	0
0	0	0	0	0	0	0	−1	1	0	−1	0	0	0	0	1	−1
0	0	0	0	0	−1	0	0	−1	1	0	0	0	0	0	0	1
0	0	0	0	0	1	0	0	0	0	0	0	0	0	0	0	0
0	0	0	0	0	1	0	0	0	0	0	0	0	0	0	0	0
0	0	0	0	−1	0	0	0	0	0	0	0	0	0	0	0	0
0	0	0	0	0	1	0	0	0	0	0	0	0	0	0	0	0
0	0	0	0	0	−1	0	0	−1	1	0	0	0	0	0	0	1
0	0	0	0	0	0	0	−1	1	0	−1	0	0	0	0	1	−1
0	0	0	0	0	0	−1	1	0	0	0	−1	0	0	1	−1	0
0	0	0	0	0	0	0	0	0	0	0	0	0	0	0	0	0
1	0	0	0	0	0	0	0	0	0	0	0	0	0	0	0	0
0	1	0	0	0	0	0	0	0	0	0	0	0	0	0	0	0
0	0	1	0	−1	0	0	0	0	0	0	0	0	0	0	0	0

y	ab	ad	ae	af	ag	ai	ak	an	ao	ar	at	av	aw	ax	
0	0	0	0	0	0	0	0	0	0	0	0	0	0	0	b
0	0	0	0	0	0	0	0	0	0	0	0	0	0	0	c
0	0	0	0	0	0	0	0	0	0	0	0	0	0	0	d
0	0	0	0	0	0	0	0	0	0	0	0	0	0	0	g
0	0	0	0	0	0	0	0	0	0	0	0	0	0	0	h
0	0	0	0	0	0	0	0	0	0	0	0	0	0	0	i
0	0	0	0	0	0	0	0	0	0	0	0	0	0	0	t
0	0	0	0	0	0	0	0	0	0	0	0	0	0	0	v
−1	0	0	0	0	0	0	0	0	0	0	0	0	0	0	x
1	−1	0	−1	−1	0	0	0	0	0	0	0	0	0	0	z
0	−1	0	−1	0	0	0	0	0	0	0	0	0	0	0	aa
0	−1	1	0	0	0	0	0	0	0	0	0	0	0	0	ac
1	−1	0	−1	−1	−1	1	0	0	0	0	0	0	0	0	ah
−1	0	0	0	0	0	−1	1	0	0	0	0	0	0	0	aj
0	0	0	0	0	0	0	−1	1	0	0	0	0	0	0	al
0	0	0	0	0	0	0	0	−1	1	0	0	0	0	0	am
0	0	0	1	1	1	0	0	0	0	1	1	1	−1	0	ap
0	0	0	1	1	0	0	0	0	0	0	1	1	−1	0	as
0	0	0	1	0	0	0	0	0	0	0	0	1	−1	0	au
0	−1	1	0	0	0	0	0	0	0	0	0	0	0	0	ay

(104)

The twist per joint are shown in Equation (100).

$$
\$_a^M = \begin{pmatrix} 0 \\ \omega_a \cos\beta \\ \omega_a \sin\beta \\ 0 \\ 0 \\ 0 \end{pmatrix}; \quad \$_b^M = \begin{pmatrix} \omega_b \cos\theta \\ 0 \\ -\omega_b \sin\theta \\ 0 \\ 0 \\ 0 \end{pmatrix}; \quad \$_c^M = \begin{pmatrix} \omega_c \cos\theta \\ 0 \\ -\omega_c \sin\theta \\ -2\omega_c \sin\theta \\ 0 \\ -2\omega_c \cos\theta \end{pmatrix}; \quad \$_d^M = \begin{pmatrix} \omega_d \cos\theta \\ 0 \\ -\omega_d \sin\theta \\ -4\omega_d \sin\theta \\ 0 \\ -4\omega_d \cos\theta \end{pmatrix}; \quad \$_e^M = \begin{pmatrix} 0 \\ \omega_e \\ 0 \\ 0 \\ 0 \\ 0 \end{pmatrix}
$$

$$
\$_f^M = \begin{pmatrix} 0 \\ \omega_f \\ \cdots \\ 2\omega_f \sin\theta) \\ 0 \\ -2\omega_f \cos\theta \end{pmatrix}; \quad \$_g^M = \begin{pmatrix} \omega_g \cos\theta \\ 0 \\ -\omega_g \sin\theta \\ -4\omega_g \sin\theta \\ -4\omega_g \cos\theta \sin\theta \\ -4\omega_g \cos\theta \end{pmatrix}; \quad \$_h^M = \begin{pmatrix} \omega_h \cos\theta \\ 0 \\ -\omega_h \sin\theta \\ -2\omega_h \sin\theta \\ -4\omega_h \cos\theta \sin\theta \\ -2\omega_h \cos\theta \end{pmatrix}; \quad \$_i^M = \begin{pmatrix} \omega_i \cos\theta \\ 0 \\ -\omega_i \sin\theta\, 0 \\ -4\omega_i \cos\theta \sin\theta \\ 0 \end{pmatrix}
$$

$$
\$_j^M = \begin{pmatrix} 0 \\ \omega_j \cos\beta \\ \omega_j \sin\beta \\ 2\omega_j \sin\theta \cos\beta \\ 2\omega_j \cos\theta \sin\beta \\ -2\omega_j \cos\theta \cos\beta \end{pmatrix}; \quad \$_k^M = \begin{pmatrix} 0 \\ \omega_k \\ 0 \\ 2\omega_k \sin\theta \\ 0 \\ -2\omega_k \cos\theta \end{pmatrix}; \quad \$_l^M = \begin{pmatrix} 0 \\ \omega_l \\ 0 \\ 2\omega_l \sin\theta \\ 0 \\ -2\omega_l \cos\theta \end{pmatrix}; \quad \$_m^M = \begin{pmatrix} \omega_m \cos\theta \\ 0 \\ \omega_m \sin\theta \\ 4\omega_m \sin\theta \\ 0 \\ -4\omega_m \cos\theta \end{pmatrix}; \quad \$_n^M = \begin{pmatrix} \omega_n \cos\theta \\ 0 \\ \omega_n \sin\theta \\ 2\omega_n \sin\theta \\ 0 \\ -2\omega_n \cos\theta \end{pmatrix}
$$

$$
\$_o^M = \begin{pmatrix} \omega_o \cos\theta \\ 0 \\ \omega_o \sin\theta \\ 0 \\ 0 \\ 0 \end{pmatrix}; \quad \$_p^M = \begin{pmatrix} 0 \\ \omega_p \\ 0 \\ 0 \\ 0 \\ 0 \end{pmatrix}; \quad \$_r^M = \begin{pmatrix} 0 \\ \omega_r \\ 0 \\ 0 \\ 0 \\ 0 \end{pmatrix}; \quad \$_s^M = \begin{pmatrix} 0 \\ \omega_s \cos\beta \\ \omega_s \sin\beta \\ \\ 0 \\ 4\omega_s \cos\theta \sin\beta \\ -4\omega_s \cos\theta \cos\beta \end{pmatrix}; \quad \$_t^M = \begin{pmatrix} \omega_t \cos\theta \\ 0 \\ \omega_t \sin\theta \\ 0 \\ 4\omega_t \cos\theta \sin\theta \\ 0 \end{pmatrix}; \quad \$_u^M = \begin{pmatrix} 0 \\ \omega_u \\ 0 \\ 0 \\ 0 \\ -4\omega_u \cos\theta \end{pmatrix}
$$

$$
\$_v^M = \begin{pmatrix} \omega_v \cos\theta \\ 0 \\ \omega_v \sin\theta \\ 2\omega_v \sin\theta \\ 4\omega_v \cos\theta \sin\theta \\ -2\omega_v \cos\theta \end{pmatrix}; \quad \$_w^M = \begin{pmatrix} 0 \\ \omega_w \\ 0 \\ 0 \\ 0 \\ -4\omega_w \cos\theta \end{pmatrix}; \quad \$_x^M = \begin{pmatrix} \omega_x \cos\theta \\ 0 \\ \omega_x \sin\theta \\ 4\omega_x \sin\theta \\ 4\omega_x \cos\theta \sin\theta \\ -4\omega_x \cos\theta \end{pmatrix}; \quad \$_y^M = \begin{pmatrix} 0 \\ \omega_y \\ 0 \\ 0 \\ 0 \\ -4\cos\theta \end{pmatrix}; \quad \$_z^M = \begin{pmatrix} \omega_z \cos\theta \\ 0 \\ \omega_z \sin\theta \\ 6\omega_z \sin\theta \\ 4\omega_z \cos\theta \sin\theta \\ -6\omega_z \cos\theta \end{pmatrix}
$$

$$
\$_{aa}^M = \begin{pmatrix} \omega_{aa} \cos\theta \\ 0 \\ \omega_{aa} \sin\theta \\ -6\omega_{aa} \sin\theta \\ -4\omega_{aa} \cos\theta \sin\theta \\ -6\omega_{aa} \cos\theta \end{pmatrix}; \quad \$_{ab}^M = \begin{pmatrix} \omega_{ab} \cos\theta \\ 0 \\ \omega_{ab} \sin\theta \\ 6\omega_{ab} \sin\theta \\ 0 \\ -6\omega_{ab} \cos\theta \end{pmatrix}; \quad \$_{ac}^M = \begin{pmatrix} \omega_{ac} \cos\theta \\ 0 \\ -\omega_{ac} \sin\theta \\ -6\omega_{ac} \sin\theta \\ 0 \\ -6\omega_{ac} \cos\theta \end{pmatrix}; \quad \$_{ad}^M = \begin{pmatrix} 0 \\ \omega_{ad} \\ 0 \\ 0 \\ 0 \\ 0 \end{pmatrix}; \quad \$_{ae}^M = \begin{pmatrix} 0 \\ \omega_{ae} \\ 0 \\ 2\omega_{ae} \sin\theta \\ 0 \\ -2\omega_{ae} \cos\theta \end{pmatrix} \tag{105}
$$

$$
\$_{af}^M = \begin{pmatrix} 0 \\ \omega_{af} \\ 0 \\ 0 \\ 0 \\ -4\omega_{af} \cos\theta \end{pmatrix}; \quad \$_{ag}^M = \begin{pmatrix} 0 \\ \omega_{ag} \\ 0 \\ 2\omega_{ag} \sin\theta \\ 0 \\ -6\omega_{ag} \cos\theta \end{pmatrix}; \quad \$_{ah}^M = \begin{pmatrix} \omega_{ah} \cos\theta \\ 0 \\ -\omega_{ah} \sin\theta \\ -6\omega_{ah} \sin\theta \\ -8\omega_{ah} \cos\theta \sin\theta \\ -6\omega_{ah} \cos\theta \end{pmatrix}; \quad \$_{ai}^M = \begin{pmatrix} 0 \\ \omega_{ai} \\ 0 \\ 2\omega_{ai} \sin\theta \\ 0 \\ -6\omega_{ai} \cos\theta \end{pmatrix}
$$

$$
\$_{aj}^M = \begin{pmatrix} \omega_{aj} \cos\theta \\ 0 \\ -\omega_{aj} \sin\theta \\ -4\omega_{aj} \sin\theta \\ -8\omega_{aj} \cos\theta \sin\theta \\ -4\omega_{aj} \cos\theta \end{pmatrix}; \quad \$_{ak}^M = \begin{pmatrix} 0 \\ \omega_{ak} \\ 0 \\ 2\omega_{ak} \sin\theta \\ 0 \\ -6\omega_{ak} \cos\theta \end{pmatrix}; \quad \$_{al}^M = \begin{pmatrix} \omega_{al} \cos\theta \\ 0 \\ -\omega_{al} \sin\theta \\ -2\omega_{al} \sin\theta \\ -8\omega_{al} \cos\theta \sin\theta \\ -2\omega_{al} \cos\theta \end{pmatrix}; \quad \$_{am}^M = \begin{pmatrix} \omega_{am} \cos\theta \\ 0 \\ -\omega_{am} \sin\theta \\ 0 \\ -8\omega_a \cos\theta \sin\theta \\ 0 \end{pmatrix}
$$

$$
\$_{an}^M = \begin{pmatrix} 0 \\ \omega_{an} \\ 0 \\ 2\omega_{an} \sin\theta \\ 0 \\ -6\omega_{an} \cos\theta \end{pmatrix}; \quad \$_{ao}^M = \begin{pmatrix} 0 \\ \omega_{ao} \cos\beta \\ \omega_{ao} \sin\beta \\ 2\omega_{ao} \sin\theta \cos\beta) \\ 6\omega_{ao} \cos\theta \sin\beta \\ 6\omega_{ao} \cos\theta \cos\beta \end{pmatrix}; \quad \$_{ap}^M = \begin{pmatrix} \omega_{ap} \cos\theta \\ 0 \\ -\omega_{ap} \sin\theta \\ -8\omega_{ap} \sin\theta \\ -8\omega_{ap} \cos\theta \sin\theta \\ -8\omega_{ap} \cos\theta \end{pmatrix}; \quad \$_{ar}^M = \begin{pmatrix} 0 \\ \omega_{ar} \cos\beta \\ \omega_{ar} \sin\beta \\ \omega_{ar}(8\sin\beta - 2\sin\theta\cos\beta) \\ 6\omega_{ar} \cos\theta \sin\beta \\ 6\omega_{ar} \cos\theta \cos\beta \end{pmatrix}
$$

$$
\$_{as}^M = \begin{pmatrix} \omega_{as} \cos\theta \\ 0 \\ -\omega_{as} \sin\theta \\ 8\omega_{as} \sin\theta \\ 4\omega_{as} \cos\theta \sin\theta \\ -8\omega_{as} \cos\theta \end{pmatrix}; \quad \$_{at}^M = \begin{pmatrix} 0 \\ \omega_{at} \cos\beta \\ \omega_{at} \sin\beta \\ 8\omega_{at} \sin\theta \\ 4\omega_{at} \cos\theta \sin\beta \\ 4\omega_{at} \cos\theta \cos\beta \end{pmatrix}; \quad \$_{au}^M = \begin{pmatrix} \omega_{au} \cos\theta \\ 0 \\ -\omega_{au} \sin\theta \\ -8\omega_{au} \sin\theta \\ -4\omega_{au} \cos\theta \sin\theta \\ -8\omega_{au} \cos\theta \end{pmatrix}; \quad \$_{av}^M = \begin{pmatrix} 0 \\ -\omega_{av} \cos\beta \\ \omega_{av} \sin\beta \\ \omega_{av}(8\sin\beta - 2\cos\beta\sin\theta) \\ 2\omega_{av} \cos\theta \sin\beta \\ 2\omega_{av} \cos\theta \cos\beta \end{pmatrix}
$$

$$
\$_{aw}^M = \begin{pmatrix} \omega_{aw} \cos\theta \\ 0 \\ \omega_{aw} \sin\theta \\ 0 \\ 4\omega_{aw} \cos\theta \sin\theta \\ 0 \end{pmatrix}; \quad \$_{ax}^M = \begin{pmatrix} 0 \\ -\omega_{ax} \cos\beta \\ \omega_{ax} \sin\beta \\ 8\omega_{ax} \sin\beta \\ 0 \\ 0 \end{pmatrix}; \quad \$_{ay}^M = \begin{pmatrix} \omega_{ay} \cos\theta \\ 0 \\ -\omega_{ay} \sin\theta \\ 8\omega_{ay} \sin\beta \\ 0 \\ -8\omega_{ay} \cos theta \end{pmatrix}
$$

By replacing the screws in the M_D matrix, subsequently in M_N, it is possible to calculate the rank of the M_N matrix and finally it is determined that the mobility of this origami array is $F_N = 1$. On the other hand, it is found that this pattern has $C_N = 72$ redundant constraints, which are distributed as shown in Equation (106) and Figure 50 .

$$
\begin{aligned}
\hat{\$}^a = [\ & 0\ \ 0\ \ 0\ \ U_1\ \ V_1\ \ W_1\ \ 0\ \ 0\ \ 0\ \ U_2\ \ V_2\ \ W_2\ \ 0\ \ 0\ \ 0\ \ U_3\ \ V_3\ \ W_3\ \ 0\ \ 0\ \ T_4\ \ U_4\ \ V_4\ \ W_4\ \ \dots \\
& \dots\ \ 0\ \ 0\ \ T_5\ \ U_5\ \ V_5\ \ W_5\ \ 0\ \ 0\ \ 0\ \ U_6\ \ V_6\ \ W_6\ \ 0\ \ 0\ \ T_7\ \ U_7\ \ V_7\ \ W_7\ \ 0\ \ 0\ \ T_8\ \ U_8\ \ V_8\ \ W_8\ \ \dots \\
& \dots\ \ 0\ \ 0\ \ T_9\ \ U_9\ \ V_9\ \ W_9\ \ 0\ \ 0\ \ T_{10}\ \ 0\ \ 0\ \ W_{10}\ \ 0\ \ S_{11}\ \ T_{11}\ \ U_{11}\ \ V_{11}\ \ W_{11}\ \ 0\ \ 0\ \ T_{12}\ \ U_{12}\ \ \dots \\
& \dots\ V_{12}\ \ W_{12}\ \ 0\ \ 0\ \ T_{13}\ \ U_{13}\ \ V_{13}\ \ W_{13}\ \ 0\ \ 0\ \ T_{14}\ \ U_{14}\ \ V_{14}\ \ W_{14}\ \ 0\ \ 0\ \ T_{15}\ \ U_{15}\ \ V_{15}\ \ W_{15}\ \ \dots \\
& \dots\ \ 0\ \ 0\ \ 0\ \ U_{16}\ \ V_{16}\ \ W_{16}\ \ 0\ \ 0\ \ 0\ \ 0\ \ 0\ \ W_{17}\ \ 0\ \ S_{18}\ \ 0\ \ U_{18}\ \ V_{18}\ \ W_{18}\ \ \dots \\
& \dots\ \ 0\ \ S_{19}\ \ T_{19}\ \ U_{19}\ \ V_{19}\ \ W_{19}\ \ 0\ \ 0\ \ T_{20}\ \ U_{20}\ \ V_{20}\ \ W_{20}\ ]
\end{aligned}
\tag{106}
$$

And:

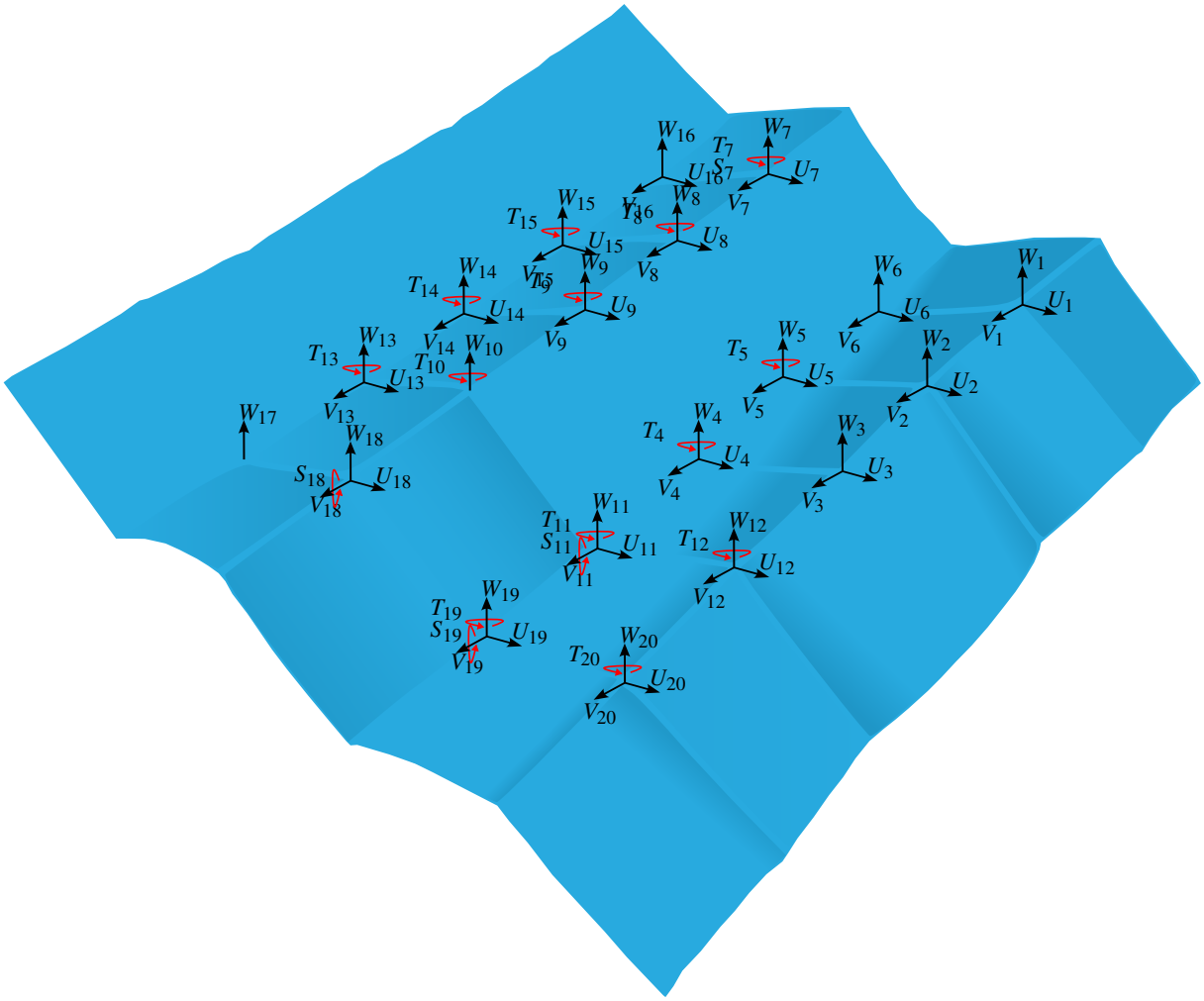

Figure 53 – 6x5 Shaped Origami

APPENDIX B – MOBILITY EQUATIONS FOR ORIGAMI-INSPIRED MECHANISMS

In this section of the dissertation, the equations used to calculate the mobility of origami and/or origami-inspired mechanisms were analyzed, and the mobility of some origami designs was determined. Subsequently, the mobility and redundant constraints of the examples of this section were calculated using Davies method, and finally, a general mobility equation for origami-inspired mechanisms was proposed, and a methodoloy for its calculation will be defined.

B.1 TACHI EQUATION

(TACHI, 2010) proposed an equation to define the mobility of origami with a fold pattern composed of multiple vertices satisfying the bird's foot condition. The bird´s foot condition consists of a set of three folds of one fold assignment (e.g. mountain), sequentially separated by angles strictly between 0 and π, plus an additional fold of the opposite assignment (LANG et al., 2018). In Figure 54, an example of a bird's foot fold at a degree 4 vertex is shown; folds a, c and d have mountain assignment, and fold b has valley assignment.

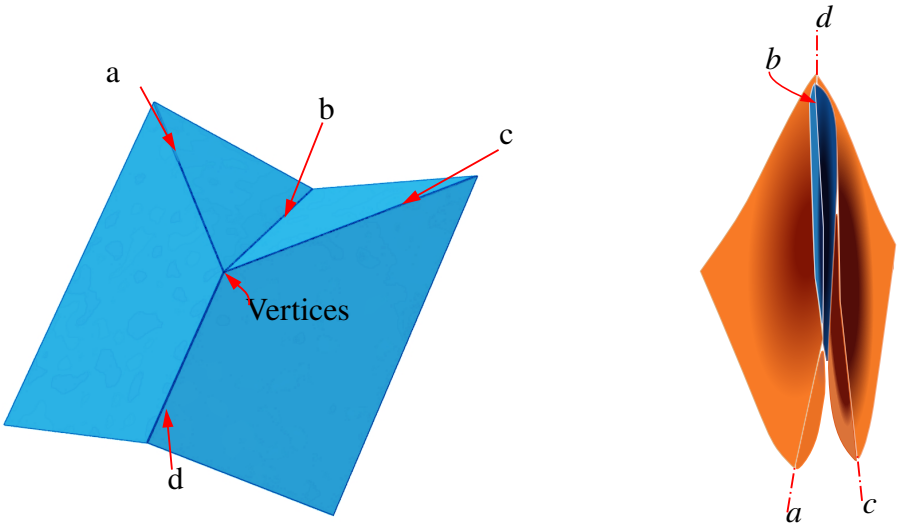

(a) Unfolded (b) Folded

Figure 54 – Bird´s-foot Origami Pattern.

If the above condition is fulfilled, it is possible to determine the number of degrees of freedom as follows

$$M = B - 3H + S - 3 - \sum_{k=4} P_k(k-3) \tag{107}$$

Where B is the number of edges on the border of the pattern. In Figure 55, you can see that origami above has eight edges on the boundary, i.e., $B = 8$.

On the other hand, H is the number of holes in the pattern; this term is used for kirigami. Therefore, for this example, H=0. S is the number of redundant constraints. Redundancy in

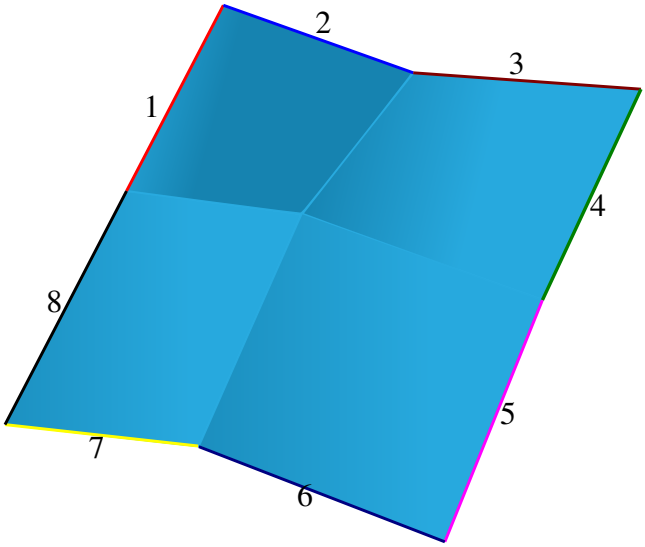

Figure 55 – Boundary Bird´s-foot origami pattern.

origami-inspired mechanisms can affect their mobility, as well as induce excessive internal loads and subsequent fatigue failure. In origami, these redundant constraints are frequently encountered due to symmetry, periodicity, and angular relationships. Each vertex has three restrictions; as building blocks are joined, the number of constraints per vertex increases and the number of folds decreases; thus, redundant constraints are added (TACHI, 2009).

Finally, the term k corresponds to the number of sides of the polygon that makes up each face of the origami, and P_k is the number of faces with a specific polygonal shape. In this case, as seen in Figure 56 the form of the faces are squares. Therefore, $k = 4$, and the number of faces with that shape is ($P_k = 4$).

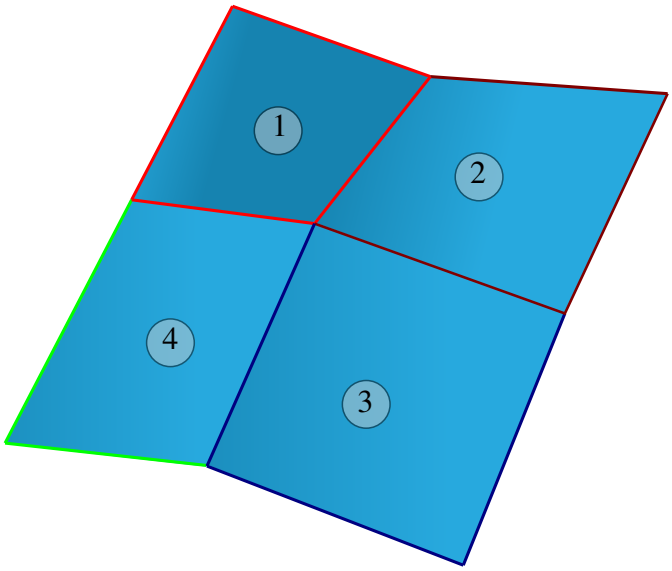

Figure 56 – Faces Bird´s-feet origami pattern.

By identifying each of the terms of the Equation (107), the degrees of freedom can be calculated using the Equation (107), then:

$$M = B - 3H + S - 3 - \sum_{k=4} P_k(k-3) \tag{108}$$

$$M = 8 - 3(0) + (0) - 3 - \sum_{k=4} (4)(4-3) = 1 \tag{109}$$

(BROWN et al., 2022), state that the redundant constraints can be determined by the difference between the observed mobility and the predicted mobility (what we know as Invariant F).

B.2 MODIFIED CHEBYCHEV-GRUBLER-KUTZBACH MOBILITY CRITERION

Generally, the mobility of the mechanisms is calculated using the modified Chebychev-Grubler-Kutzbach mobility criterion, with all its joints expanded (MARTINS; MURAI, 2020), which is formulated as follows:

$$M = \lambda(n - j - 1) + j + q \tag{110}$$

Where λ is the order of the screw system, in the case of origami, this is considered spherical, i.e., $\lambda = 3$. n is the number of facets of the origami, j is the number of internal folds of the origami, and q defines the redundant constraints of the origami. For the example of Figure 10, number of facets is equal to 4 ($n = 4$), number of folds inside the pattern is 4 ($j = 4$), and there are no redundant constraints. If the mobility of the origami is computed employing the Equation (110), one has:

$$M = 1 \tag{111}$$

It can be observed that the two equations yield the same result, so it can be considered that both can be used for the calculation of mobility in origami. It must be remembered that the Equation (107) is restricted for origami patterns that fulfills the bird's foot condition. Therefore, a relation between the two equations is made.

B.3 RELATIONSHIP BETWEEN THE TACHI EQUATION AND THE MOBILITY CRITERION

It should be reminded that a general mobility equation for origami inspired mechanisms is sought. Therefore, factors related to kirigami are eliminated from either equation. Thus, in Equation (107), factor $H = 0$ and the S term is replaced by q, leading to:

$$M = B + q - 3 - \sum_{k=4} P_k(k-3) \tag{112}$$

and

$$M = \lambda(n - j - 1) + j + q \tag{113}$$

In this case, λ is equal to 3 and multiplies terms inside the parentheses, leaving:

$$M = 3n - 3j - 3 + j + q \tag{114}$$

equating Equação (112) and Equação (114), we have that:

$$B + q - 3 - \sum_{k=4} P_k(k-3) = 3n - 2j - 3 + q \tag{115}$$

Eliminating same terms we have that:

$$B - \sum_{k=4} P_k(k-3) = 3n - 2j \tag{116}$$

From the Equação (116) some deductions can be drawn such as:

- There is a relationship between external folds and facets of origami, with the joints and links of a kinematic chain.

Some examples are developed in order to determine the mobility of origami using the above two equations, in the following sections.

B.4 ORIGAMI WITH VERTEX OF DEGREE 4 (D4V)

The spherical four-bar mechanism is composed of 4 links ($n = 4$), and four joints ($j = 4$), and its working space is spherical ($\lambda = 3$). It can be represented in different ways as an origami with vertex of degree 4, some of these are presented below, and its mobility is calculated using Equation (107) and Equation (17).

B.4.1 Origami D4V with M=1, B=8 and k=4

The mobility of this origami was calculated in the development of section B.1 and section B.2. It was found that by applying the two equations, the result was 1 DOF. Additionally, the two sides of the equality shown in Equation (116) are calculated to corroborate the conclusions of section B.3.

$$B - \sum_{k=4} P_k(k-3) = 3n - 2j \tag{117}$$

then,

$$4 = 4 \tag{118}$$

B.4.2 Origami D4V with M=1, B=6 and k=3,4

The origami representing a vertex degree 4 (D4V) pattern of this type is shown in Figure 57; it has three valley-type folds (a, b and d) and one mountain-type fold (b). it has six

edges on the boundary ($B = 6$), and it has two types of geometric figures (two triangles ($k = 3$) and two parallelepipeds ($k = 4$)).

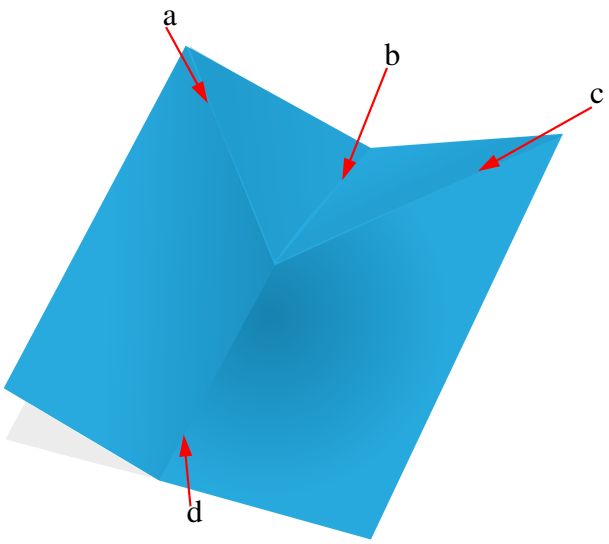

Figure 57 – Origami D4V with 6 borders

Therefore, the mobility by applying the Equation (107) is:

$$M = B - 3H + S - 3 - \sum_{k=4} P_k(k-3) \tag{119}$$

$$M = 1 \tag{120}$$

In the same way, by applying the Equation (116) it is observed that the equality is maintained.

$$B - \sum_{k=4} P_k(k-3) = 3n - 2j \tag{121}$$

$$4 = 4 \tag{122}$$

B.4.3 Origami D4V with M=1, B=4 and k=3

Another pattern for D4V is shown in the Figure 58; this representation fulfills the bird's foot condition since it has three folds (a, c and d) with valley type assignment and is sequentially separated by right angles, and one fold with mountain assignment (b). This pattern is composed of four edges on the boundary ($B = 4$). Additionally, the geometric figures within the pattern are all triangular.

By calculating the mobility using the Equation (107) we obtain that the degrees of freedom of this block is the same as the previous ones:

$$M = B - 3H + S - 3 - \sum_{k=4} P_k(k-3) \tag{123}$$

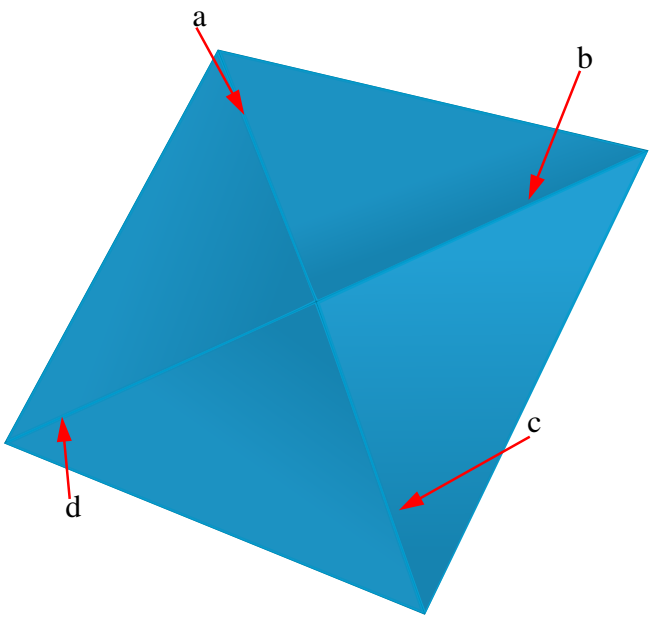

Figure 58 – Origami D4V with 4 borders

$$M = 1 \tag{124}$$

While applying the Equation (116) it is evident that the proportions are maintained.

$$4 = 4 \tag{125}$$